2011

# A STUDY ON WIRELESS COMMUNICATION ERROR PERFORMANCE AND PATH LOSS PREDICTION

Isnin, Ismail

# A STUDY ON WIRELESS COMMUNICATION [illegible] BEHAVIOR ANCE AND PATH LOSS PREDICTION



[illegible]

Ph.D. 201[illegible]


# A STUDY ON WIRELESS COMMUNICATION ERROR PERFORMANCE AND PATH LOSS PREDICTION

**Ismail Fauzi Isnin**

**Ph.D.**
**April 2011**


# A STUDY ON WIRELESS COMMUNICATION ERROR PERFORMANCE AND PATH LOSS PREDICTION

**Ismail Fauzi Isnin**

A thesis submitted to the University of Plymouth
in partial fulfilment for the degree of

**Doctor of Philosophy**

School of Computing and Mathematics
Faculty of Science and Technology
University of Plymouth
United Kingdom

**April 2011**

# A Study on Wireless Communication Error Performance and Path Loss Prediction

Ismail Fauzi Isnin

## Abstract

One channel model that characterises multipath fading effect of a wireless channel is called Flat Rayleigh Fading channel model. Given the properties of Flat Rayleigh Fading channel, an equation to find the capacity of a Flat Rayleigh fading channel with hard decision decoding is derived. The difference of power requirement to achieve the Additive White Gaussian Noise (AWGN) capacity over a Flat Rayleigh Fading channel fading is found to increase exponentially with $E_s/N_0$. Upper and lower bounds of error performance of linear block codes over a Flat Rayleigh Fading channel are also studied.

With the condition that the excess delay of a channel is known earlier, it is shown that a correlator with shorter length, according to excess delay of the channel, can be constructed for use in wireless channel response measurements. Therefore, a rule of construction of a shorter length correlator is defined, involving concatenation of parts of a Constant Amplitude Zero Auto-Correlation (CAZAC) sequence.

Simulation of [136,68,24] Double Circulant Code with Dorsch List Decoding is also done in order to evaluate error performance of the channel coding scheme over one of the IEEE Wireless Metropolitan Area Network (WirelessMAN) channel models, the Stanford University Interim Channel Model No. 5 (SUI-5) channel. Performance of the channel coding was severely degraded over the SUI-5 channel when it is compared to its performance over the AWGN channel.

Indoor path losses within three multifloor office buildings were investigated at 433 MHz, 869 MHz and 1249 MHz. The work involved series of extensive received signal strength measurements within the buildings for all of the considered frequencies. Results have shown that indoor path loss is higher within a square footprint building than indoor path loss in a rectangular building. Parameters of Log-Distance Path Loss and Floor Attenuation Factor Path Loss models have been derived from the measurement data. In addition, a new indoor path loss prediction model was derived to cater for path loss prediction within multifloor buildings with indoor atriums. The model performs with better prediction accuracy when compared with Log-Distance Path Loss and Floor Attenuation Factor Path Loss models.

# Contents

# Acronyms

| | |
|---|---|
| $\pi/4$ DQPSK | $\pi/4$ Differential Quadriphase Phase Shift Keying |
| 1G | First Generation |
| 2G | 2nd Generation |
| 3G | Third Generation |
| 4G | Fourth Generation |
| AMPS | Advance Mobile Phone Service |
| AWGN | Additive White Gaussian Noise |
| BBG | Babbage Building |
| BPSK | Binary Phase Shift Keying |
| BSC | Binary Symmetric Channel |
| CAZAC | Constant Amplitude Zero Auto-Correlation |
| CDMA | Code Division Multiple Access |
| CRC | Cyclic Redundancy Check |
| dB | Decibles |
| DC | direct current |
| DCS-1800 | Digital Cellular System 1800 |
| ECSD | Enhanced Circuit Switched Data |
| EDGE | Enhanced Data Rate for Global/GSM Evolution |
| ETACS | European Total Access Communication System |
| ETSI | European Telecommunications Standards Institute |
| FAF | Floor Attenuation Factor |

FDMA . . . . . Frequency Division Multiple Access

FM . . . . . Frequency Modulation

FOMA . . . . . Freedom of Mobile Access

FSK . . . . . Frequency Shift Keying

GERAN . . . . . GSM/EDGE Radio Access Network

GMSK . . . . . Gaussian Minimum Shift Keying

GPRS . . . . . Global Packet Radio System

GSM . . . . . Global System for Mobile

HSCSD . . . . . High Speed Circuit Switched Data

ISI . . . . . Intersymbol Interference

ITU . . . . . International Telecommunication Union

LOS . . . . . Line-of-Sight

NLOS . . . . . Non Line-of-Sight

NMT . . . . . Nordic Mobile Telephone System

PDC . . . . . Personal Digital Cellular

QPSK . . . . . Quadrature Phase Shift Keying

RLV . . . . . Roland Levinsky Building

RS-232C . . . . . Recommended Standard 232 C Revision

SMB . . . . . Smeaton Building

SMS . . . . . Short Messaging Service

SNR . . . . . Signal to Noise Ratio

SUI-5 . . . . . Stanford University Interim Channel Model No. 5

TDMA . . . . . Time Division Multiple Access

TIA/EIA . . . . . Telecommunication Industry Association/Electronic Industries Alliance

UHF . . . . . Ultra High Frequency

| | |
|---|---|
| UMTS | Universal Mobile Telephone System |
| USB | Universal Serial Bus |
| UTRAN | UMTS Terrestrial Access Network |
| W-CDMA | Wideband Code Division Multiple Access |
| WirelessMAN | Wireless Metropolitan Area Network |

# List of Tables

# List of Figures

# Acknowledgements

I would like to express my gratitude to everyone who has helped and supported me in this work.

First of all, It has been a privilege to have Professor Martin Tomlinson as my director of studies. I would like to thank Professor Martin Tomlinson for all the kind help, support, guidance and encouragement during my study. Thanks for your priceless supervision throughout the years which has helped me to improve my research skills and knowledge in the field of digital communication and error control coding.

To my other supervisors, I would like to thank Dr Mohammed Zaki Ahmed for all the kind help, support, guidance and encouragement during my study. Thanks for your help when I was looking for a university to do my PhD study and introduced me with the field of digital communication and error control coding. I would like to thank Dr Marcel Ambroze for your kind help in our discussion on the Dorsch decoding algorithm.

I would like to acknowledge Professor Michael Darnell and Dr Cen Jun Tjhai, my external and internal examiners respectively, for their valuable and helpful feedback on this thesis.

The Ministry of Higher Education of Malaysia and Universiti Teknologi Malaysia for awarding me the scholarship for this study.

My colleagues in the Fixed and Mobile Communications Research Group (CJ, Purav Shah, Jing Cai, Li Yang, Xin Xu and Mubarak Jibril), for their kind friendship, assistances and knowledge sharing. Thanks to CJ for his kind helps especially when I was trying to get used to UNIX-based operating systems and during the discussion on Dorsh decoding algorithm.

Malaysian community in Plymouth for all their helps, friendship and support.

My beloved wife, Zaitun, for her love, pray, support and company.

Last but not least, my beloved family - my parents, brothers and sisters, for their love, pray and support.

# Author's Declaration

At no time during the registration for the degree of Doctor of Philosophy has the author been registered for any other University award without prior agreement of the Graduate Committee.

This study was financed with the aid of scholarships from Malaysia Ministry of Higher Education and Universiti Teknologi Malaysia, Malaysia.

A programme of advanced study was undertaken, which included extensive reading of literature relevant to research project, extensive on-site measurements and experiments on indoor wireless transmission system and preparation of research papers for publication.

The author has published papers in the proceeding of following international conferences:

1. SPIE International Conference on Wireless Sensing and Processing IV, Orlando, Florida, USA, 13 - 17 April 2009 in the Proceeding of SPIE, Volume 7349, page 734908.

2. SPIE International Conference on Wireless Sensing, Localization and Processing V, Orlando, Florida, USA, 5 - 9 April 2010 in the Proceeding of SPIE, Volume 7706, page 77060G.

Word count of main body of the thesis : 22415

Signed : 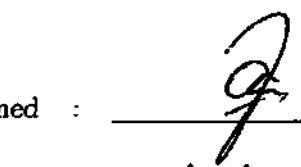

Date : 11/4/2011

# Chapter 1

# Introduction

Design and implementation of a wireless system is not as straightforward as the implementation of wired systems. This is because wireless system performance is limited by detrimental effects of wireless communication channels. Wireless channels are random, time varying and suffer from interference from their surroundings and environments.

In wireless signal transmission, signal radio waves are radiated with various angle of departure at the transmitter antenna. This generates multipath signal components of the signal that propagate through different paths to the receiver. Each of multipath components is reflected, diffracted and scattered in different ways while propagating to the receiver, depending the propagation environment. Reflection, diffraction and scattering are three basic propagation mechanisms of radio wave propagation [Rappaport, 1996]. Due to multipath propagation, multipath components are received by the receiver with varying delay and amplitude, random phase and angle of arrival.

Received signal strength at an instantaneous time is the result of summation of multipath components that arrive at that moment. Received signal strength is due to such fluctuation, even at small travel distance or high sampling rate. This is because multipath components arriving at the receiver are known to have varying amplitude and phase in both time and space dimensions. This rapid fluctuation of received signal strength is known as multipath fading or small scale fading.

Another effect in a wireless channel that is due to multipath propagation is known as Intersymbol Interference (ISI). Intersymbol interference refers to the effect of one or more multipath components of previous symbols arriving at the receiver within the detection period of succeeding symbols. In other words, ISI occurs when the delay of a symbol

multipath components exceeds the symbol period, and interferes with succeeding symbols.

If small-scale fading refers to fading effects within very small travel distance, another type of fading that occurs to wireless signals over a large travel distance is known as large-scale fading. Large-scale fading refers to the effect of signal strength attenuation over large transmitter and receiver distances. The large-scale fading is also known as path loss.

Generally, the work presented in this thesis is related to these three wireless channel effects.

## 1.1 Thesis Aim, Objectives and Organisation

The aim of the thesis is to study and contribute to the knowledge of wireless communications. The first objective of this thesis is to analyse and contribute in area of capacity and error performance of communications over a small-scale multipath fading channel, which is known as a multipath Rayleigh fading channel. The second objective is to study and contribute in the area that relates to a multipath ISI channel. Specifically, these areas are channel impulse response measurement and error performance of a multipath ISI channel. The third objective is to study and contribute in the area of path loss in a wireless communication channel. The last objective is restricted to indoor path loss prediction within multifloor buildings.

The thesis is arranged into eight chapters including this Introduction Chapter.

In order to have an overview of technology used in common wireless systems, a review of technology evolution of a mobile wireless system is done in Chapter 2. The mobile wireless system was chosen since it is the most common wireless system that has been publicly deployed worldwide. The review mainly concerns features, modulation, multiple access and error control coding schemes of the existing mobile systems. Additionally, the review has also reviewed characteristics and challenges of the next generation mobile system.

Mathematical models of three fundamental digital communication channels - the hard decision Binary Symmetric Channel (BSC), the Additive White Gaussian Noise (AWGN) channel and the Flat Rayleigh Fading multipath channel, are explained in the beginning of Chapter 3. Later, description of hard decision and soft decision channel capacity of the AWGN channel are presented and the channel capacity of a hard decision of Rayleigh

fading channel is derived. Relative to the capacity of AWGN channel, the extra power requirement of communication over a Rayleigh fading channel to achieve the same capacity is analysed and plotted for the case of hard decision channel. Similarly, the extra power requirement of communication over a hard decision AWGN channel is analysed and plotted for the capacity of a soft decision AWGN channel is to be achieved. A literature study of lower and an upper bounds of error performance of a general block code over AWGN and Flat Rayleigh fading channels is presented in Chapter 4.

It is well known that equalization is a technique to mitigate the effects of ISI. Equalization involves estimation of channel impulse response at the receiver. Estimated channel impulse response is found from periodic autocorrelation function of training sequence and a periodic correlator at the receiver. Chapter 5 presents a general rule of construction of the correlator whose its length is optimised according to maximum excess delay of the channel impulse response.

In Chapter 6, the performance of a coding scheme is investigated over the SUI-5 channel. SUI-5 channel model is one of the IEEE 802.16 Wireless Metropolitan Area Network (WirelessMAN) channel models. The channel model characterises effects of multipath fading and ISI of a fixed wireless broadband channel. The encoder of the channel coding scheme consists of [136,68,24] Double Circulant Code; the decoder is the Dorsch List Decoding type.

Chapter 7 presents work on topic of indoor path loss prediction within multifloor office buildings. Three multifloor office buildings were selected as measurement sites. Each building represents common features of multifloor office buildings such as a rectangular building footprint, square building footprint and building with an indoor atrium. Series of extensive on-site measurements of received signal strength were conducted at carrier frequencies of 433 MHz, 869 MHz and 1249 MHz within each of the buildings. Parameters involving Log-Distance and Floor Attenuation Factor path loss models are derived and presented. A new indoor path loss prediction model for use in path loss prediction within a multifloor building with an indoor atrium is described.

Conclusions from work presented in this thesis and a list of recommended future research directions are given in Chapter 8.

## 1.2 Contributions to Knowledge

The list below summarises the contributions made by the thesis. In Section 8.2, eight specific original contributions to the knowledge and practice are presented.

**Chapter 2**

- A review of existing and future mobile wireless systems which discusses the evolution of mobile wireless systems features, channel coding, multiple access and modulation schemes.

**Chapter 3**

- Capacity of Binary Flat Rayleigh Fading channel with hard decision decoding has been derived, by the substitution of the channel bit error probability over AWGN channel with the channel bit error probability over a Flat Rayleigh Fading channel, into the Binary Symmetric Channel capacity equation.

- For hard decision decoding, the difference of power requirement to achieve a specified AWGN channel capacity, over a Flat Rayleigh fading channel, has been calculated and plotted in Figure 3.9. The difference is defined as loss due to fading. The result shows that the loss due to fading exponentially increases as received Signal to Noise Ratio (SNR) per bit over the AWGN channel increases.

- For the AWGN channel, the difference of power requirement to achieve the capacity of soft decision decoding by the hard decision decoding has been calculated and plotted in Figure 3.8. The difference is defined as loss due to hard decision decoding. The result shows that the loss due to hard decision decoding exponentially decreases as the received SNR per bit increases.

**Chapter 4**

- The chapter contains literature on upper and lower bounds of error performance for general linear block codes over AWGN and Flat Rayleigh Fading channels.

**Chapter 5**

- A rule of optimised length correlator construction, for use in channel impulse response measurement, is explained. The length of the correlator depends on maximum excess delay of the channel impulse response.

**Chapter 6**

- The chapter contains a description of a simulation model that considers channel coding, Root Raised Cosine pulse shaping filtering, multipath channel filtering and Zero Forcing equalization filtering.

- Simulation results which present codeword error probability for the [136,68,24] Double Circulant Code with Dorsch List Decoding over AWGN and SUI-5 channels, are given.

**Chapter 7**

- Parameters of Log-Distance Path Loss Prediction model are presented, for use during indoor path loss prediction within multifloor buildings at carrier frequencies of 433 MHz, 869 MHz and 1249 MHz.

- Parameters of the Floor Attenuation Factor Path Loss Prediction model are presented, for use during indoor path loss prediction within multifloor buildings at carrier frequencies of 433 MHz, 869 MHz and 1249 MHz.

- It is shown that path loss rate is higher within office multifloor buildings with square footprints than path loss rate within office multifloor buildings with rectangular footprints.

- It is shown that the standard deviation of the path loss distribution from its mean is related to the propagation type between transmitter and receiver. Higher standard deviation is found for Line-of-Sight (LOS) and vice versa. This result has supported and shown agreement with findings in earlier literatures [Turkmani et al., 1987, Turkmani and Parsons, 1988].

- It is shown that the path loss rate decreases as the carrier frequency increases, within a waveguided environment where transmitter and receiver are in LOS. This result has supported and shown agreement with findings in earlier literature [Yamaguchi et al., 1986].

- It is shown that the path loss rate increases as the number of floor obstructions between transmitter and receiver increases. This result has supported and shown agreement with findings in earlier literatures [Seidel and Rappaport, 1992, Phaiboon, 2002].

- It is shown that the loss due to first floor obstruction encountered is the highest in most of the considered environments. Independent loss due to subsequent floors decreases non-linearly. This result has supported and shown agreement with findings in earlier literatures [Seidel and Rappaport, 1992, Phaiboon, 2002].

- A new indoor path loss prediction model is presented for use in path loss prediction within multifloor buildings with an indoor atrium. The model shows better prediction accuracy within such environment.

- It is shown that the Log-Distance model with path loss exponent for the Same Floor environment is better suited than the Free Space Path Loss model to predict LOS path loss, surrounding the indoor atrium of the multifloor building.

- It is shown that the path loss of the middle floor is higher than the path loss of the ground floor with the condition that transmitter and receiver are Non Line-of-Sight (NLOS), and the transmitter position is on the edge of the atrium of a higher floor.

# Chapter 2

# Existing Mobile Systems: Modulation, Multiple Access and Channel Coding

At this time, there are three generations of mobile phone systems that have been publicly deployed. They are commonly called First Generation (1G), 2nd Generation (2G) and Third Generation (3G) systems [Kaaranen et al., 2005]. Mobile system technology evolves from one generation to next generation with enhanced and additional features that fulfill user demands and, at the same time, promising better return value to service providers and other parties who have invested on it.

Generally, in the era of 1G systems, mobile phone systems were designed to provide voice or speech services while in, the era of 2G systems, mobile systems started to offer text-based communication and non real-time packet data services on top of enhanced voice services. With the introduction of 3G systems, mobile users have been exposed to audio-based and video-based services and enhanced packet data services. Mobile users are now able to have voice conversation with friends or family members and see their face simultaneously.

This chapter provides a general overview of the evolution of practical mobile systems and the main characteristics of each generation. At the same time, this chapter also generally identifies types of modulation scheme, multiple access and error control codes that have been applied on those systems. Therefore, the review in this chapter is not

intended to cover all aspects of a mobile system: instead, it is limited by concentrating on the most important topics. To summarize the review, related tables regarding the applied modulation, multiple access and channel coding schemes are provided at the end of this chapter.

Furthermore in this chapter, there is a section that reviews literature that concentrates on the characteristics and expectations of future mobile systems and their challenges. Readers are given a general picture of the challenges in the realization of the next generation mobile systems.

## 2.1 1st Generation

One of characteristics of 1G systems is that the type of modulation used in the transmission of voice data and system control data is different. For transmission of voice data, the systems used the analogue Frequency Modulation (FM) while, for the transmission of system control data, the systems used digital Frequency Shift Keying (FSK) modulation. During the 1G system era, the network coverage was only within national-scope. All of 1G systems used Frequency Division Multiple Access (FDMA) as their multiple access technique. Examples of 1G mobile phone systems are Advance Mobile Phone Service (AMPS), European Total Access Communication System (ETACS) and Nordic Mobile Telephone System (NMT).

### 2.1.1 Advance Mobile Phone Service (AMPS)

AMPS is the first 1G system that had been introduced in late 1970's in the United States of America [Brand and Aghvami, 2002]. Design processes of AMPS started in 1970. It was publicly deployed in Chicago, USA in 1984. AMPS operated within the 824 to 849 MHz frequency band for uplink transmission and the 869 to 894 MHz frequency band for downlink transmission [1]. These provided 25 MHz frequency bands for both uplink and downlink; FDMA was used to divide a 25 MHz band into 832 subchannels. The size of each subchannel was 30 kHz. From total of 832 available subchannels, 666 subchannels were allocated for user voice transmission purposes and the rest were allocated for transmission of control data.

[1] Uplink transmission is transmission from a mobile station to a base station: downlink transmission is transmission from a base station to a mobile station

In AMPS, the modulation scheme that was used for voice transmission was analogue FM with frequency deviation of 12 kHz. While for control data transmission, it was digitally modulated using FSK with frequency deviation of 8 kHz. The data rate for control data was 10 kbps. The channel coding scheme that was applied in AMPS control data transmission was BCH(40,28) and BCH(48,36) for downlink and uplink transmissions respectively.

Later, there were several systems that were developed and derived from AMPS such as Extended AMPS (E-AMPS) and Narrowband AMPS (N-AMPS). In N-AMPS, size of a subchannel was 10 kHz.

### 2.1.2 European Total Access Communications System (ETACS)

ETACS is a 1G system that operated mainly in Europe. ETACS was derived from the AMPS. However, differences between ETACS and AMPS are their operating frequency bands and sizes of a subchannel. The ETACS subchannel was smaller than AMPS subchannel.

Similar to AMPS, ETACS used FDMA as its multiple access protocol. ETACS operated in the 890 to 915 MHz frequency band for uplink transmission, and from 935 to 960 MHz for downlink purposes. With the size of a subchannel equal to 25 KHz, ETACS systems were able to operate with 1000 subchannels. Therefore, the capacity of ETACS is larger than AMPS.

ETACS used Frequency Modulation with an 8 kHz frequency deviation scheme to deliver its analogue voice transmission service. While for control data transmission, FSK digital modulation was applied with frequency deviation of 6.4 kHz. The data rate for ETACS control data transmission was 8 kbps.

There was no difference in the channel coding scheme that was applied to both ETACS and AMPS; BCH(40,28) and BCH(48,36) were used for downlink and uplink transmission respectively.

A variant of ETACS was known as Narrowband ETACS (N-ETACS) which operated in a lower frequency band than ETACS. The size of a subchannel of N-ETACS was 12.5 kHz which is a half of the size of a ETACS subchannel.

## 2.2 2nd Generation

Several weaknesses that had been present in 1G systems were limited coverage of system due to limited system capacity, less integration between systems and high transmission power requirement.

In 2G systems, digital modulation has been used for both user data and control data transmissions. Time Division Multiple Access (TDMA) and Code Division Multiple Access (CDMA) are the most common multiple access protocols that have been applied in 2G systems.

Since there is no longer analogue voice transmission in 2G systems, another significance difference of 2G systems from 1G systems was the application of voice codec technology. With voice codec technology, the human voice is encoded from an analogue signal to a digital form before it is transmitted. At the receiver end, digitally encoded data was then decoded back to analogue form. The quality of received voice signal is better than in one 1G systems.

Examples of 2G mobile systems are Global System for Mobile (GSM), Digital AMPS (D-AMPS), CdmaOne and Personal Digital Cellular (PDC).

### 2.2.1 Global System for Mobile Communications (GSM)

GSM was the most successful 2G mobile system with regard to its worldwide distribution and deployment [Vriendt et al., 2002]. GSM specifications were made by European Telecommunications Standards Institute (ETSI) in 1989, and it was commercialized in 1991. Besides voice conversational and voice message services, GSM has offered a text message service which is also known as Short Messaging Service (SMS). SMS is a connectionless packet service and it is based on a Circuit-switched data (CSD) service. The maximum number of characters in an SMS message is limited to 160 characters per text message.

Frequency bands that have been allocated for GSM to operate are the same bands as ETACS, which are the band 890 to 915 MHz for uplink and the band 935 to 960 MHz for downlink. Obviously, GSM is the system that has replaced ETACS.

In the 25 MHz frequency bands that have been allocated for uplink and downlink purposes, each band is divided into 250 subchannels. The size of each subchannel is 200

kHz. A 200 kHz subchannel can be shared by up to eight users using TDMA scheme. With TDMA, each user is given a timeslot to use the subchannel.

The modulation scheme that has been used in GSM is Gaussian Minimum Shift Keying (GMSK).

In terms of error control coding schemes that have been used in GSM, Cyclic Redundancy Check (CRC) coding is used for error detection purposes, while Convolutional Code and Fire Codes are used for error correction purposes. Many enhancements and improvements have been carried out on GSM systems. Some of these have contributed to improvements in the transmission rate of GSM. The conventional GSM transmission rate was 9.6 kbps. After optimization work on its channel coding scheme, the GSM transmission rate was increased to 14.4 kbps.

Several new technologies have also been introduced in the optimization of GSM systems, such as Enhanced Circuit Switched Data (ECSD), High Speed Circuit Switched Data (HSCSD), Global Packet Radio System (GPRS), Enhanced Data Rate for Global/GSM Evolution (EDGE) and Enhanced GPRS (E-GPRS) [Kaaranen et al., 2005]. ECSD and HSCSD were designed to increase capacity of GSM circuit switched data services, while GPRS, EDGE and E-GPRS are technologies that increase capacity of GSM packet switched data services.

A cellular system that has been derived from GSM is known as Digital Cellular System 1800 (DCS-1800). The DCS-1800 system was designed and optimized as a personal communication cellular system. DCS-1800 operates in frequency bands of 1710 to 1785 MHz for the uplink and 1805 to 1880 MHz for the downlink.

### 2.2.2 Digital AMPS (D-AMPS)

Digital AMPS (D-AMPS) is a digital cellular system in the USA. D-AMPS was derived from AMPS and D-AMPS was standardized under Interim Standard 54 (IS-54) by Telecommunication Industry Association/Electronic Industries Alliance (TIA/EIA) in 1990.

Significant differences between D-AMPS and the original AMPS are the type of modulation scheme and multiple access scheme that have been used in voice data transmission. D-AMPS implements a 4-ary $\pi/4$ Differential Quadriphase Phase Shift Keying ($\pi/4$ DQPSK) modulation scheme which has managed to produce a 48.6 kbps modulated bit

rate transmission. For control data transmission, the same FSK modulation scheme as used in AMPS remains and thus the transmission bitrate is 10 kbps. D-AMPS uses CRC codes and Convolutional Codes as its error control coding schemes.

In terms of channel size, the size of a subchannel in D-AMPS is still the same size as in AMPS, which is 30 kHz per subchannel. However, each subchannel is shared by three users using a TDMA scheme instead of one user as in AMPS. Therefore, the capacity of D-AMPS is three times higher than AMPS.

One of later developments of D-AMPS is the Interim Standard 136 (IS-136). Some of the main changes that have been standardized in IS-136 standard are the application of a $\pi/4$ DQPSK modulation scheme for control data transmission and the implementation of Paging and SMS.

### 2.2.3 CdmaOne

Another cellular system that is categorized as a 2G system is CdmaOne. The specification of the CdmaOne system is given in Interim Standard 95 A (IS-95A) standard. CdmaOne was first deployed in 1995.

CdmaOne uses CDMA as its multiple access scheme which enables up to 64 users shares a single 1.25 MHz channel using a spread spectrum mechanism. Each user is distinguished from other users by assigning an unique pseudo-random code at transmitter and receiver ends.

The uplink modulation scheme of CdmaOne is different from the downlink modulation scheme. Binary Phase Shift Keying (BPSK) is used for the uplink and Quadrature Phase Shift Keying (QPSK) is used for the downlink. Even though the modulation type is different from uplink and downlink, both links end up with 1.2288 Mbps channel bit rate transmission. The IS-95A system throughput is 14.4 kbps. CRC and Convolutional code are applied in CdmaOne for error control purposes.

The next evolution of CdmaOne was the IS-95B specification which was published in 1995 [CDMA Development Group Website, 2007]. IS-95B is categorized in the 2.5G system category. In IS-95B, a packet-switched data service is implemented and its data bit rate is 64 kbps.

### 2.2.4 PDC

Besides GSM that was specified by ETSI and CdmaOne approved by the USA, Japan also has its own 2G mobile communication standard, which is called Personal Digital Cellular (PDC). PDC is based on the D-AMPS (IS-54) cellular system. PDC uses the same modulation scheme as D-AMPS which is $\pi/4$ DQPSK. PDC system allocates 25 KHz for a single subchannel and its channel data rate is 42 kbps. Thus, the bandwidth efficiency of the PDC system equals to 1.68 bps/Hz [Rappaport, 1996]. In terms of the channel coding scheme used in the system, PDC uses CRC and convolutional codes with constraint length of 5 and coding rate of 9/17 [Rappaport, 1996]. The most widely known service that has been offered in PDC was 'i-mode'. The i-mode service enables users to access Internet from mobile phones. However, PDC was not widely deployed outside of Japan.

## 2.3 3rd Generation

3rd generation systems offer higher number of applications than 1G and 2G systems. With 3G systems, users are able to have higher speeds of packet-switched and circuit-switched data transmission. High speed packet-switched data transmission allows the mobile phone user to use electronic mail with an attachment service, Internet surfing, on-line transactions, database access, location information services and large file transfer [Evans and Baughan, 2000]. High speed circuit-switched data transmission allows users to have high quality voice conversation and audio-video conversation services [Tachikawa, 2003].

### 2.3.1 Freedom of Mobile Access (FOMA)

The first 3G system deployed is called Freedom of Mobile Access (FOMA). FOMA was firstly deployed in October 2001, in Japan. FOMA is based on the IMT-2000 system, which uses Wideband Code Division Multiple Access (W-CDMA) technology. In FOMA, packet-switched data transmission can achieve up to 64 kbps for the uplink and 384 kbps for the downlink. With such data rates, users are able to browse and surf the Internet, send and receive emails and download 'i-appli' applications and multimedia files conveniently. Circuit-switched services, such as voice and video conversations, are supported by up to 64 kbps transmission speed [Tachikawa, 2003].

### 2.3.2 Universal Mobile Telephone System (UMTS)

A European 3G cellular system standard that was proposed by ETSI is called the Universal Mobile Telephone System (UMTS). UMTS generally operates at in the 2 GHz frequency band. However, band allocation in one country might differ from other countries according to the local government wireless policies and planning.

The main radio interface of UMTS is called the UMTS Terrestrial Access Network (UTRAN). In UMTS, the W-CDMA multiple access scheme is used over a 5 MHz frequency band for the uplink and another 5 MHz frequency band for downlink transmission. The modulation scheme applied in UMTS is QPSK with root raised cosine roll-off of 0.22 for pulse shaping. the transmission chip rate is 3.84 Mcps. Since QPSK is used, the maximum channel bit rate is 7.68 Mbps, twice the chip rate. As mentioned in [Take, 2004], the bandwidth of a 3G system could be up to 144 kbps for high speed movement, 384 kbps for low speed movement and 2 Mbps for stationary or indoor environments.

If UTRAN is unreliable in some areas, UMTS will automatically activate its alternative radio interface which is called the GSM/EDGE Radio Access Network (GERAN). Basically, GERAN is a combination of GSM radio interfaces and EDGE technology.

Furthermore, the types of error control codes that have been applied in UMTS are CRC for error detection, whilst convolutional and Turbo coding are used for error correction coding.

## 2.4 4G Features and Challenges

Even though 3G systems have already provided various types of mobile applications and services, mobile communication technology is still continuously evolving. Needs and expectations of users, service providers and hardware vendors continuously increase. Features of Fourth Generation (4G) systems were discussed in terms of the user perspective in [Hui and Yeung, 2003]. High usability of services which enable users to use mobile services and applications anytime and anywhere become the first expectation of users. also, users also expect to use mobile services on any platforms or devices, with services being delivered through different technologies seamlessly. A global standard of specifications that covers all aspects of systems, or integration of existing and new systems, provides possible solutions to realise this environment. For example, IP-based transmission is supported by all

mobile systems and technologies. Users also expect to have low cost multimedia services on their mobile system. Users also would like to have an ideal system that could support their individual needs, based on their personal interests and intentions. Some of these future system user expectation are also supported in [Take, 2004]. In [Evans and Baughan, 2000], 4G systems are also expected to have an autonomous and automated initiated machine to machine interaction feature. As discussed in [Tachikawa, 2003], some features that are proposed to the 4G system are listed below:

- Systems with an operating system that is capable of integrating cellular networks, fixed-wireless access networks and wireless LANs.
- High speed transmission that can support peak hour traffic at about 50-100 Mbps.
- Larger system capacity, at about 10 times that of 3G systems.
- Support for the next generation Internet such as IPV6 and higher Quality of Service.
- Seamless services
- Flexible network architecture
- Use of the microwave band at 3-6 GHz
- Low system cost which is less than 0.1 percent of cost of 3G systems.

From [Evans and Baughan, 2000, Akyildiz et al., 2008, Kelley, 2007, Zheng et al., 2009], several aspects that need to be highly dynamic features of 4G systems are given below:

- User traffic
- Air interface and terminal.
- Radio environment.
- Quality of Service.
- Mobility Pattern.
- Software Radio
- Cognitive Radio

## 2.5 Summary

In this chapter, a review of the evolution of mobile systems technologies, ie modulation schemes, multiple access and channel coding schemes, is presented. Mobile systems that have been reviewed are ETACS and AMPS for 1G generation systems, GSM, D-AMPS and CdmaOne for 2G mobile systems and UMTS for 3G mobile systems. Table 2.1 shows modulation schemes and bandwidth efficiency of the reviewed mobile systems. Table 2.2 listed types of channel coding schemes that have been applied in the reviewed mobile systems. Finally, Table 2.3 summarizes multiple access schemes as applied in the reviewed systems.

| System | Modulation Scheme | Bandwidth Efficiency |
|---|---|---|
| AMPS | FM (voice data)<br>FSK (control data) | N/A<br>10 kbps / 30 kHz = 0.33 bps/Hz |
| ETACS | FM (voice data)<br>FSK (control data) | N/A<br>8 kbps / 25 kHz = 0.32 bps/Hz |
| GSM | GMSK | 270.83 kbps / 200 kHz = 1.35 bps/Hz |
| D-AMPS (IS-54) | 4-ary $\pi/4$ DQPSK | 48.6 kbps / 30 kHz = 1.62 bps/Hz |
| PDC | 4-ary $\pi/4$ DQPSK | 42 kbps / 25 kHz = 1.68 bps/Hz |
| CdmaOne | BPSK and QPSK | Spread spectrum modulation |
| UMTS | QPSK | Spread spectrum modulation |

Table 2.1: Modulation schemes and bandwidth efficiency of cellular systems.

| System | Error Control Code |
|---|---|
| AMPS and ETACS | BCH Code |
| GSM | CRC, Convolutional Code (r=1/2, K=5) and FIRE Code |
| D-AMPS (IS-54) | CRC and Conv. Code (r=1/2,K=6) |
| PDC | CRC and Conv. Code (r=9/17,K=5) |
| CdmaOne (IS-95) | CRC and Conv. Code (r=1/2(downlink) ,r=1/3 (uplink),K=5) |
| UMTS | CRC, Convolutional Code and Turbo Coding |

Table 2.2: Error Control Coding schemes of cellular systems. K = length of the convolutional codes memory.

| System | Multiple access scheme |
|---|---|
| AMPS and ETACS | FDMA |
| GSM | TDMA |
| D-AMPS (IS-54) and PDC | TDMA |
| CdmaOne (IS-95) | CDMA |
| UMTS | W-CDMA-FDD |

Table 2.3: Multiple access schemes of cellular systems

# Chapter 3

# Analysis of AWGN and Rayleigh Fading Channel Capacities

## 3.1 Communication Channel Models

In digital communication system research and design, the communication channel is one of important basic components that needs to be taken into consideration. This is because the communication channel is the factor that mainly influences the performance of communication systems. The channel has its own properties and distortion characteristics which corrupt the transmitted signal. At a certain level of corruption, the transmitted signal cannot be recovered at the receiver and error is considered to have occurred. The most common channel related effect usually considered in any digital communication system is that of white noise. If wireless communication system is considered, another additional common effect that needs to be considered is known as the multipath fading effect.

In order to consider an effect of a communication channel in theoretical study, effects and properties of the channel are mathematically modelled. Those channel models mathematically corrupt the signal by simulating characteristics and behaviour of actual communication channels. Three types of channel models are described in this chapter: the Binary Symmetric Channel (BSC), the Additive White Gaussian Noise Channel (AWGN) and the Rayleigh Multipath Fading Channel.

### 3.1.1 Binary Symmetric Channel (BSC)

The Binary Symmetric Channel (BSC) is a very simple communication channel model. The properties of the BSC are a set of binary channel input symbols $X = \{0, 1\}$, a set of binary channel output symbols $Y = \{0, 1\}$ and sets of conditional probabilities $\{p, (1-p)\}$ which are also known as the transition probabilities of a channel symbol.

$$P(0|1) = P(1|0) = p \text{ and } P(1|1) = P(0|0) = (1-p) \tag{3.1}$$

$p$ is the probability of a transmitted symbol being received and demodulated as an error, while, $(1-p)$ is the probability of a transmitted symbol being received and demodulated correctly. Since the BSC is a symmetric channel, transition probabilities of each channel symbols are symmetrical. Figure 3.1 shows the BSC as described above.

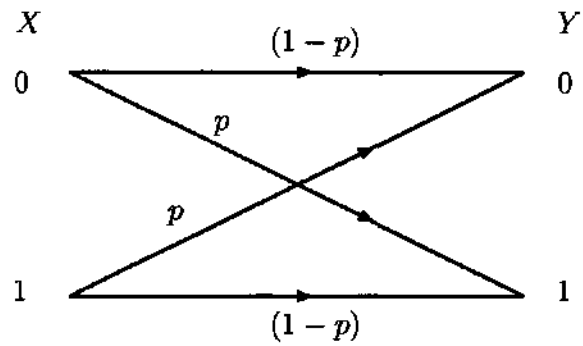


Figure 3.1: the Binary Symmetric Channel.

The BSC is considered as a hard decision channel model. The BSC satisfies the characteristic of a hard decision channel since both input symbol set and output symbol set, are sets of the same symbols. Output symbols of a hard decision channel are considered as the output of hard decision quantisation of the demodulator output at the receiver.

### 3.1.2 Additive White Gaussian Noise Channel

The Additive White Gaussian Noise (AWGN) Channel is commonly used to model the thermal noise phenomenon. Thermal noise is a very common source of performance degradation of communication systems. This thermal noise energy is generated by electronic circuits and components of physical communication devices, especially at the receiver side. Noise energy corrupts the signal additively. Mathematically, the AWGN channel is modelled as shown in Figure 3.2.

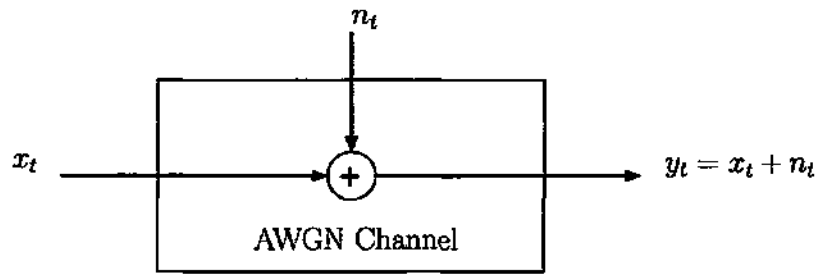


Figure 3.2: the Additive White Gaussian Noise Channel.

As shown in Figure 3.2, assume $t$ is an instantaneous time of signal transmission, the thermal noise value is denoted as $n_t$, the input signal value is denoted as $x_t$ and the received signal value after thermal noise corruption is denoted as $y_t$.

The thermal noise value $n_t$ is a random value and it is independent of $x_t$. The random value of $n_t$ is characterised by its probability density function (p.d.f) that follows the Gaussian Distribution as given in (3.2) with mean, $\mu = 0$ and variance, $\sigma^2 = \frac{N_0}{2}$. $\frac{N_0}{2}$ is the thermal noise power spectral density over all frequencies in frequency domain.

$$\text{pdf}(n_t) = \frac{1}{\sqrt{2\pi\sigma^2}} \exp - \frac{(n_t - \mu)^2}{2\sigma^2} \tag{3.2}$$

$y_t$ is the sum of $x_t$ and random value $n_t$. Thus, $y_t$ is also a random variable which follows the Gaussian distribution with the same variance as the distribution of $n_t$, but its mean value is $\mu = x_t$ instead of zero. The conditional probability of a signal $x_t$ transmitted over the AWGN channel and received as $y_t$ is given as (3.3) below,

$$p\left(y_t|x_t\right) = \frac{1}{\sqrt{2\pi\sigma^2}} \exp - \frac{(y_t - x_t)^2}{2\sigma^2} \tag{3.3}$$

The AWGN channel is considered as a soft decision channel. This is because the AWGN channel is characterised by a different set of channel input symbols and channel output symbols. As shown by Figure 3.3, the values of received signal $y_t$, which is considered as channel output symbols are from a set of continuous symbols within the range $(-\infty ... +\infty)$. The value of $x_t$ is usually from a discrete input symbol set, depending on the type of modulation used. As an example, consider antipodal BPSK modulation to be applied which maps binary channel bits 0 and 1 to -1 and +1 respectively. Therefore, set of channel input symbols consists of {-1,1}.

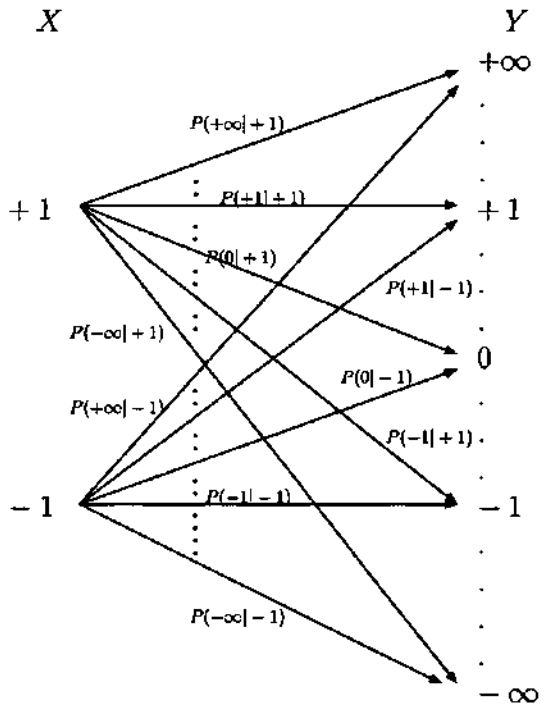


Figure 3.3: The Additive White Gaussian Noise Channel as a Soft Decision Channel.

### 3.1.3 Rayleigh Flat-Fading Channel

Besides the noise effect that commonly corrupts transmitted signals in communication systems, the fading effect is also recognised as one of signal impairments which occurs, especially in wireless transmission communication systems. Since wireless transmission is a non-guided transmission medium, unlike a cable transmission line, a signal is radiated at various angles from the transmitter antenna thus generates multiple path propagation of signal components that travel over different paths from transmitter to receiver. These multiple path signals are called multipath signal components.

Due to the different transmission paths, these multipath signal components are characterised by different time delay, phase shift, frequency shift and amplitude values by the time these signals are detected by the receiver. Based on these parameters, several categories of fading channels are defined such as Frequency Selective or Frequency Flat Fading, Slow or Fast Fading. For a Flat-Fading type of channel, this is defined by the time-delay spread of multipath components being less than channel symbol period from time-domain viewpoint. In the frequency domain, flat fading it is defined by the channel coherent bandwidth being higher than the channel symbol bandwidth [Sklar, 2001, Proakis, 1995].

A mathematical model of signal transmission over a small scale flat-fading channel is

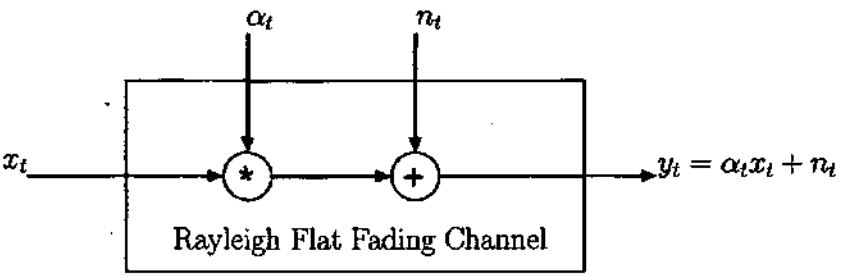


Figure 3.4: the Rayleigh Flat Fading Channel

given by (3.4) and shown in Figure 3.4. At time instant $t$, $x_t$ is the transmitted signal value, $\alpha_t$ is the fading gain, $n_t$ is the AWGN gain and $y_t$ is the received signal value.

$$y_t = \alpha_t x_t + n_t \tag{3.4}$$

where $\alpha_t$ is a random value.

Suppose that none of multipath signal components received are line-of-sight, the pdf of the $\alpha_t$ distribution is said to follow the Rayleigh pdf. The Rayleigh pdf is given as [Proakis, 1995].

$$\text{pdf}(\alpha_t) = \frac{\alpha_t}{\sigma^2} \exp\left(-\frac{\alpha_t^2}{2\sigma^2}\right), \ \alpha_t \geq 0 \tag{3.5}$$

where $\alpha_t = \sqrt{c_{1t}^2 + c_{2t}^2}$.

$c_1$ and $c_2$ are independent Gaussian random variables each from an independent Gaussian generator. Each Gaussian generator follows a $N\left(0, \sigma^2\right)$ distribution, which means a Gaussian/Normal random distribution with mean = 0 and variance = $\sigma^2$.

### Rayleigh Fading Power Distribution

The AWGN channel is a non-fading channel. This means that the mean of the received SNR per bit is time invariant or in other words, it is constant over time. It is different when compared to a Rayleigh Fading channel. Since the Rayleigh Fading channel is a time-variant fading channel. This means that in every bit period the transmitted signal is assumed to be faded or attenuated by a random value of fading power. If the random fading gain at time instant $t$ is given as $\alpha_t$, the fading power at time instant $t$ is denoted as $\alpha_t^2$. Suppose that pdf of the random variable $\alpha_t$ is following the Rayleigh distribution as given by (3.5) with a certain value of $\sigma^2$: with the same value of $\sigma^2$, the pdf of $\alpha^2$ is

given by the Chi-Square distribution with two degrees of freedom [Proakis, 1995]:

$$\text{pdf}(\alpha^2) = \frac{1}{2\sigma^2} \exp\left(-\frac{\alpha^2}{2\sigma^2}\right), \ \alpha^2 \geq 0 \tag{3.6}$$

where $2\sigma^2 = E(\alpha^2)$, is the mean of the $\alpha^2$ distribution.

Suppose that the mean of SNR per channel bit of a non-fading channel $E_c/N_0$ and the fading power at instantaneous time $t$, $\alpha_t^2$ are known, the instantaneous received SNR per channel bit at time $t$ for a channel subject to fading is then given as,

$$\gamma_t = \frac{E_c}{N_0}\alpha_t^2. \tag{3.7}$$

The average of received SNR, $\bar{\gamma}$, is given as

$$\bar{\gamma} = \frac{E_c}{N_0}E(\alpha^2) \tag{3.8}$$

The pdf of $\gamma_t$ also follows the distribution of Chi Square with two degrees of freedom:

$$\text{pdf}(\gamma_t) = \frac{1}{\bar{\gamma}} \exp\left(-\frac{\gamma_t}{\bar{\gamma}}\right) \tag{3.9}$$

## 3.2 Capacity of Binary Input AWGN and Rayleigh Fading channels with Hard Decision Decoding

In [Cover and Thomas, 1991], the capacity of a channel is the maximum average mutual information between the input symbols and output symbols of the channel. Assuming that $X$ and $Y$ are discrete input symbol set and discrete output symbol sets respectively, therefore the average mutual information of such channel is given as

$$\begin{aligned} C &= I(X;Y) \\ &= \sum_{x\in X}\sum_{y\in Y} p(x,y)\log_a\left(\frac{p(y|x)}{p(y)}\right) \end{aligned} \tag{3.10}$$

where $p(x,y) = p(x)p(y|x)$ is the joint probability of input symbol $x$ and output symbol $y$, $p(y|x)$ is the conditional probability of having $y$ when given $x$ and $p(x)$ is the probability of symbol $x$. In modelling communication channel, the conditional probability is also known as the transitional probability which is defined as the probability of receiving $y$ symbol when $x$ symbol is transmitted.

For the Hard Decision decoding case, the BSC is used since it is a special channel model that represents a channel with binary input and binary output; thus it describes a binary channel with a hard decision decoding method. As shown in Figure 3.1, input and output symbol sets of the channel consists of two channel equally probable symbols of 0 and 1. Thus

$$X = Y = \{0, 1\}$$

and probability of each symbol is

$$p(x=0) = p(x=1) = \frac{1}{2} \quad \text{and} \quad p(y=0) = p(y=1) = \frac{1}{2}$$

The transitional probability of receiving output symbol being different to transmitted symbol, $p(y=1|x=0) = p(y=0|x=1) = p$, and the transitional probability of receiving output symbol being the same as transmitted symbol, $p(y=1|x=0) = p(y=0|x=1) = (1-p)$. If these values are substituted into (3.10), therefore, the capacity of the BSC channel is found as

$$\begin{aligned}
C(p) &= \sum_{x\in X}\sum_{y\in Y} p(x,y)\log_a\left(\frac{p(y|x)}{p(y)}\right) \\
&= \sum_{x=0}^{1}\sum_{y=0}^{1} p(x)p(y|x)\log_a\left(\frac{p(y|x)}{p(y)}\right) \\
&= p(x=0)p(y=0|x=0)\log_a\left(\frac{p(y=0|x=0)}{p(y=0)}\right) \\
&\quad + p(x=0)p(y=1|x=0)\log_a\left(\frac{p(y=1|x=0)}{p(y=1)}\right) \\
&\quad + p(x=1)p(y=0|x=1)\log_a\left(\frac{p(y=0|x=1)}{p(y=0)}\right) \\
&\quad + p(x=1)p(y=1|x=1)\log_a\left(\frac{p(y=1|x=1)}{p(y=1)}\right) \\
&= 1 + p\,\log_a(p) + (1-p)\,\log_a(1-p)
\end{aligned} \tag{3.11}$$

The unit of channel capacity is nats per channel symbol if $a = e$. Alternatively, if $a = 2$,

the unit of channel capacity is bits per channel symbol.

In the case of an uncoded system with binary antipodal BPSK signaling over the AWGN channel, the average probability of a channel bit in error is given as [Proakis, 1995],

$$P_n(E_c/N_0) = \frac{1}{2}\,\mathrm{erfc}\left(\sqrt{\frac{E_c}{N_0}}\right) \tag{3.12}$$

where $\frac{E_c}{N_0}$ is the SNR per channel bit.

The capacity of the AWGN BSC channel can be calculated by inserting (3.12) into (3.11) as shown below:

$$\begin{aligned} C_{Hard}(E_c/N_0) &= 1 - H(P_n) \\ &= 1 - [-P_n \log_a(P_n) - (1-P_n)\log_a(1-P_n)] \\ &= 1 + P_n \log_a(P_n) + (1-P_n)\log_a(1-P_n) \\ &= 1 + \frac{1}{2}\,\mathrm{erfc}\left(\sqrt{\frac{E_c}{N_0}}\right) \log_a\left(\frac{1}{2}\,\mathrm{erfc}\left(\sqrt{\frac{E_c}{N_0}}\right)\right) + \\ &\quad \left(1 - \frac{1}{2}\,\mathrm{erfc}\left(\sqrt{\frac{E_c}{N_0}}\right)\right) \log_a\left(1 - \frac{1}{2}\,\mathrm{erfc}\left(\sqrt{\frac{E_c}{N_0}}\right)\right) \end{aligned} \tag{3.13}$$

For the case of a time-variant channel, such as Rayleigh fading channel which has variate mean of received SNR at the receiver, (3.11) could be used with the $p$ value in the equation to represent average channel bit error probability of a Rayleigh Fading channel. In [Proakis, 2000], the average channel bit error probability of a time-variant Rayleigh fading channel was derived by integrating (3.12) with the pdf of received SNR per channel bit of Rayleigh Fading channel, which is given by (3.9). The average probability of channel

bit in error for a time-variant Rayleigh fading channel with binary antipodal signaling is:

$$\begin{aligned}
P_r(\bar{\gamma}) &= \int_0^{\infty} P_n(\gamma_t)\ \mathrm{pdf}(\gamma_t)\ d\gamma_t \\
&= \int_0^{\infty} \frac{1}{2}\mathrm{erfc}\left(\sqrt{\gamma_t}\right)\ \frac{1}{\bar{\gamma}} \exp\left(\frac{-\gamma_t}{\bar{\gamma}}\right)\ d\gamma_t \\
&= \frac{1}{2}\int_0^{\infty} \mathrm{erfc}\left(\sqrt{\gamma_t}\right)\ \frac{1}{\bar{\gamma}} \exp\left(\frac{-\gamma_t}{\bar{\gamma}}\right)\ d\gamma_t \\
&= \frac{1}{2}\left[\frac{\left(-\frac{\bar{\gamma}\sqrt{\bar{\gamma}+\bar{\gamma}^2}\ \mathrm{erf}\left(\frac{1+\bar{\gamma}\sqrt{\gamma_t}}{\sqrt{\bar{\gamma}+\bar{\gamma}^2}}\right)}{1+\bar{\gamma}} - \bar{\gamma}\exp^{\frac{-\gamma_t}{\bar{\gamma}}}\ \mathrm{erfc}\left(\sqrt{\gamma_t}\right)\right)}{\bar{\gamma}}\right]_0^{\infty} \\
&= -\frac{1}{2}\left(\sqrt{\frac{\bar{\gamma}}{1+\bar{\gamma}}}\right) - \frac{1}{2}\left(\frac{-\bar{\gamma}}{\bar{\gamma}}\right) \\
&= \frac{1}{2}\left(1 - \sqrt{\frac{\bar{\gamma}}{1+\bar{\gamma}}}\right).
\end{aligned} \tag{3.14}$$

The channel capacity of a hard decision channel, (3.11), is a function of error bit probability and probability of error bit for a Rayleigh fading channel as given in (3.14); therefore, the channel capacity of Rayleigh fading with hard decision decoding as a function of average of SNR,$\bar{\gamma}$, is given as

$$\begin{aligned}
C_{Fading}(\bar{\gamma}) &= C(P_r) \\
&= 1 - [-P_r\ \log_a(P_r) - (1-P_r)\ \log_a(1-P_r)] \\
&= 1 + P_r\ \log_a(P_r) + (1-P_r)\ \log_a(1-P_r) \\
&= 1 + \frac{1}{2}\left(1 - \sqrt{\frac{\bar{\gamma}}{1+\bar{\gamma}}}\right)\ \log_a\left(\frac{1}{2}\left(1 - \sqrt{\frac{\bar{\gamma}}{1+\bar{\gamma}}}\right)\right) + \\
&\quad \left(1 - \frac{1}{2}\left(1 - \sqrt{\frac{\bar{\gamma}}{1+\bar{\gamma}}}\right)\right)\ \log_a\left(1 - \frac{1}{2}\left(1 - \sqrt{\frac{\bar{\gamma}}{1+\bar{\gamma}}}\right)\right)
\end{aligned} \tag{3.15}$$

In order to plot $C_{Hard}$ and $C_{Fading}$ on the same axis as in Figure 3.7, $C_{Fading}$ is substituted into a function of $E_c/N_0$ by assuming $E(\alpha^2) = 1$. Thus,

$$\begin{aligned}
C_{Fading}\left(\frac{E_c}{N_0}\right) &= 1 + \frac{1}{2}\left(1 - \sqrt{\frac{\frac{E_c}{N_0}}{1+\frac{E_c}{N_0}}}\right)\ \log_a\left(\frac{1}{2}\left(1 - \sqrt{\frac{\frac{E_c}{N_0}}{1+\frac{E_c}{N_0}}}\right)\right) + \\
&\quad \left(1 - \frac{1}{2}\left(1 - \sqrt{\frac{\frac{E_c}{N_0}}{1+\frac{E_c}{N_0}}}\right)\right)\ \log_a\left(1 - \frac{1}{2}\left(1 - \sqrt{\frac{\frac{E_c}{N_0}}{1+\frac{E_c}{N_0}}}\right)\right)
\end{aligned} \tag{3.16}$$

(3.13) and (3.16) may be used to calculate the capacity of the hard decision AWGN and Rayleigh fading channel for binary orthogonal signaling system with $P_n$ value in regard to the binary orthogonal signaling. The average probability of a channel bit in error for the binary orthogonal signalling is given as

$$P_n(E_c/N_0) = \frac{1}{2}\,\mathrm{erfc}\left(\sqrt{\frac{E_c}{2N_0}}\right) \tag{3.17}$$

Figure 3.5 and Figure 3.6 show the channel capacity comparison between binary antipodal and binary orthogonal signaling over a hard decision AWGN and a hard decision Rayleigh fading channel respectively.

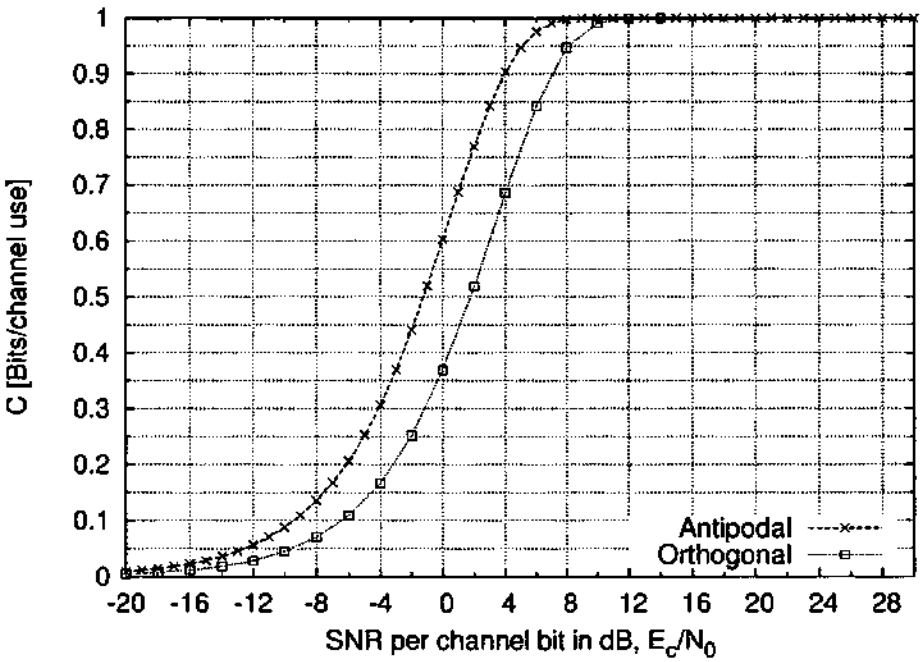


Figure 3.5: Channel capacity of AWGN channel with binary antipodal and binary orthogonal signalling

## 3.3 Capacity of Binary Input AWGN channel with Soft Decision Decoding

In contrast to a hard decision channel model, the number of output symbols is higher than number of input symbols in a soft decision channel. A set of channel output symbols may be defined as a range of continuous values. Suppose that the input of the channel is a discrete symbol set consisting of $q$ symbols, and the channel output symbol is defined

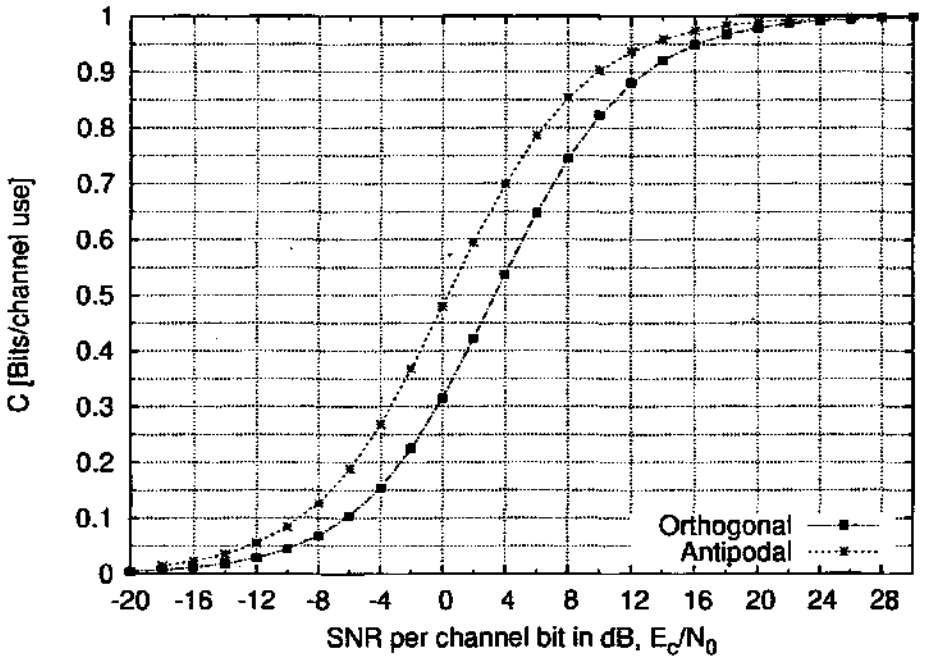


Figure 3.6: Channel capacity of Rayleigh channel with binary antipodal and binary orthogonal signalling

as a continuous range between $\infty$ and $-\infty$. The capacity of such a channel in bits per channel use is the maximum average mutual information between the discrete input $X = \{x_0, x_1, \ldots, x_{q-1}\}$ and the output $Y = [\infty, -\infty]$ and is given in [Proakis, 2000] as :

$$C = \max_{P(x_i)} \sum_{i=0}^{q-1} \int_{-\infty}^{\infty} p(y|x_i)p(x_i) \log_2 \frac{p(y|x_i)}{p(y)} dy \tag{3.18}$$

where $p(y|x_i)$ is the conditional probability of getting an output symbol $y$ when the input symbol is $x_i$, and

$$p(y) = \sum_{k=0}^{q-1} p(y|x_k)p(x_k). \tag{3.19}$$

Suppose that the input of a binary input channel is from a discrete symbol set consisting of $X = \{1, -1\}$; therefore $p(X = 1) = p(X = -1) = 1/2$. The channel output is a continuous symbol set which is defined as a range of values, $Y = \{-\infty, \ldots, \infty\}$. Therefore, the capacity of a binary input AWGN channel with soft decision decoding is given as,

$$C_{Soft} = \frac{1}{2} \int_{-\infty}^{\infty} p(y|X = 1) \log_2 \frac{p(y|X = 1)}{p(y)} dy + \frac{1}{2} \int_{-\infty}^{\infty} p(y|X = -1) \log_2 \frac{p(y|X = -1)}{p(y)} dy \tag{3.20}$$

where the pdf of $p(y|X)$ follows the Gaussian distribution and it is given by (3.3).

In order to visually show the differences between (3.13), (3.15) and (3.20), each equation is numerically solved and plotted for $-20$ dB $\leq \frac{E_c}{N_0} \leq 30$ dB. Figure 3.7 shows curves of hard and soft decision binary input AWGN channel capacities and hard decision Rayleigh fading channel capacity.

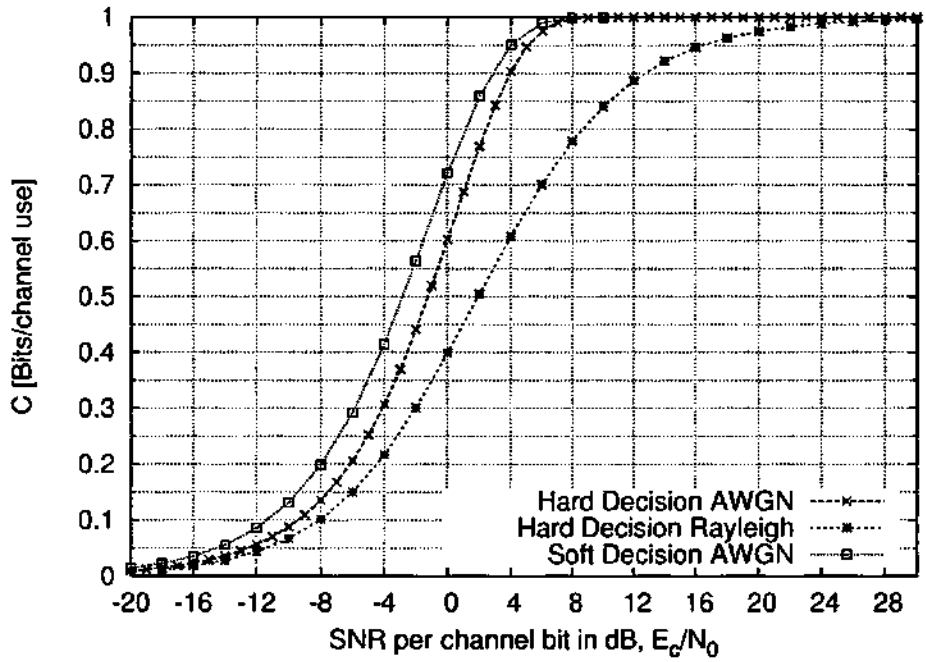


Figure 3.7: AWGN and Rayleigh fading channel capacities for antipodal BPSK signalling

## 3.4 Power Loss due to Hard Decision Decoding

As shown in Figure 3.7, the capacity of AWGN channel is affected by the type of decoding scheme applied in the system. The capacity of an AWGN channel with a soft decoding scheme is higher than the capacity of a AWGN channel with hard decision decoding over a certain range of $E_c/N_0$. In other words, more power is required if hard decision decoding is applied to achieve the same channel capacity as a system with soft decision decoding. This additional power that is required by hard decision decoding to achieve the same capacity as soft decision decoding at a given mean $E_c/N_0$ is defined as power loss due to hard decision decoding.

Given a certain value of capacity, $A_{Soft}$ and $A_{Hard}$ are respective required values of $E_c/N_0$ in (3.20) and (3.13) to achieve the capacity. Therefore, the power loss due to hard

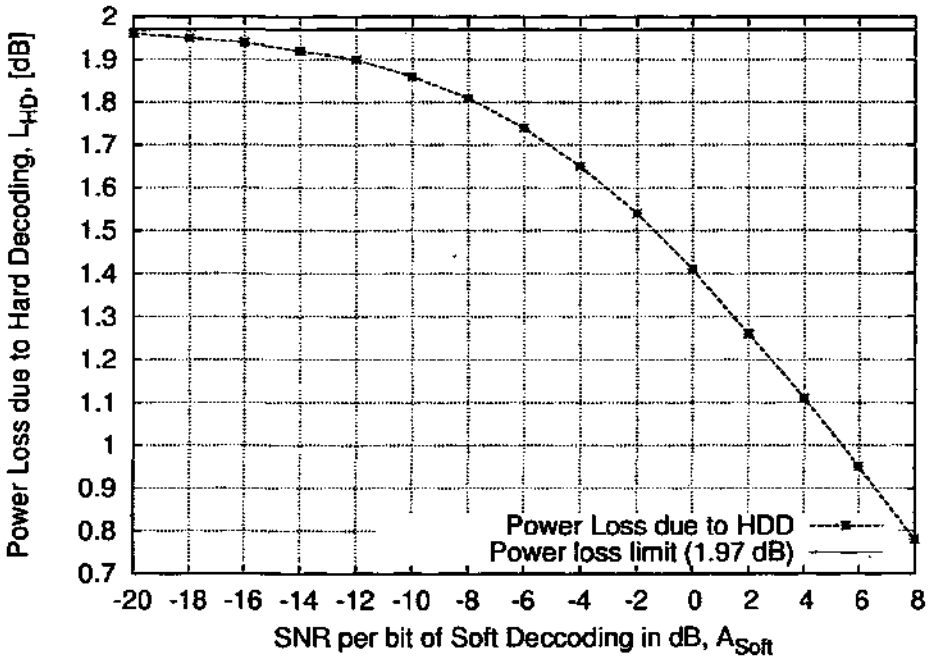


Figure 3.8: Power Loss due to Hard Decision Decoding over AWGN channel

decision decoding, $L_{HD}$, is defined as

$$L_{HD} = A_{Hard} - A_{Soft} \tag{3.21}$$

In order to reveal the curve of loss due to hard decision decoding for the case of the AWGN channel, $L_{HD}$ is plotted against $A_{Soft}$ as shown in Figure 3.8. In [Proakis, 2000], it is mentioned that the limit of power loss due to a hard decision decoding scheme is $\approx$ 1.97 dB as the capacity is approaching zero for case of an AWGN channel. With the limit of soft decision decoding gain equal $\approx$ 1.97 dB at very low $E_c/N_0$, soft decision decoding gain is about 1.9 dB, 1.4 dB and 0.78 dB at $E_c/N_0$ equal to -12 dB, 0 dB and 8 dB respectively. From the results it is concluded that soft decision decoding implementation is certainly useful if the $E_c/N_0$ is in a low region. In a much higher $E_c/N_0$ region, performance of hard decision decoding is believed to be as good as soft decision decoding. At such stage, hard decision decoding is preferable in practice since hard decision decoding complexity is less than soft decision decoding.

## 3.5 Power Loss due to Fading

As shown in Figure 3.7, it is obvious that the fading phenomenon limits the capacity of the wireless channel. Consequently, more power is required to achieve the same capacity as can be achieved over an AWGN channel. This extra power requirement is considered as power loss due to fading effects. In this analysis, power loss due to fading is considered for the case of hard decision decoding.

Given a certain value of capacity, $A_{Fading}$ and $A_{Hard}$ are respective required values of $E_c/N_0$ in (3.15) and (3.13) to achieve the capacity. Therefore, power loss due to the fading effect is defined as

$$L_{Fading} = A_{Fading} - A_{Hard} \tag{3.22}$$

A graph of $L_{Fading}$ against $A_{Hard}$ is plotted and shown in Figure 3.9.

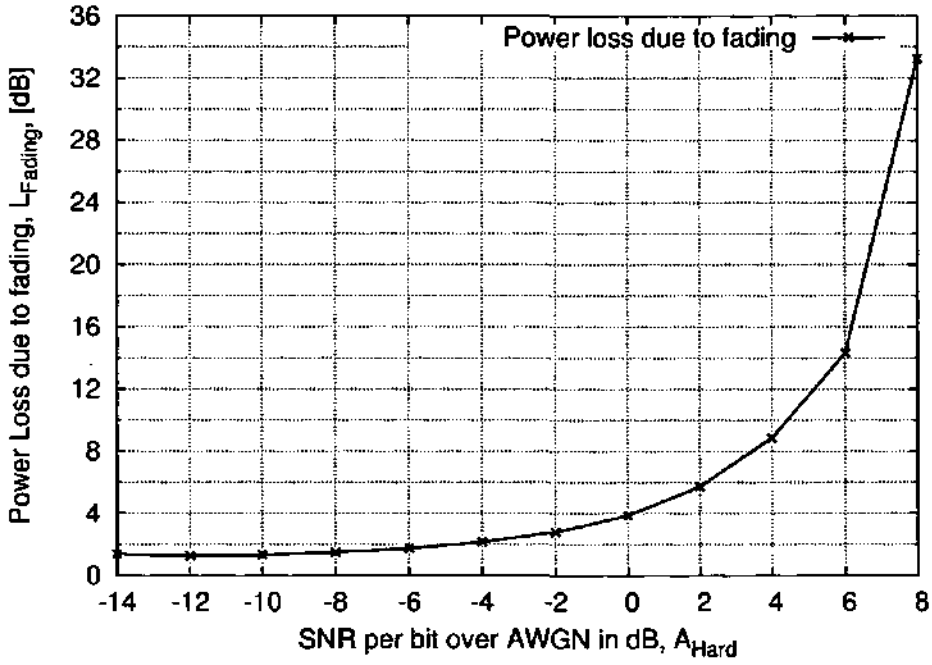


Figure 3.9: Power Loss due to Fading over Hard Decision BSC channel

As shown in Figure 3.9, power loss due to fading increases exponentially as SNR per bit increases. At $A_{Hard}$ equal to -14 dB, 0 dB and 8 dB, it is found that the power loss due to fading is about 1.4 dB, 3.9 dB and 33.3 dB, respectively.

## 3.6 Summary

The communication channel is an important component to be considered in the design of a good communication system. In theoretical design and analysis of a communication system, the communication channel is usually described by mathematical models. The AWGN channel model is the most common channel model that characterises signal distortion due to thermal noise effects. Secondly, the Rayleigh flat fading channel is channel model that characterises the effect of signal fading due to the multipath phenomenon.

The capacity of a binary antipodal signalling AWGN channel with hard decision and soft decision decoding is compared and the power loss due to the hard decision decoding is found. It is found that the power loss due to hard decision decoding decreases exponentially as $SNR$ increases. It is concluded that hard decision decoding is going to be as good as soft decision decoding at high $SNR$. At low $SNR$, hard decision decoding is found to perform worse with a limit of loss of 1.97 dB.

The AWGN channel is well known as channel with a non-variant mean whereas the Rayleigh fading channel is a mean varying channel. Therefore, capacity analysis of Rayleigh fading channels was done by combining the well established AWGN capacity formulas and the distribution of the Rayleigh fading power variable. The capacity of Rayleigh flat fading channel is analysed for binary antipodal signaling channel with hard decision decoding. Power loss due to fading over a hard decision channel is also analysed and presented. It is found that the severity of fading effects exponentially increase as $SNR$ increases.

# Chapter 4

# Error Performance Analysis of Linear Block Codes over AWGN and Rayleigh Fading channels

## 4.1 Error Performance Analysis of an Uncoded System over AWGN and Rayleigh Fading Channels

Suppose that no channel coding scheme is applied to a digital communication system. This means each of channel bits transmitted through channel represents an information bit, and the energy per information bit is equal to energy per channel bit, $E_b = E_c$. With known $E_b$, the average probability of an information bit in error for an antipodal BPSK system over an AWGN channel, $P_b$, can be calculated using (3.12). Since, $E_b = E_c$, therefore, average probability of channel bit in error, $P_c$, is equal to average probability of information bit in error, $P_b$.

$$P_c = P_b = \frac{1}{2}\text{erfc}\left(\sqrt{\frac{E_b}{N_0}}\right) \tag{4.1}$$

For the case of a time-variant channel such as Rayleigh fading, the average error probability of an information bit of system with a antipodal BPSK modulation is given by (3.14). Since, $E_c = E_b$ for an uncoded system, the channel bit error probability over a Rayleigh fading channel with known mean of received SNR per channel bit, $E_c/N_0$ is

given as,

$$P_c\left(\frac{E_c}{N_0}\right) = P_b\left(\frac{E_b}{N_0}\right) = \frac{1}{2}\left(1 - \sqrt{\frac{\frac{E_c}{N_0}}{1+\frac{E_c}{N_0}}}\right) = \frac{1}{2}\left(1 - \sqrt{\frac{\frac{E_b}{N_0}}{1+\frac{E_b}{N_0}}}\right) \tag{4.2}$$

Using the Binomial Series, (4.2) can be simplified to an approximation. For $E_b/N_0 \gg 0$, an approximation of average error probability of information bit is found to be,

$$P_b\left(\frac{E_b}{N_0}\right) \approx \frac{1}{4\frac{E_b}{N_0}} \tag{4.3}$$

Derivation of this approximation is given in Appendix A.

For comparison of uncoded system error performance over AWGN and Rayleigh fading channels, (4.1), (4.2) and its approximation (4.3) are plotted together in Figure 4.1. The X-axis is the SNR per information bit in dB units, while the Y-axis is the information bit error probability. It is obvious that the error performance is much better over the AWGN channel as compared to the Rayleigh Fading channel. The additional power required by the system to achieve the same error rate as over the AWGN channel appears to be inversely proportional as the error rate is reduced. For example, in order to achieve $P_b = 10^{-2}$, approximately 10 dB more SNR per bit is required by the system for transmission over Rayleigh Fading channel. If the expected error level is reduced to $P_b = 10^{-3}$, it is shown that approximately 17 dB more SNR per bit is needed.

The error performance curves of Rayleigh Fading and its approximation seem to converge at $E_b/N_0 \geq 14$ dB. At $E_b/N_0 \gg 0$, it is seen that the error probability linearly decreases as power increases. For every 10 dB power incrementation, the error probability of a channel bit approximately decreases by $10^{-1}$.

From this performance comparison, it could be said that the fading effect is more severe than the effect of thermal noise for wireless digital communication systems.

## 4.2 Error Performance of Linear Block Codes over an AWGN channel

For the coded system case, suppose that a system is using an $(n, k, d_{min})$ code as its error control coding encoder, $k$ is the number of information bits being fed into the encoder,

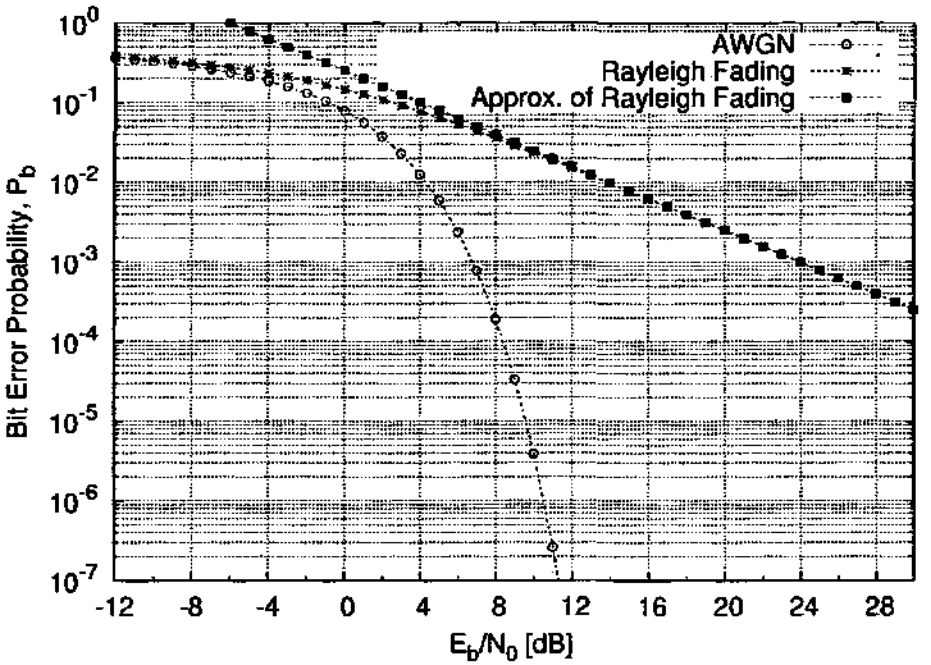


Figure 4.1: Bit error probability of uncoded BPSK system over AWGN and Rayleigh Fading channels

$n$ = length of a codeword generated by the encoder and $d_{min}$ is the minimum Hamming distance of the code; hence, the code rate of the encoder is $R = k/n$.

When channel coding is applied, the energy per channel bit, also known as the energy per coded bit, $E_c$, is no longer the same as the energy per information bit, $E_b$. The relation between $E_b$ and $E_c$ for a coded system is given as:

$$E_c = E_b R = E_b \frac{k}{n} \tag{4.4}$$

For a fair error performance comparison with the uncoded system analyzed in Section 4.1, the same BPSK signaling, channel bandwidth and noise power are applied. For the time-invariant AWGN channel case, the average probability of error of a coded bit is equal to :

$$P_c = \frac{1}{2}\text{erfc}\left(\sqrt{\frac{E_c}{N_0}}\right) = \frac{1}{2}\text{erfc}\left(\sqrt{\frac{E_b}{N_0}R}\right) \tag{4.5}$$

One of the properties of a block code is that it has maximum number of errors in a codeword that can be corrected, which is denoted as $t$. The $t$ of a block code can be

calculated when the $d_{min}$ of the code is known where

$$t = \lfloor (d_{min} - 1)/2 \rfloor \tag{4.6}$$

With a known maximum number of correctable errors $t$, codeword length $n$ and channel bit error probability $P_c = p$, the codeword error probability of a block code, which is denoted as $P_M$, can be calculated using [Proakis, 1995]:

$$P_M \leq \sum_{m=t+1}^{n} \binom{n}{m} p^m \ (1-p)^{n-m} \tag{4.7}$$

(4.7) is applicable if hard decision decoding is applied at the receiver. This bound is known as an exact bound for perfect codes, whereby the equality case is achieved. If a code is not a perfect code, then this bound represents an upper bound of codeword error probability which satisfies the inequality case.

Another upper bound which is looser than (4.7) is known as Union Bound which is given as [Proakis, 2000],

$$P_M \leq (M-1) \sum_{m=\lfloor d_{min}/2 \rfloor + 1}^{d_{min}} \binom{d_{min}}{m} p^m \ (1-p)^{d_{min}-m} \tag{4.8}$$

where $d_{min}$ is the Minimum Hamming distance of the code and $M = 2^k$ is the number of codewords of the code.

If soft decision decoding is applied at the receiver, decoder output should to be the codeword that has the minimum Euclidean distance between it and the received signal. The probability of codeword error between two codewords is also influenced by the Hamming distance between the transmitted codeword and decoded codeword. For example in the case of a linear block code, it is assumed that all-zeroes codeword, denoted as $c_1$, is transmitted, and the $m$-th codeword, which is denoted as $c_m$, being decided as the most likely transmitted codeword at the receiver. The Hamming distance between the $c_1$ codeword and an $c_m$ codeword is denoted as

$$d(c_1, c_m) = w_m$$

where $w_m$ is the Hamming weight of the $m$-th codeword and $m = 2, \ldots, M$ since the

all-zeroes codeword is excluded from the set of possible received codeword.

The probability of the all-zeroes codeword, $c_1$, being wrongly decoded to a non-all-zeroes codeword, $c_m$, is denoted as $P_2$, and written as a function of $w_m$, is given as [Proakis, 2000],

$$P_2(c_1, c_m) = Q\left(\sqrt{2\frac{E_b}{N_0}w_m R}\right) \tag{4.9}$$

where $R$ is the code rate and $Q(.)$ is area under the tail of the Gaussian PDF which is given as

$$Q(x) = \frac{1}{2}\text{erfc}\left(\frac{x}{\sqrt{2}}\right) \tag{4.10}$$

Suppose that the Hamming weights of all $M$ codewords are known: therefore, $P_M$ is upper bounded as [Proakis, 2000]

$$P_M \leq \sum_{m=2}^{M} Q\left(\sqrt{2\frac{E_b}{N_0}w_m R}\right). \tag{4.11}$$

If only the weight distribution of a code is known, then (4.11) is modified to give

$$P_M \leq \sum_{w=d_{min}}^{n} f(w)\ Q\left(\sqrt{2\frac{E_b}{N_0}wR}\right) \tag{4.12}$$

where $f(w)$ is the frequency of codewords with Hamming weight $= w$.

If the minimum Hamming weight of the code is known, $d_{min}$, a looser upper bound could be used in order to estimate the codeword error probability of a code. The bound is given as

$$P_M \leq (M-1)\ Q\left(\sqrt{2\frac{E_b}{N_0}d_{min}R}\right) \tag{4.13}$$

The error performance of several well-known block codes is compared over the AWGN channel. As shown in Figure 4.2 and Figure 4.3, the three block codes that have been chosen for comparison are Repetition (3, 1, 3), Extended Golay (24, 12, 8) and Extended BCH (128, 64, 22) codes. As a comparison benchmark between the uncoded system and the coded system performance, an error curve of an uncoded system is also plotted in both figures.

Figure 4.2 shows error curves of the chosen codes over an AWGN channel with hard

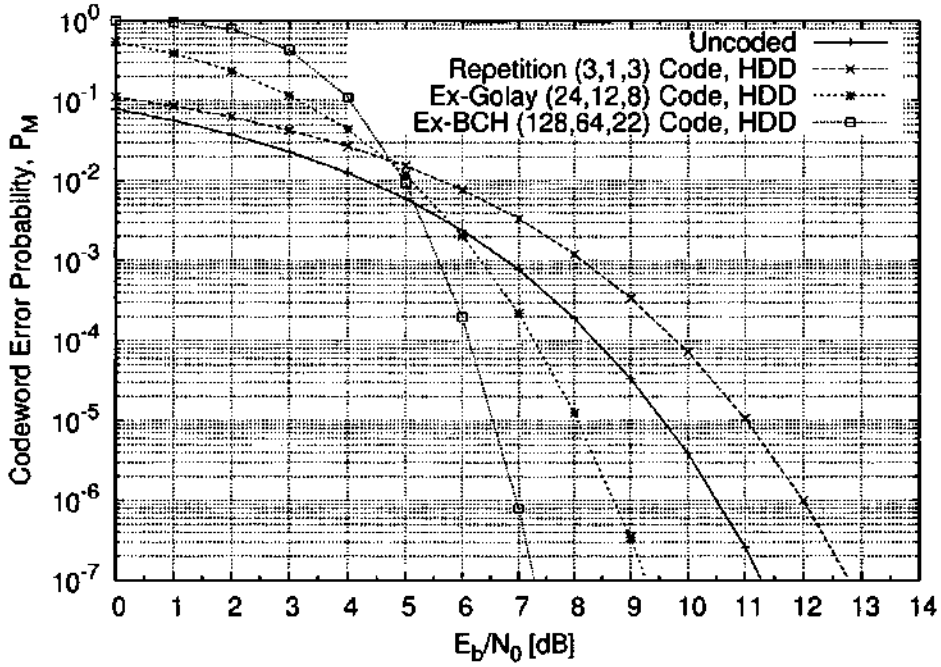


Figure 4.2: Error performance of Extended Golay, Extended BCH and Repetition block codes over AWGN channel with Hard Decision Decoding.

decision decoding. The codeword error probability curves plotted in the figure are from (4.7). For the case of hard decision decoding, as shown in the figure, it is found that the BCH code is the best among the codes. At $P_M = 10^{-5}$, the coding gain of the BCH code is approximately as much as 3 dB. With the Golay code, even though it is not as good as the BCH code, it has achieved almost 1.5 dB coding gain compared to the uncoded system. The opposite result is observed for the case of the Repetition code. It is found that the Repetition code is the worst code used for transmission over the AWGN channel due to its error performance being worse than of the uncoded system.

If the decoder implements soft decision decoding, the error performance of the selected codes is as shown in Figure 4.3. The codeword error probability of the codes is calculated using (4.11). The weight distributions of the Extended Golay(24, 12, 8) code and the Extended BCH(128, 64, 22) are given in Appendix C. Again, the BCH code seems to be the best code since its error performance is better than Golay and Repetition codes. At $P_M = 10^{-5}$, the coding gains of BCH and Golay codes are approximately 6 dB and 3.5 dB respectively. Interestingly, the Repetition code error performance is exactly the same as the uncoded system. This means that the Repetition code does not have any coding gain over AWGN channel with a soft decision decoding scheme.

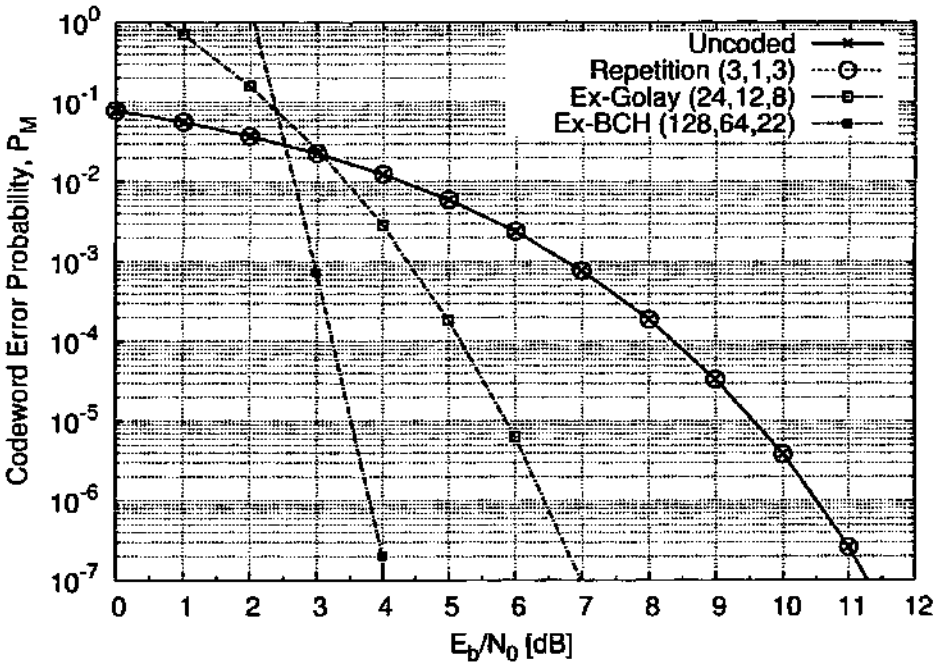


Figure 4.3: Error performance of Extended Golay, Extended BCH and Repetition block codes over AWGN channel with Soft Decision Decoding.

## 4.3 Error Performance of Linear Block Codes over Rayleigh Fading channel

For the case of an uncoded system over a Rayleigh Fading channel, the channel bit error probability is given by (4.2). If channel coding is applied, and the signaling scheme is the antipodal BPSK, then the error probability of a channel bit is given as [Proakis, 1995]:

$$P_{c,R}\left(\frac{E_c}{N_0}\right) = \frac{1}{2}\left(1 - \sqrt{\frac{\frac{E_c}{N_0}}{1+\frac{E_c}{N_0}}}\right) = \frac{1}{2}\left(1 - \sqrt{\frac{\frac{E_b}{N_0}R}{1+\frac{E_b}{N_0}R}}\right) \tag{4.14}$$

where $R = k/n$ is rate of the code, $n$ is codeword length and $k$ is the number of information bits input to the encoder. bookmark

The codeword error probability of a block code over a Rayleigh Fading channel with hard decision decoding can be calculated using the same equation given by (4.7). The only thing that needs to change is the probability of channel bit in error $p$ which is now given by (4.14). The codeword error probability of three block codes over a Rayleigh fading channel with hard decision decoding is plotted in Figure 4.4. The block codes considered are Repetition(3, 1, 3), the Golay(23,12,7) and the BCH(127,64,21) codes.

At $P_M = 10^{-5}$, the BCH code is found to perform better than the other considered

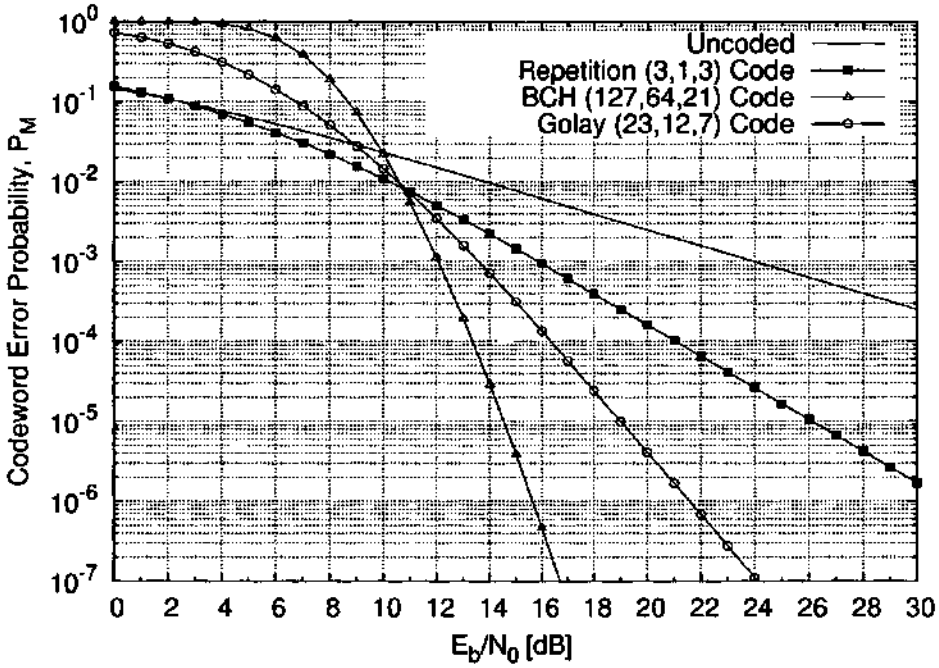


Figure 4.4: Error performances of Golay, BCH and Repetition block codes over Rayleigh Fading channel with Hard Decision Decoding.

codes. The power gain achieved by the BCH code over the Golay and the Repetition code is approximately 4 dB and 11 dB respectively. The Repetition code case is seen to be the worse one. One interesting observation to highlight is that the performance of the Repetition code is better than an uncoded system over a Rayleigh fading channel. The coding gain of the Repetition code is approximately 8 dB at $P_M = 10^{-3}$.

The codeword error probability bounds of a linear block code over soft decision decoding scheme can be calculated using the diversity error performance formula. This is because, channel coding is a kind of time diversity. In [Proakis, 2000], the error probability of transmission with $n$-diversity scheme for binary antipodal PSK system is given as

$$P_2(n) = \left(\frac{1-\mu}{2}\right)^n \sum_{x=0}^{n-1} \binom{n-1+x}{x} \left(\frac{1+\mu}{2}\right)^x \tag{4.15}$$

where $n$ is the order of diversity and $\mu$ is given as,

$$\mu = \sqrt{\frac{\frac{E_c}{N0}}{1+\frac{E_c}{N0}}} = \sqrt{\frac{\frac{E_b}{N0}R}{1+\frac{E_b}{N0}R}} \tag{4.16}$$

The derivation of (4.15) is shown in Appendix B.

To explain the concept of channel coding as a time diversity scheme, the Repetition

code concept in a binary symbol system is taken as an example. In a Repetition code codebook, there are only two codewords available, the all-zeroes codeword denoted as $c_1$ and the all-ones codeword denoted as $c_2$. Assume that Repetition(7,1,7) code is taken as the considered code. An information bit 0 will be encoded into the $c_1$ codeword by replicating the 0 by seven times, and vice versa for generation of the $c_2$ codeword. The energy per codeword bit is $E_c = E_b/7$. Assuming that all-zeroes codeword, $c_1$ is transmitted through a time-variant channel, such as fading channel. Each of seven transmitted codeword bits are subject to independent fading and noise. The transmission of the $c_1$ may also be viewed as the time diversity transmission of order 7. Therefore, the probability of $c_1$ codeword bits being received as $c_2$ codeword bits at the receiver, or equivalently the codeword error probability of the Repetition(7,1,7) code may calculated using (4.15) with $n = 7$.

Note that the relationship between the value of $n$ to use in (4.15), with Hamming distance between all-zeroes codeword and all-ones codeword

$$n = d(c_1, c_2) = 7$$

where $d(c_1, c_2)$ is the Hamming distance between $c_1$ and $c_2$ codewords. This means that the error probability between two codeword is dependent on their Hamming distance.

Other than Repetition code, (n,k,d) linear block codes would have $M = 2^k$ codewords in total, including the all-zeroes codeword, $c_1$. If the all-zeroes codeword is again assumed being the transmitted codeword and it is known that

$$d(c_1, c_m) = w_m$$

where $m = 2, \ldots, M$ , $c_m$ is the $m$-th codeword of the code and $w_m$ is Hamming weight of the $m$-th codeword. Therefore the decoding error probability of the linear block code could be calculated using the weight of other $M - 1$ non-all-zeroes codewords as below [Proakis, 2000]

$$\begin{aligned} P_M &< \sum_{m=2}^{M} P_2(w_m) \\ &< \sum_{m=2}^{M} \left(\frac{1-\mu}{2}\right)^{w_m} \sum_{x=0}^{w_m-1} \binom{w_m - 1 + x}{x} \left(\frac{1+\mu}{2}\right)^{x} \end{aligned} \tag{4.17}$$

If only $d_{min}$ of the code is known, then a looser upper bound than (4.17) could be used, which is given as [Proakis, 2000]:

$$P_M < \sum_{m=2}^{M} P_2(w_m) < (M-1) P_2(d_{min}) < 2^k \binom{2d_{min}-1}{d_{min}} \left( \begin{matrix} 1 \\ 4\frac{E_b}{N_0} R \end{matrix} \right)^{d_{min}} \tag{4.18}$$

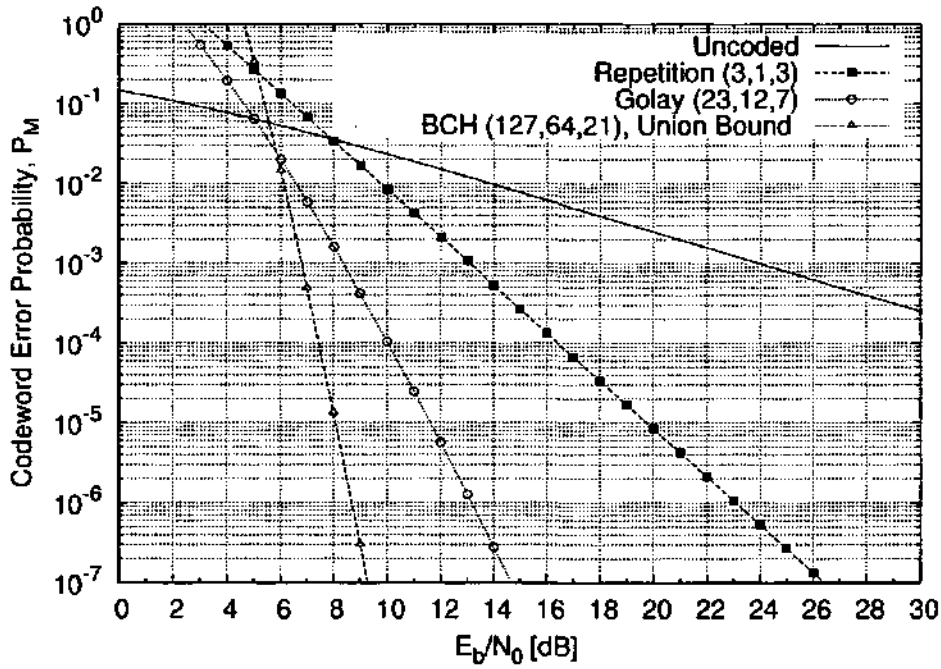


Figure 4.5: Error performances of the Golay(23,12,7), the BCH(127,64,21) and the Repetition(3,1,3) block codes over Rayleigh Fading channel with Soft Decision Decoding.

In Figure 4.5, the error performance of block codes over a Rayleigh fading channel with a soft decision decoding scheme is shown. Due to the limit of floating number precision in calculating the BCH curve using (4.17), the BCH curve is calculated from the looser bound, (4.18). Golay and Repetition curves are calculated using (4.17). A bound calculated from the weight distribution as given by (4.17) is always tighter to the actual codeword error performance, than a bound calculated using (4.18). Therefore it is believed that the BCH code could achieve $10^{-5}$ error level at $E_b/N_0$ less than 8 dB while, for Golay and Repetition codes, approximately 11 dB and 20 dB are required to achieve similar error level, respectively.

At error level $P_M = 10^{-5}$, the gain achieved by the Repetition(3,1,3) code with soft decision decoding is about 6 dB from its hard decoding performance. For the Golay(23,12,7) and the BCH(127,64,21), the gain due to soft decision decoding are about 7.5 dB and 7 dB, respectively.

## 4.4 Summary

From the literature study of channel coding in this chapter, it is found that there are several bounds that could be used in order to estimate error performance of a block code over AWGN or Rayleigh Fading channels. Weight distribution and $d_{min}$ are two variables that are useful in providing bounds of error performance of a block code. The bound that uses weight distribution as a parameter is a closer prediction to actual error probability than the bound that uses $d_{min}$. The bound is known as the Exact Bound for a perfect code. In the case of non perfect codes, the bound is considered as an upper bound of error performance of the code. In the latter, it is assumed that the Hamming weight of all codewords is equal to $d_{min}$. This assumption results in a looser error probability bound. This is because the smaller the value of Hamming distance between any two codewords, then the higher the probability of a codeword being decoded as another codeword. The bound that has been derived from weight distribution is considered as a lower bound, and the bound calculated using $d_{min}$ is considered as an upper bound of a linear block code.

From error performance comparison of an uncoded system over AWGN and Rayleigh Fading channels, it is shown that the effect of multipath fading on the system performance is more severe than the effect of thermal noise. In order to achieve comparable bit error probability of a communication over fading channel to that over an AWGN channel, higher power is required by the system. It is shown that an uncoded system requires approximately 10 dB SNR per bit in order to achieve a bit error probability lower than $10^{-5}$. Over a fading channel however, it is more than 30 dB SNR per bit is required by the system.

One of the solutions that is applicable to reduce system power requirement is to implement channel coding. Three block codes, the Repetition(3,1,3), the Extended Golay(24,12,8) and the Extended BCH(128,64,22) codes, have been compared in terms of codeword error performance over the AWGN channel. For the Rayleigh Fading channel, the Golay(23,12,7) and the BCH(127,64,21) codes, have been compared in terms of codeword error performance together with the repetition(3,1,3) code. As a conclusion, the Repetition code scheme is found unsuitable for implementation if the channel type is AWGN. The system performs even worse than an uncoded system if a Repetition code is used with a hard decision decoding scheme. The best performance that could be achieved by Repetition coding with soft decision decoding over an AWGN channel is the same as

the performance of an uncoded system. For the other two codes, it is shown that, either with soft decision or hard decision decoding, both coding schemes could reduce the system power requirement. If the channel is a Rayleigh fading channel, it is found that all the considered block codes do improve power requirement of system.

The error performance of a block code is influenced by the value of $d_{min}$ of the code. Higher the $d_{min}$ of the code will result lower the error probability. Therefore, it is not a surprising result to find that the considered BCH codes perform better than the other considered codes, then followed by the Golay code and the Repetition code, consecutively.

# Chapter 5

# Shortened Training Sequence for Mobile Channel Response Measurement

## 5.1 Introduction

In wireless digital communication data transmission, data are transmitted from the transmitter to the receiver in the form of packets. Besides a sequence of data, each of transmitted packets also contains a sequence that is known as the training sequence. The training sequence consists of unique words with good correlation properties.

The good correlation property means that the correlation function of the sequence is everywhere zero except at multiples of the period where the autocorrelation function has a single maximum peak [Frank and Zadoff, 1962]. This property is also called as the Constant Amplitude Zero Auto-Correlation (CAZAC) property in [IEEE-Std-802.16, 2004]. This property is very useful for measuring the impulse response of the channel for the equalization process on the receiver side, especially for a communication over time variant channels such as a wireless channel. One of well known sequence that has this property is called Frank sequence [Frank and Zadoff, 1962, Frank, 1963]. Proofs of several useful properties of Frank sequence are given in [Fan and Darnell, 1995].

## 5.2 Unique word with CAZAC properties

Defining a complex unique word sequence with length $N$ symbols, consisting of real and imaginary parts which are denoted as $Q[n]$ and $I[n]$ respectively. $n$ is an integer representing the index of a symbol in the sequence; therefore, $0 \leq n < N$. The sequence are derived from Frank-Zadoff sequence [Frank and Zadoff, 1962] and could be generated using the formula given in [IEEE-Std-802.16, 2004], as

$$I[n] = \cos(\theta[n]) \quad \text{and} \quad Q[n] = sin(\theta[n]) \tag{5.1}$$

where

$$\theta[n = p + q\sqrt{N}] = \frac{2\pi\ p\ q\ r}{\sqrt{N}} \tag{5.2}$$

and $p = 0, 1, \ldots, \sqrt{N} - 1$, $q = 0, 1, \ldots, \sqrt{N} - 1$ and $r = 1, 3$ or co-prime with $\sqrt{N}$.

As an example, a unique word with $N = 16$ is chosen and the sequence is given as

$$\begin{array}{cccccccccccccccc} \mathrm{Q} & = & 0 & - & 0 & + & - & + & - & + & 0 & - & 0 & + & + & + & + & + \\ \mathrm{I} & = & + & 0 & - & 0 & 0 & 0 & 0 & 0 & - & 0 & + & 0 & 0 & 0 & 0 & 0 \end{array} \tag{5.3}$$

and its periodic auto-correlation function is shown in Figure 5.1. Note that the periodic auto-correlation function as shown in Figure 5.1 is an up-sampled and filtered version. The sequence are upsampled with 32 samples per symbol. It is found that every correlation peak is a perfect peak with zero sidelobes. These correlation peaks are separated from each other by $N$ symbol periods. This means that the channel impulse response that can be perfectly equalized over not more than $2N$ symbol periods.

However, periodic correlation is not practically efficient in real applications because one perfect peak is enough to obtain the channel response. Furthermore, implementation of periodic correlation requires a large size of correlator buffer and also more complex computation is involved. If the unique word length is equal to $N$, ideally only one correlation peak with zero sidelobes is expected. Then the length of the periodic correlator must be at least $3N$. The correlation function of these two sequences is shown in Figure 5.2. It is observed that one perfect correlation peak appears in the middle. The length of channel impulse response that can be perfectly equalized is also equal to $2N$ symbol periods. This implementation is more efficient compared to the previous one. Advantages from this

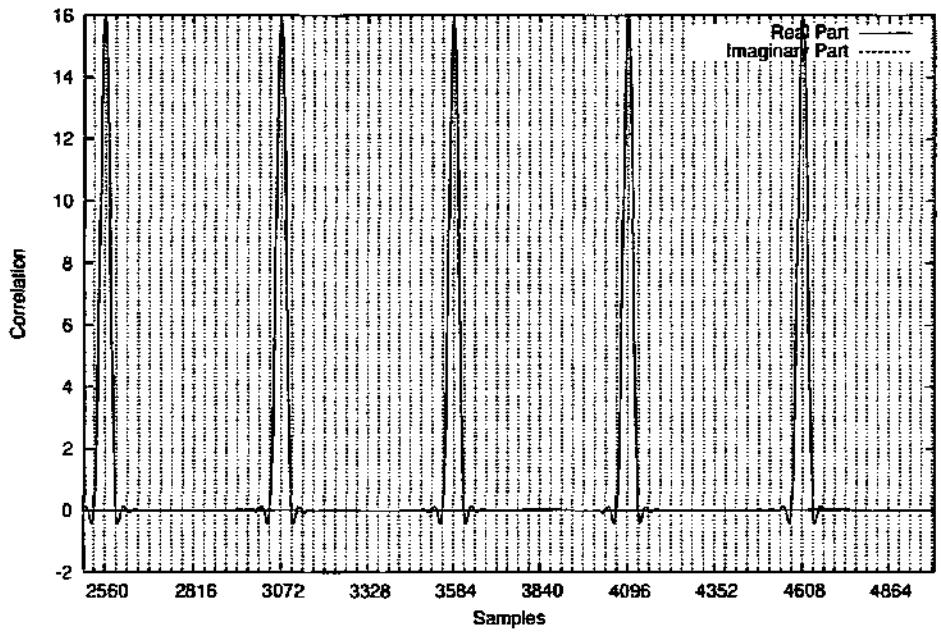


Figure 5.1: Auto-correlation function of periodic correlator. $N = 16$

implementation are that obviously less computation is required and a smaller correlator size than for periodic auto-correlation. It is found that the minimum size of correlator is equal to $3N$.

## 5.3 Shorter sequence for more efficient channel estimation

However, the channel impulse response is not always in the same state and might have different lengths for different environments. For wireless communication channels, the channel impulse response is time variant and environmentally-influenced. If the length of a pre-echo of the channel response is denoted as $C_h$ and the post-echo of the channel response is denoted as $C_t$, then the total length of channel response, denoted as $C_l$, is given as

$$C_l = C_h + C_t \tag{5.4}$$

where length is in symbol period units.

As described in the previous section, it is found that a periodic sequence with minimum length $3N$ is required in order to have a Dirac impulse function form of its correlation function. Also, it is found that the total length of Dirac function is equal to $2N$. The length of the left zero-sidelobe is the same as the length of the right zero-sidelobe, which is $N$ symbol periods. If length of the channel response is known to be $C_l$ symbol periods,

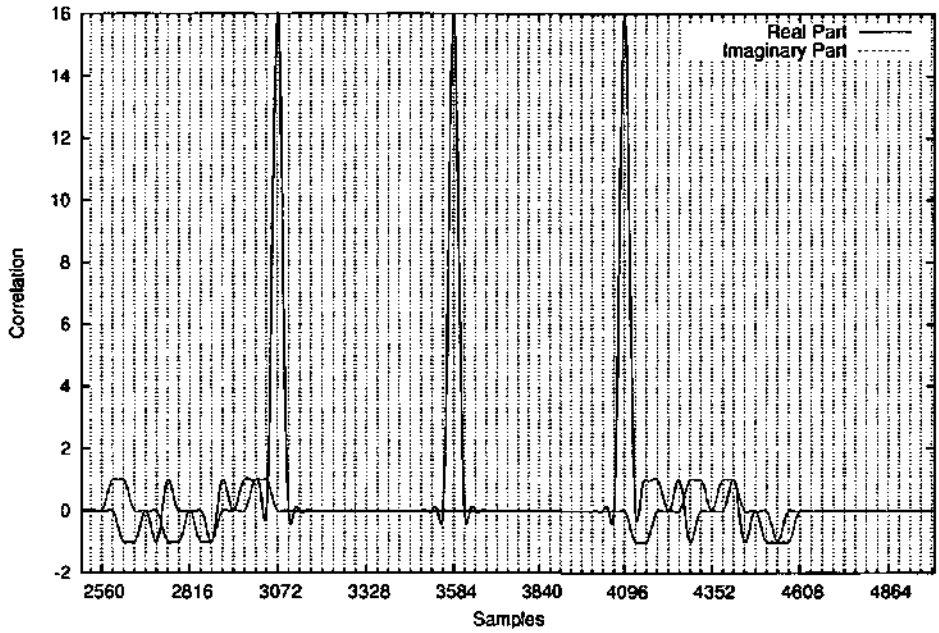


Figure 5.2: Auto-correlation function of periodic correlator with length of $3N$. $N = 16$.

a more efficient solution is achieved if there is a sequence of correlator with length shorter than $3N$ but still capable of replicating the channel response with length equal to or longer than $C_l$. This solution means reducing computation overhead in estimation of channel impulse response for every packet received.

In order to construct a shorter correlator with length less than $3N$, concatenation of partial sequences at the beginning and end of the unique word is found to work. The output of the concatenation process is an aperiodic correlator sequence with length shorter than $3N$ symbols. To describe the operation, assume the length of original sequence before concatenation is $N$ symbols. Then, the sequence that is going to be concatenated at the beginning of the unique word is called the Head Sequence and its length is denoted as $L_h$. The sequence that is concatenated at the end of the unique word is called the Tail Sequence, and its length is denoted as $L_t$. Therefore, after concatenation, the length of aperiodic correlator sequence is $L_a = N + L_h + L_t$.

It is important to note here that the sequence that will be concatenated at the head is actually the last $L_h$ symbols from the original unique word. Similarly, the sequence that will be concatenated at the end is actually the first $L_t$ symbols of the original unique word. To illustrate these rules, the Head Sequence is marked with forward-slash pattern while back-slash pattern is used to mark the Tail Sequence as shown in Figure 5.3.

Assume that the length of the original complex sequence, $N = 16$ symbols. The

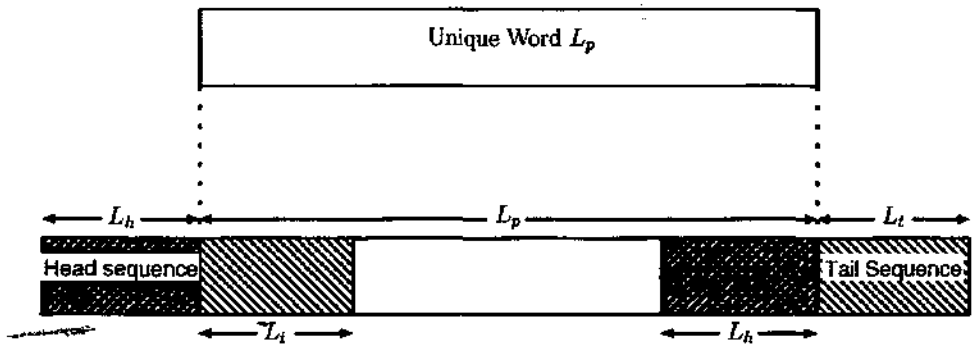


Figure 5.3: Concatenation rules

lengths of the Head Sequence and the Tail Sequence are the same, $L_h = L_t = 4$ symbols. The correlation function between the aperiodic correlator and the original unique word is shown in Figure 5.4. From the figure, it is found that a perfect peak with zero sidelobes

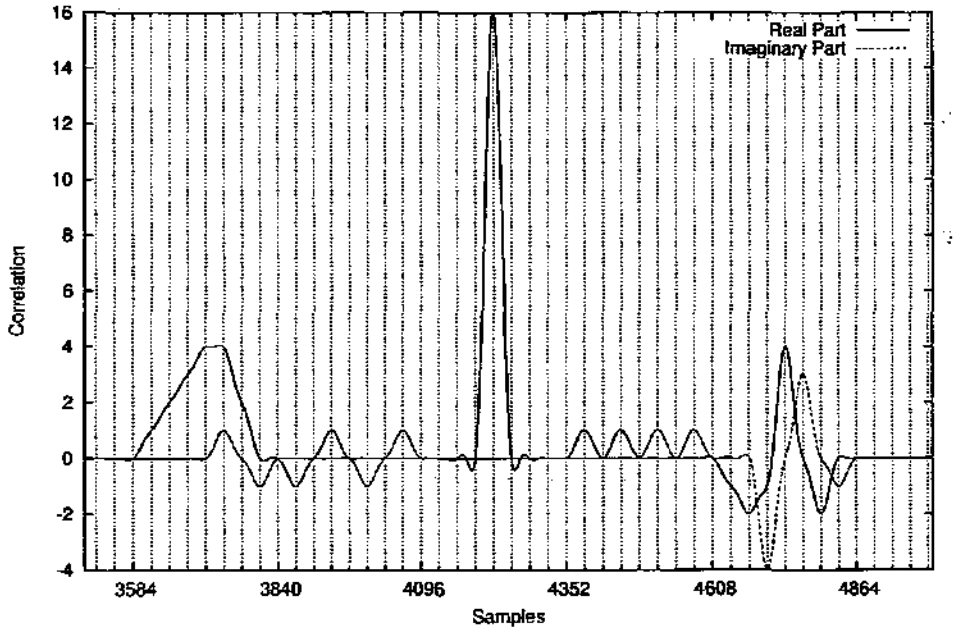


Figure 5.4: Aperiodic cross-correlation function with $N = 16$, $L_h = L_t = 4$

does appear in the cross-correlation function. Then length of the zero sidelobe sections on each side are shorter than $N$. In fact, the lengths of the sidelobes are equal to $L_h = L_t = 4$. Thus, this makes the length of the zero sidelobes $L_h + L_t$ symbol periods.

A hypothesis is made at this stage which suggests that the length of the zero sidelobes of the crosscorrelation function is affected by the length of the Head and Tail sequences. A set of head and tail sequences lengths are prepared as shown in Table 5.1, for use in the construction of different length aperiodic correlators. Each of the aperiodic correlators is constructed by following the concatenation rules as illustrated in Figure 5.3.

| Original Sequence Length, $N$ | Configuration | Concatenated Sequence Length, $L_a$ | Head Sequence Length | Tail Sequence Length |
|---|---|---|---|---|
| 16 | 1 | 24 | 7 | 1 |
| | 2 | 24 | 3 | 5 |
| | 3 | 27 | 4 | 7 |
| | 4 | 27 | 8 | 3 |

Table 5.1: Concatenation configurations

The correlation functions between the original unique word and aperiodic correlators from Configuration 1, 2, 3 and 4 of Table 5.1 are shown in Figures 5.5(a), 5.5(b), 5.5(c) and 5.5(d), respectively. For Figure 5.5(a), the lengths of the Head sequence and Tail sequence are equal to 7 and 1 respectively. It is found that the left zero-sidelobe length is as long as 7 symbols period and the right zero-sidelobe is 1 symbol period. For Configuration 2, head and tail sequence lengths are equal to 3 and 5 symbols. The corresponding correlation function is shown in Figure 5.5(b), and shows that the left zero-sidelobe length is again equal to head sequence length which is 3 symbols; the right zero-sidelobe length is equal to the tail sequence length which is 5 symbols. Similar observation can be made for Configurations 3 and 4. Clearly, the left and right zero-sidelobes lengths are determined from lengths of the head sequences and tail sequences, respectively.

## 5.4 Summary

From the observations that have been made above, it is concluded that a shorter correlator sequence can be customised according to the delay of the multipath components of a communication channel. If the lengths of pre-echo $C_h$, and post-echo $C_t$, of the channel response are known, then the bounds boundary of head sequence length $L_t$, and tail sequence length $L_t$, are given as,

$$L_h \geq C_h \text{ and } L_t \geq C_t \tag{5.5}$$

Therefore the length of correlator sequence, $L_a$ is given as,

$$L_a \geq N + L_h + L_t \tag{5.6}$$

where $N$ is the length of unique word sequence.

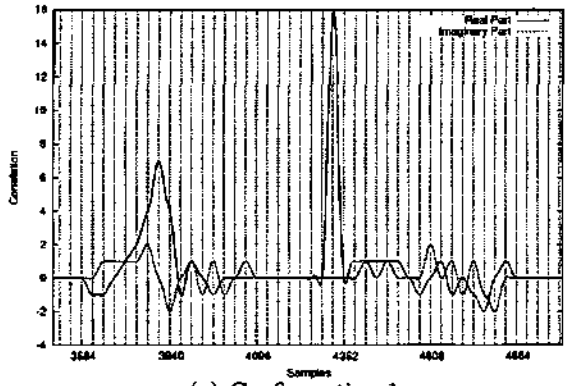


(a) Configuration 1

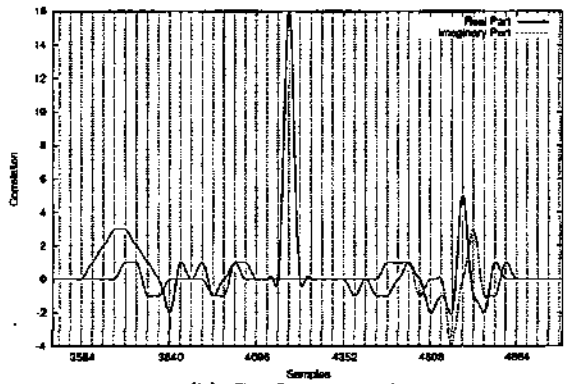


(b) Configuration 2

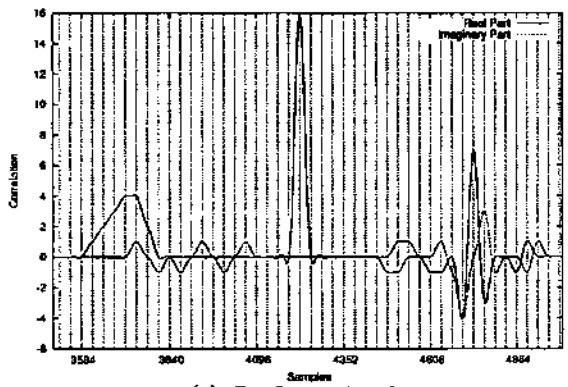


(c) Configuration 3

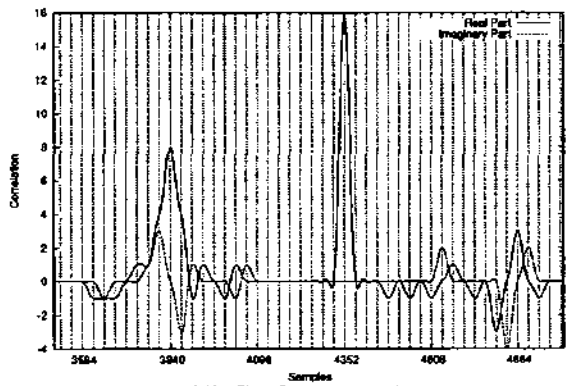


(d) Configuration 4

Figure 5.5: Cross-correlation functions of configurations from Table 5.1

# Chapter 6

# Error performance of [136,68,24] Double Circulant Code with Dorsch List Decoding over SUI-5 Channel

## 6.1 Introduction & Background

Wireless broadband systems have been actively researched recently because they offer a capability for high bit-rate transmission over up to tens of miles distance wirelessly. This feature also promises a lower cost system compared to cable based systems. A wireless broadband system has also been standardised by the IEEE known as Wireless Metropolitan Area Networks (WirelessMAN). WirelessMAN (WiMax) system specifications are written in the IEEE 802.16 standard [IEEE-Std-802.16, 2004].

In the standard, the channel model that has been proposed in [Erceg et al., 2001], has been accepted for use in simulations, design, development and testing of technologies suitable for fixed broadband wireless applications. A set of six channel models has been provided in [Erceg et al., 2001]. The set of channel models is called the Modified Stanford University Interim (SUI) channel models. The Modified Stanford University Interim (SUI) Channel model is a set of channel models that has been proposed to represent channel characteristics of fixed broadband wireless channels. There are six channel models in the

SUI channel model set, which are called SUI-1 to SUI-6, respectively. SUI-1 and SUI-2 are channel models for mostly flat terrain with light tree density. SUI-5 and SUI-6 are for hilly terrain with moderate and heavy tree density. SUI-3 and SUI-4 are for intermediate terrain between the two formerly mentioned terrains. Each of the channel models provides parameter values of multipath fading with omnidirectional and 30° directional receiving antennas. Multipath fading is modelled as a tapped-delay line with 3 taps and non-uniform delays. The gain of each tap is characterised by a Ricean or a Rayleigh distribution and a maximum Doppler frequency.

In this chapter, a simulation model of a wireless communication system over one of the SUI channel models has been developed. Specifically, the channel model that was considered in this work is the SUI-5 channel model. The system is equipped with a [136,68,24] double circulant code as its error correction encoder and Dorsch List Decoding as its error correction decoder. The purpose of this simulation is to reveal the performance of the channel coding scheme over the SUI-5 channel. The model of system considers the up-sampling and down-sampling process, pulse shaping filtering, the application of training sequence, equalizer filtering and channel coding schemes.

### 6.1.1 SUI-5 Channel

The multipath channel of the SUI model is characterised by a three tapped-line delay model. Each tap would have its own delay profile and power profile with its corresponding K-factor of a Ricean distribution. Generally, the Modified SUI-5 channel model is proposed to model the multipath fading communication channel for fixed wireless broadband access over hilly terrain with moderate and high tree density environments. Within such environments, it is common to have non-line of sight propagation paths becoming the dominant propagation paths. The specification of the SUI-5 channel model that has been applied in this work is the SUI-5 with an omnidirectional antenna and the percentage of the coverage area of a cell is 90%. Table 6.1 shows selected parameters and their values.

## 6.2 Simulation Model

In order to explain the simulation model, the diagram in Figure 6.1 shows the overview of system model.

Table 6.1: SUI-5 Channel Model

| | Tap 1 | Tap 2 | Tap 3 | Unit |
|---|---|---|---|---|
| Delay | 0 | 4 | 10 | $\mu$s |
| Power (omni antenna) | 0 | -5 | -10 | dB |
| 90 % K-factor (omni) | 0 | 0 | 0 | |
| Normalization factor | - 1.5113 | - 1.5113 | - 1.5113 | dB |

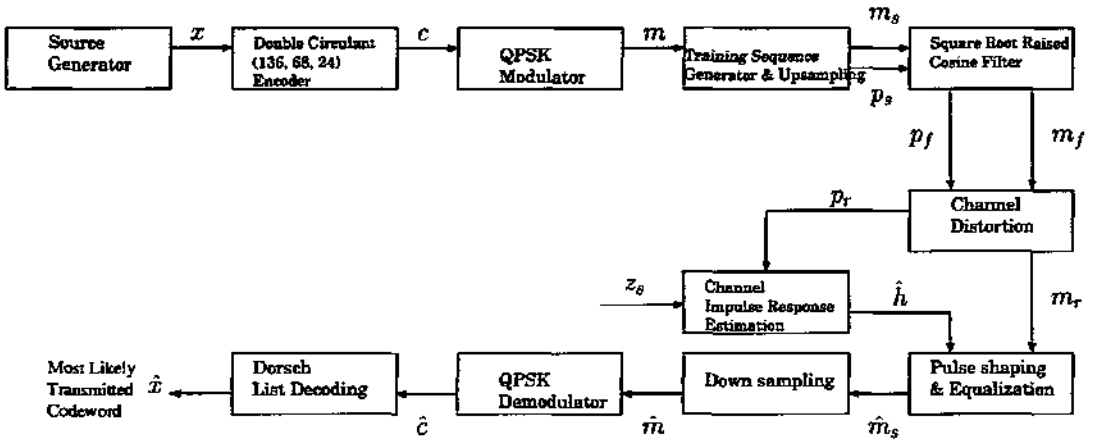


Figure 6.1: Simulation model overview

The Source Generator block represents a random binary generator that generates a vector of binary information bits with length $k$, denoted as

$$\mathbf{x} = [x_0, x_1, x_2, \ldots, x_{k-1}]. \tag{6.1}$$

The vector $\mathbf{x}$ is then inserted into the Encoder block and it encoded to become a codeword vector with length $n$. The type of code that has been applied is the [136, 68, 24] double circulant code; the same code has been used in [Tomlinson et al., 2007], with $n = 136$ as codeword length, $k = 68$ as information bit length and $d_{min} = 24$ as the minimum distance of the code. The code rate is $r = \frac{k}{n} = 1/2$. The output of the Encoder block is called the encoded vector, denoted as

$$\mathbf{c} = [c_0, c_1, c_2, \ldots, c_{n-1}]. \tag{6.2}$$

$c$ is then mapped with a Gray encoded QPSK mapping scheme in order to generate a vector of discrete information-bearing complex-valued symbols denoted as

$$\mathbf{m} = [m_0, m_1, m_2, \ldots, m_{n/2-1}] \tag{6.3}$$

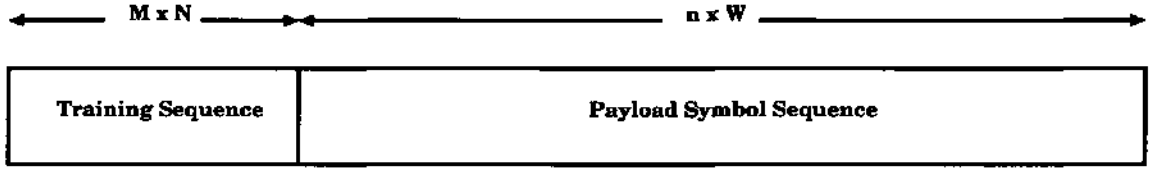


Figure 6.2: Mapping of training sequence and payload blocks in a burst of packet.

Since $m$ is a periodic symbol vector with symbol period equal to $T$, therefore, $m_i \equiv m(iT)$.

Data packets are assumed to be transmitted burst by burst, with every burst consisting of a block of training sequence followed by a payload block. The training sequence consists of a single or a periodic arrangement of unique words with CAZAC properties. A unique word is generated using (5.1). $M$ is the number of unique words in a training sequence, and $N$ is the length of a unique word. $W$ is number of encoded codewords in a payload field. The general arrangement of the training sequence and payload block is shown in Figure 6.2. For simplicity of the simulation model and of the computation load, $M = 1$, $N = 256$ and $W = 1$ are applied. Furthermore, the training sequence and the payload sequence are treated as independent blocks but both blocks are assumed to be distorted by the same channel response. The training sequence is denoted as $p$.

The training sequence, $p$, and payload symbols, $m$, are up-sampled with four samples per symbol, before the pulse shaping filtering. In order to apply the Nyquist Criterion pulse shaping, vectors $m$ and $p$ are convolved with $g_T(t)$, where $g_T(t)$ is time-domain response of transmitter pulse shaping filter. The filter $g_T(t)$ is known as Square Root Raised Cosine filter which has a band-limited frequency response characteristic $G_T(f) = FFT(g_T(t)) = \sqrt{|X_{rc}(f)|}$. The filter of $X_{rc}$ is known as a Raised Cosine filter and it characteristic function is given by [Proakis, 2000],

$$X_{rc}(f) = \left\{ \begin{array}{ll} T & ; \left(0 \leq |f| \leq \frac{1-\beta}{2T}\right) \\ \frac{T}{2}\left\{1 + cos\left[\frac{1-\beta}{2T}\left(|f| - \frac{1-\beta}{2T}\right)\right]\right\} & ; \left(\frac{1-\beta}{2T} \leq |f| \leq \frac{1+\beta}{2T}\right) \\ 0 & ; |f| > \left(\frac{1+\beta}{2T}\right) \end{array} \right\}$$

where $\beta$ is the roll-off factor of the filter. The range of the $\beta$ values is $0 \leq \beta \leq 1$; $\beta = 0.25$ has been chosen for the system model because it is a compulsory $\beta$ value to be supported as specified in the WiMax standard [IEEE-Std-802.16, 2004]. Since convolution in time domain is equivalent to multiplication in frequency domain, and it is faster and simpler

to implement, therefore the pulse shaping filtering is done in frequency domain as below

$$M_f(f) = M_s(f) \times G_T(f) \text{ and } P_f(f) = P_s(f) \times G_T(f) \tag{6.4}$$

where $M_s(f) = FFT(m_s)$ is the Fourier transform of $m_s$ and $M_f(f)$ is the filtered payload in the frequency domain. Similarly, $P_s(f) = FFT(p_s)$ is Fourier transform of $p_s$ and $P_f(f)$ is the filtered training sequence in frequency domain. Therefore, filtered payload and training sequences in the time domain are equal to $IFFT(M_f(f)) = m_f(t)$ and $IFFT(P_f(f)) = p_f(t)$, where IFFT means Inverse Fourier Transform.

In the channel distortion block, filtered sequences, $m_f(t)$ and $p_f(t)$, are convolved with channel impulse response, $h(t)$. The channel impulse response, $h(t)$, is generated from the SUI-5 channel model that was proposed in [Erceg et al., 2001] [1]. The characteristics of the SUI-5 channel have been mentioned in Section 6.1.1. The channel impulse response is time varying. A channel response will only be used for one burst. A new and independent channel response is generated and will be convolved in the next burst. It is assumed that the same channel impulse response applies for both payload and training sequence convolutions. Convolution of payload and training sequence with channel impulse response is also done in the frequency domain.

$$M_d(f) = M_f(f) \times H(f) \text{ and } P_d(f) = P_f(f) \times H(f) \tag{6.5}$$

where $H(f) = FFT(h(t))$, is the Fourier transform of the time-domain channel impulse response $h(t)$. $M_d(f)$ and $P_d(f)$ are distorted payload sequence and distorted training sequence in the frequency domain, respectively. Distorted sequences in the time domain, $m_d(t)$ and $p_d(t)$ are obtained by applying IFFT to $M_d(f)$ and $P_d(f)$ respectively. Additive white noise is added to $m_d(t)$ and $p_d(t)$ to produce distorted and noisy payload and training sequence vectors, $m_r(t)$ and $p_r(t)$. The addition is done in the time domain. Therefore, the complete equation for the channel distortion block in the time domain is given as

$$m_r(t) = m_d(t) + n_1(t) \text{ and } p_r(t) = p_d(t) + n_2(t) \tag{6.6}$$

where $n_1(t)$ and $n_2(t)$ are noise random values generated from two independent Gaussian

[1] Example of implementation of SUI channel is given in Appendix B of [Erceg et al., 2001].

random generators with identical variance.

At the receiving end, the training sequence, $p_r(t)$, is then correlated with a correlator sequence, $z(t)$. The correlator sequence is a periodic sequence of unique words. As much as three unique words are concatenated and upsampled to generate the $z_s(t)$. Due to the CAZAC properties of the unique word, correlation of $p_r(t)$ and $z_s(t)$ will return the estimation of channel impulse response, $\hat{h}(t)$. With a known estimation of the channel impulse response, the filter at the receiver side is constructed by combining the Zero Forcing equaliser and Square Root Raised Cosine pulse shaping filter as below

$$F(f) = \frac{1}{\hat{H}(f)} \times G_R(f). \tag{6.7}$$

where $G_R(f) = G_T(f)$. In order to realise an equalised and pulse shaped received payload vector, $\hat{m}_s(t)$, the distorted and noisy payload vector, $m_r(t)$, is convolved with the receiver filter, $f(t)$ in frequency domain as below

$$\hat{m}(t) = IFFT(\hat{M}(f)) = IFFT(M_r(f) \times F(f)). \tag{6.8}$$

Vector $\hat{m}_s(t)$ is then down-sampled before it is decoded by QPSK soft decision demodulator. The QPSK demodulator returns the soft value of the received vector which is denoted as $\hat{r}$ along with the vector bits reliability order. From the $\hat{r}$, the hard decoded encoded bit $\hat{b}$ is generated using hard decision decoding. Reliability of each hard decoded bits is ordered based on the soft values of $\hat{r}$. $\hat{b}$ and its bit reliability order are then fed into an Extended Dorsch List decoder to find the most likely transmitted codeword $\hat{x}$.

The decoder treats the $n-k$ least reliability bits of $\hat{b}$ as erasure bits and the other $k$ bits as the information bits. The first candidate codeword is found by solving the $n-k$ erasure bits of $\hat{b}$ with the $k$ information bits remain unchanged. With $k$ information bits of $\hat{b}$, there are $2^k$ possible information bits combination may be found, by inverting at least one bit and finally up to all $k$ information bits of $\hat{b}$ are inverted. Provided these $2^k$ possible information bit combinations, a complete list of $2^k$ candidate codewords is generated by solving erasures bits for each information bit combinations. The candidate codeword that has the highest correlation value with the down-sampled received vector is chosen as the most likely transmitted codeword, $\hat{x}$. Detail explanation of the Dorsch list decoder used

in the simulation is explained in [Tomlinson et al., 2007].

## 6.3 Performance of Simulation Model over SUI-5 Channel

The error performance of the coding scheme described in Section 6.2 is shown in Figure 6.3. The decoder was set to have $w \leq 2$ where $w$ is the number of invertible information bits in $\hat{b}$. Therefore the maximum size of the codeword list of the decoder is equal to $\sum_{w=1}^{2} \binom{k=68}{w} = 2346$ codewords. If $w = 1$ is considered, the size of codeword list equals $\binom{k=68}{w=1} = 68$ codewords. Along with the curves over the SUI-5 channel, performance curves of the same coding scheme over an AWGN channel are also plotted for comparison.

It is found that the performance of the [136,68,24] Double Circulant code with Dorsch List Decoding is badly impaired by the multipath and fading effects of the SUI-5 channel. Even though the channel coding scheme that has been applied is quite outstanding over an AWGN channel, the decoder has been affected by the poor performance of the equalizer. A Zero Forcing equalizer does the forcing of the impulse response of the channel and equalizer to zero at all except one at symbol periods. This technique does remove the ISI. However, it also eliminates received power of delayed paths while retaining the received power of the first tap. Manipulation of received power of delayed paths, rather than eliminating it, would be useful to reduce the fading depth of the received power. Application of other equaliser algorithms is believed will improve fading effects mitigation.

## 6.4 Summary

The Stanford University Interim (SUI) Channel Model is a set of six channel models that has been proposed to represent communication channels of fixed wireless broadband access in various environments [Erceg et al., 2001]. Each of the channel models may be categorised into different terrain types and level of tree density within the coverage areas. In fact, the set of channel models have been used as the channel models for simulation, design and assessment of systems that conform to the IEEE 802.16 WirelessMAN standard.

Hence, it is interesting to investigate the level of impairment of the SUI channel to communication systems. Therefore a simulation model has been developed to simulate a wireless communication system over one of proposed fixed wireless broadband channels, the SUI-5 channel. The SUI-5 channel model is categorised to represent hilly terrain

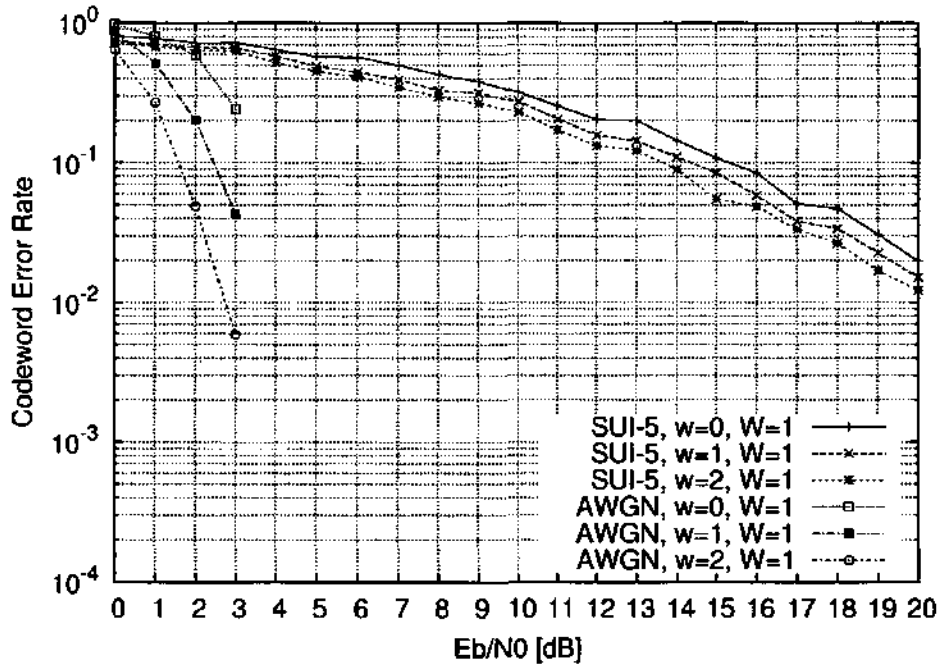


Figure 6.3: Error Performance of [136,68,24] Double Circulant Code with Dorsch List Decoding over SUI-5 Channel. $W = 1$. $w = 0, 1, 2$.

with medium or high tree density. A channel coding scheme of a [136,68,24] Double Circulant Code with a Dorsch List Decoding was applied due to its impressive performance over an AWGN channel [Tomlinson et al., 2007]. Due to time varying and multipath fading properties of the communication channel, application of the training sequence and an adaptive equaliser using a Zero Forcing algorithm are considered in the simulation model. The training sequence consists of a unique word that has the Constant Amplitude Zero Auto-Correlation (CAZAC) properties as specified in the IEEE 802.16 WirelessMAN Standard [IEEE-Std-802.16, 2004]. Additionally, up-sampling and pulse shaping filtering are also considered in the simulation.

Results of simulation have found that the combination of channel coding and equalization that have been applied in the system is not adequate to mitigate the effects of ISI and fading over the SUI-5 multipath channel. The error performance of the system over the SUI-5 channel is quite significantly different from the error performance of the system over an AWGN channel. Furthermore, increasing the size of codeword list does not improve the codeword error probability at a rate better than improvements made over an AWGN channel. It is believed that the performance of the channel coding has been affected by the poor performance of the equalizer. A better equalization scheme is required to mitigate

the fading effect in the received vectors.

# Chapter 7

# Path Loss Predictions within multi-floored buildings at 433 MHz, 869 MHz and 1249 MHz

## 7.1 Introduction and Background

Wireless solutions are becoming popular for indoor systems such as multimedia systems, security and monitoring systems [Hwang and Baek, 2007] and etc. Therefore exploration of propagation characteristics at various carrier frequencies is necessary to support future deployment of various indoor wireless systems. One important area to support the implementation of efficient wireless systems is a knowledge of the coverage area of a transmitter within a given environment. Good knowledge on the coverage area then becomes an input to the hardware location planning phase which influences system performance and cost. Propagation models that are commonly used to predict the coverage area of a transmitter are categorised as a large-scale propagation models. Large-scale propagation models characterize the attenuation of received signal strength over a large distance (large-scale) between transmitter and receiver. The distance between transmitter and receiver could be up to tens of meters for indoor environments or up to tens of kilometres for outdoor environments. In this chapter, path loss characteristics have been derived at three different Ultra High Frequency (UHF) [1] carrier frequencies. Those carrier frequencies are

[1] UHF band is between 300 MHz and 3000 MHz (3 GHz). Its wavelengths is between 10 cm to 1 metre. UHF is numbered as Band No. 9 in International Telecommunication Union (ITU) Radio Band Number.

433 MHz, 869 MHz and 1249 MHz. Propagation of signals at different frequencies in an exactly the same environment shows different characteristics. This is due to the different wavelengths of the signals. Signal paths at different frequencies are reflected, diffracted and scattered differently to each other.

Received signal strength measurements have been carried out within three University of Plymouth buildings. Each building represents features typical of an office building. The first building is a building with a rectangular shaped footprint. The second building is a building with a square shape footprint. Comparison of path loss model parameters between these two office buildings is to find the relationship between building footprint and path loss. The third building is a building with an indoor atrium. It is also useful to investigate the characteristics of path loss within this type of building. Details of each building are described in Section 7.3.

### 7.1.1 Free Space Propagation Models

Large scale propagation models commonly predict the average received signal level for a given transmitter-to-receiver distance (T-R distance). If the signal is propagating in an environment where there is no obstruction between transmitter and receiver, and the surrounding is an empty space, the environment is known as a free space environment. Therefore, with no obstruction between transmitter and receiver, a clear and a line-of-sight propagation path is presumably present. Predicting received power within a free space environment could be done by using the well-known Friis free space equation, which is given as

$$P_r(d) = \frac{P_t G_t G_r \lambda^2}{(4\pi)^2 d^2 L} \tag{7.1}$$

where $P_t$ and $P_r$ are transmit power and received power, respectively. $G_t$ and $G_r$ are the gain of the transmitter antenna and the gain of the receiver antenna, respectively. $\lambda$ is the wavelength in meters. $L$ is the system loss and $d$ is the distance between transmitter and receiver antennas. $P_t$ and $P_r$ must be in the same units. $G_t$ and $G_r$ are dimensionless. $L = 1$ if there is no loss caused by the system.

However, Equation (7.1) is only valid for predicting $P_r$ when $d$ is in the far-field region [Rappaport, 1996]. The far-field region is the region beyond the far-field distance, $d_f$,

which is given by

$$d_f = \frac{2D^2}{\lambda} \tag{7.2}$$

where $D$ is the largest physical linear dimension of the antenna and $\lambda$ is signal wavelength. $d_f$ must satisfy $d_f \gg D$ and $d_f \gg \lambda$. The far-field region and the far-field distance are also known as *Fraunhofer region* and *Fraunhofer distance*, respectively.

With known transmitted power and distance between transmitter and receiver, the path loss of free space propagation, which is denoted by $PL_0$, can be calculated using

$$PL_0(d)\ [\text{dB}] = 10\log_{10}\frac{P_t}{P_r(d)} = -10\log_{10}\left[\frac{G_t G_r \lambda^2}{(4\pi)^2 d^2 L}\right]. \tag{7.3}$$

## 7.2 Measurement Apparatus

### 7.2.1 Measurement apparatus for the 433 MHz system

Figure 7.1(a) shows the block diagram of the 433 MHz transmitter measurement setup. Generally, the transmitter side measurement apparatus consists of a direct current (DC) power supply, the 433 MHz transmitter module and a 1/4 wavelength monopole whip antenna. The 433 MHz transmitter module uses a TX2EH-433-64-5V Radiometrix chip. For detailed specifications of the transmitter chip and the antenna, readers are referred to the Radiometrix webpage [Radiometrix Ltd. ]. With a 5V input voltage supplied from the power supply to the transmitter module, the actual output power of the 433 MHz transmitter module, $P_o(433)$ is equal to +21.12 dBm. Measurement of the actual output power of transmitter module has been done earlier. The center frequency of the transmitter, $f(433)$, is 433.9 MHz. From [Radiometrix Ltd. ], the antenna gain, $G_t(433)$, is equal to 0 dB. Since there is no connecting cable between the transmitter module and the transmitting antenna, it is assumed that there is no loss between both components. Thus the radiated power, $P_t(433)$, of 433 MHz transmitter is also equal to +21.12 dBm. All of the equipments are arranged on top of a trolley for relocation flexibility, as shown in Figure 7.1(b). The antenna is set to be at 1.25 meters above the floor.

The block diagram of the 433 MHz receiver measurement apparatus setup is shown in Figure 7.2(a). The receiver consists of a helical antenna, an Anritsu MS2661B spectrum analyser and a computer. The antenna and spectrum analyser are connected to

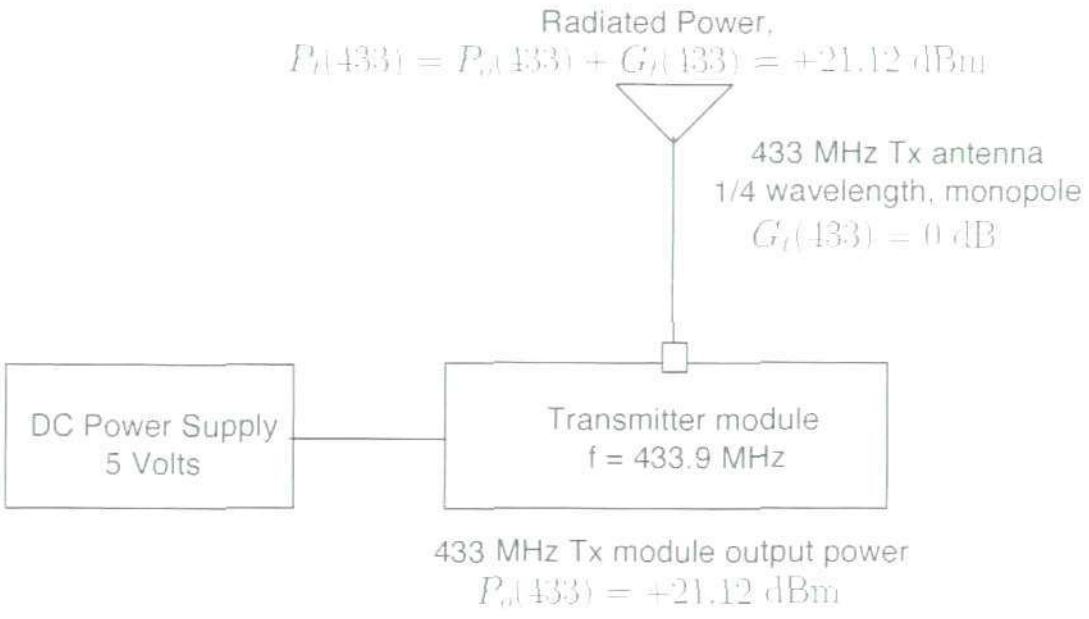


(a) 433 MHz Transmitter block diagram

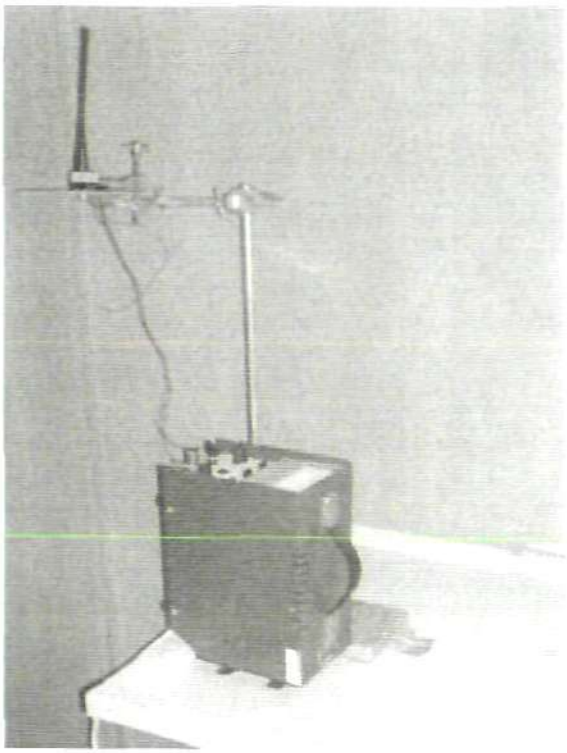

(b) Photo of the 433 MHz transmitter apparatus arrangement on top of a trolley

Figure 7.1: 433 MHz transmitter measurement apparatus

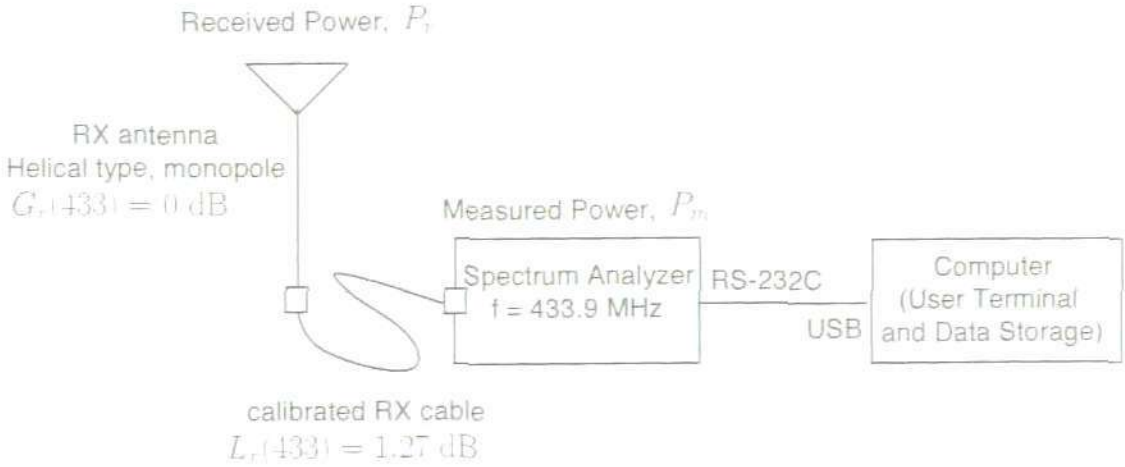


(a) 433 MHz Receiver block diagram

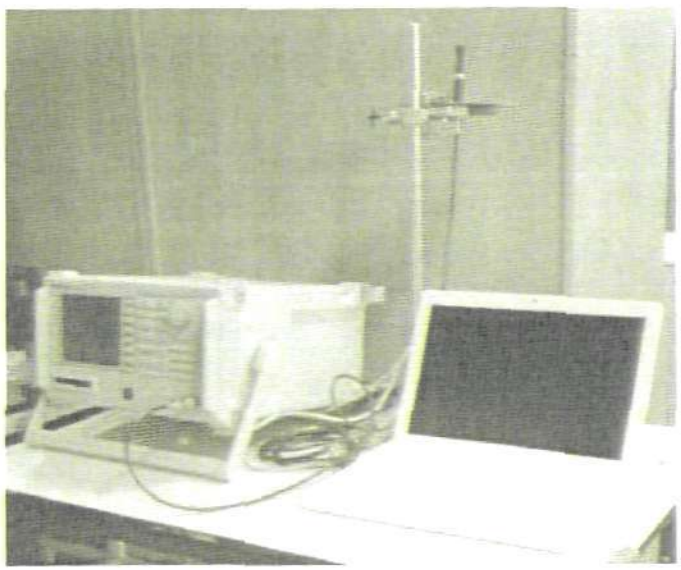

(b) Photo of the 433 MHz receiver apparatus arrangement on top of a trolley

Figure 7.2: 433 MHz receiver measurement apparatus

each other by a calibrated cable. The gain of the antenna, $G_r(433)$ is equal to 0 dB [Radiometrix Ltd. ] and the loss due to the connecting cable, $CL_r(433)$, is equal to 1.27 dB. The spectrum analyser function is to measure the received signal strength. The peak frequency of the spectrum analyser is set to the center frequency of the transmitter, 433.9 MHz, and the resolution bandwidth of the spectrum analyser is set to 30 kHz. The spectrum analyser is capable of measuring a received signal strength between 0 and -80 dBm. The computer is installed with a customized data acquisition program that enables the user to change spectrum analyser configurations, retrieve signal strength reading from the spectrum analyser and store the measurement readings. The computer and spectrum analyser are connected to each other by a Universal Serial Bus (USB) to Recommended Standard 232 C Revision (RS-232C) cable.

### 7.2.2 Measurement apparatus for the 869 MHz system

The block diagram of the 869 MHz transmitter measurement apparatus is shown in Figure 7.3(a). The transmitter consists of a DC power supply, the 869 MHz transmitter module and a helical antenna. The same power supply used in the 433 MHz transmitter system is again used in the 869 MHz transmitter system. The 869 MHz transmitter module is built from a TX3H-869.50-10 Radiometrix chip with center frequency, $f(869) = 869.5$ MHz. With 5V input voltage, the output power of the transmitter module, $P_o(869) = +24.25$ dBm. Since there is no cable between transmitter module and transmitting antenna, therefore the transmit power of the transmitter, $P_t(869) = +24.25$ dBm. The physical arrangement of the equipment is similar to the 433 MHz transmitter arrangement shown in Figure 7.1(b), except that a different transmitter module, antenna type and antenna height that have been used. The transmitter antenna has been set to be 1.27 meters above the floor. The antenna gain, $G_t(869)$, is equal to 0 dB [Radiometrix Ltd. ]. The transmitter module and the transmitter antenna of the 869 MHz transmitter system are shown in Figure 7.3(b).

Figure 7.4(a) shows the block diagram of the 869 MHz receiver system. Equipped with a 3/4 wavelength monopole whip antenna, the received signal strength is measured by the spectrum analyser at the center frequency $f(869)$. It is assumed that the antenna gain, $G_r = 0$ dB. The resolution bandwidth of the spectrum analyser is set to 30 kHz and the dynamic range of the spectrum analyser is 0 to -80 dBm. The computer is setup the same

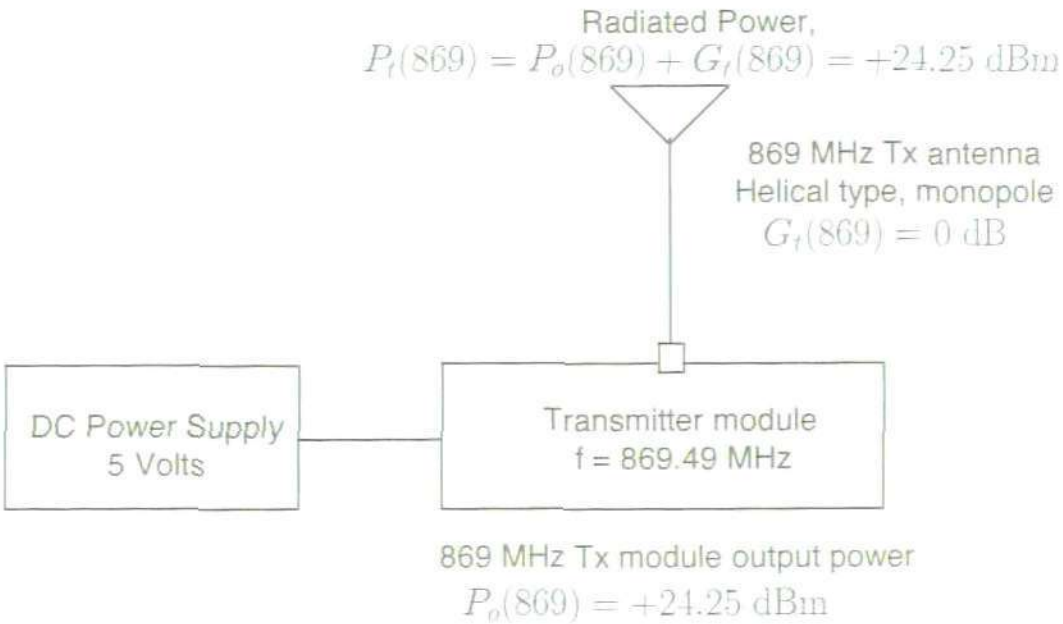


(a) 869 MHz Transmitter block diagram

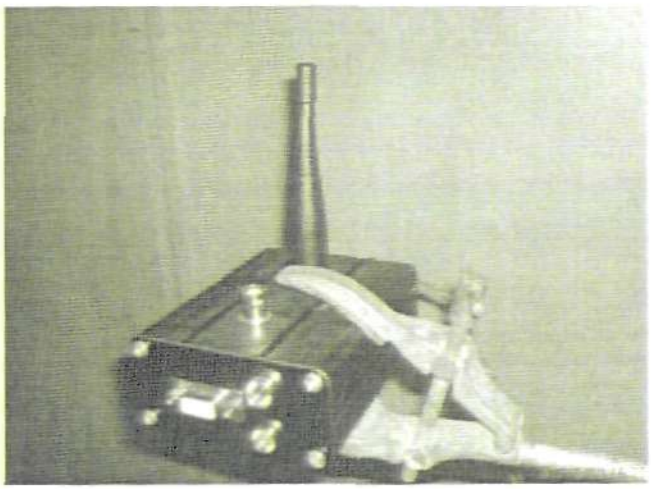

(b) Photo of the 869 MHz transmitter module and antenna

Figure 7.3: 869 MHz transmitter measurement apparatus

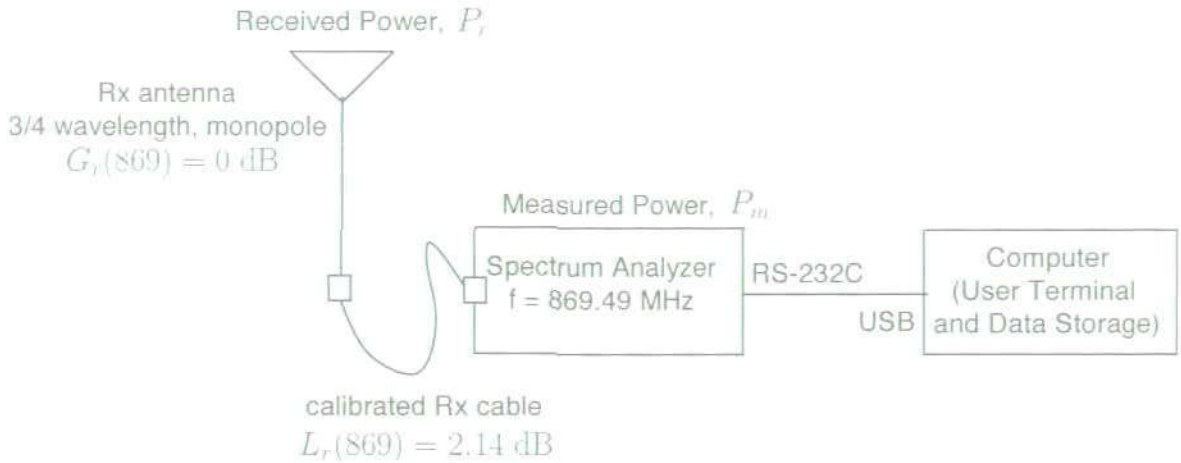


(a) 869 MHz Receiver block diagram

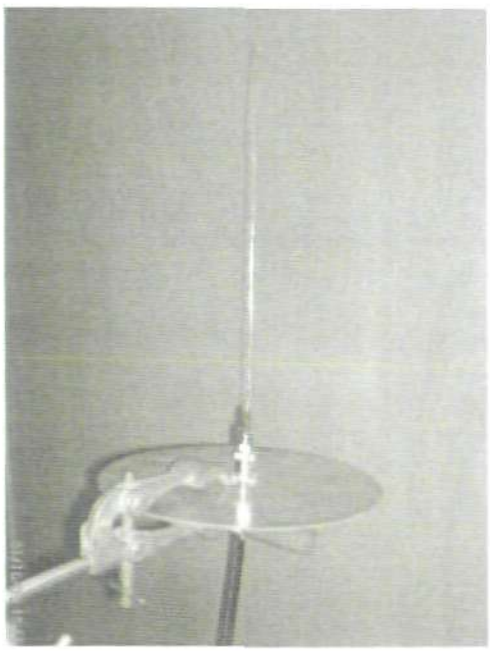

(b) Photo of the 869 MHz receiver antenna

Figure 7.4: 869 MHz receiver measurement apparatus

way as described for the 433 MHz receiver system configuration. The antenna of the 869 MHz receiver system is shown in Figure 7.4(b).

### 7.2.3 Measurement apparatus for the 1249 MHz system

The 1249 MHz transmitter system consists of a DC power supply with a 12V output, a 1249.36 MHz transmitter module and a 1/2 wavelength dipole antenna. With 12V DC input voltage, the transmitter output power, $P_o(1249)$, is equal to +31.19 dBm. There is a cable which connects the transmitter module and the transmitter antenna. Its loss, $CL_t(1249)$, has been measured at 1249 MHz signal frequency and is found to be 2.51 dB. Therefore, the transmitted power of the system, $P_t(1249) = P_o(1249) - CL_t(1249) = 28.68$ dB. Theoretically, the gain of a dipole antenna is 1.64 or 2.15 dB above an isotropic antenna [Rappaport, 1996]; therefore, the gain of the 1249 MHz transmitter antenna, $G_t(1249)$, is assumed to be 2.15 dB. The block diagram and photo of the equipment arrangement of the 1249 MHz transmitter system are shown in Figure 7.5(a) and Figure 7.5(b) respectively.

The receiver antenna of the 1249 MHz system is identical to its transmitter antenna. Therefore, its gain, $G_r(1249)$, is also assumed to be 2.15 dB. The antenna is connected to the spectrum analyser by a calibrated cable. The cable loss, $CL_r(1249)$ is 0.58 dB. The resolution bandwidth and dynamic range of the spectrum analyser remain at 30 kHz and 0 to -80 dBm, respectively. However, its center frequency is set equal to transmitter center frequency, $f(1249) = 1249.36$ MHz. The block diagram and photo of the equipment arrangement of the 1249 MHz receiver system are shown in Figure 7.6(a) and Figure 7.6(b) respectively.

To summarize the information presented in this section, Table 7.1 gives a summary of 433 MHz, 869 MHz and 1249 MHz measurement apparatus configurations. Measurement system parameters are consistent for a flat fading model.

## 7.3 Locations of Measurements

Three of University of Plymouth's buildings were chosen to be the measurement sites for the measurement of received signal strength within buildings. The buildings are known as the Smeaton Building, the Babbage Building and the Roland Levinsky Building. Detailed information and descriptions of each building are given as follows:

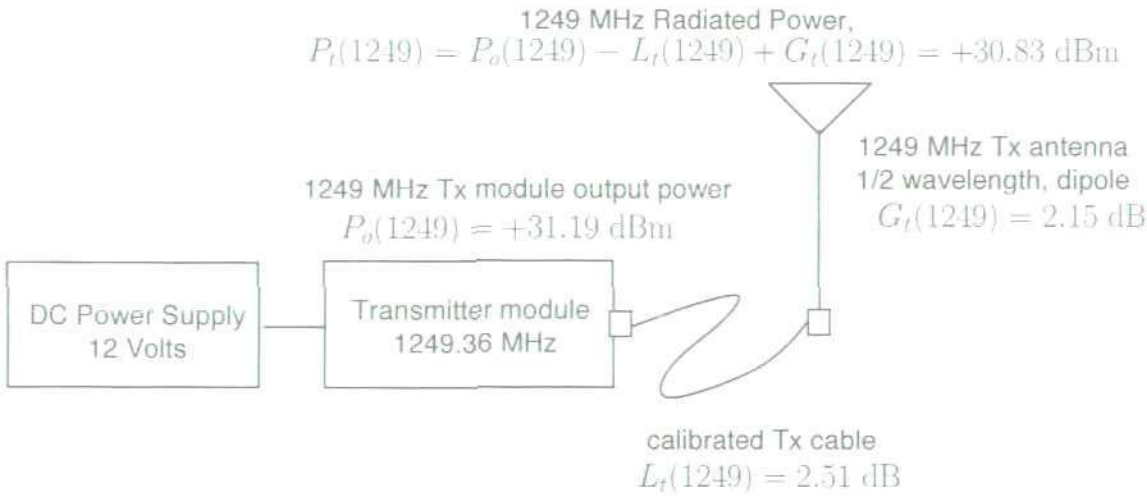


(a) 1249 MHz Transmitter block diagram

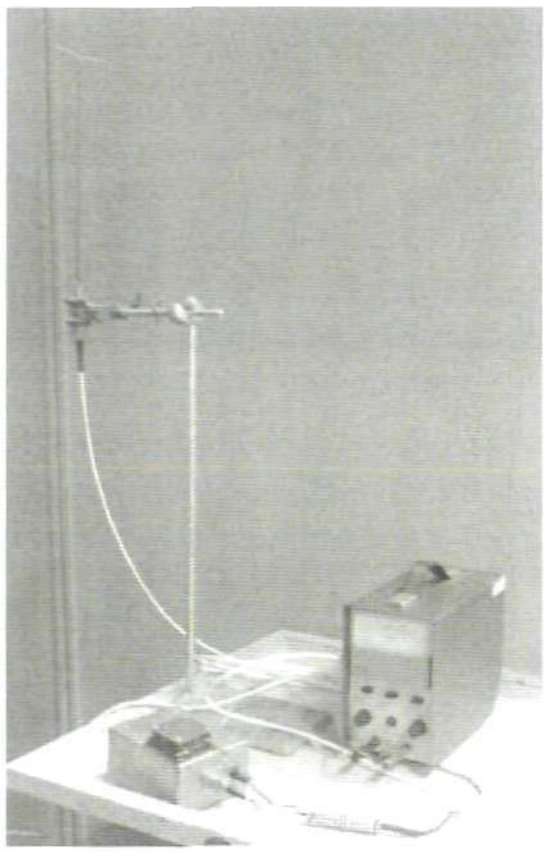

(b) Photo of the 1249 MHz transmitter apparatus arrangement on top of a trolley

Figure 7.5: 1249 MHz transmitter measurement apparatus

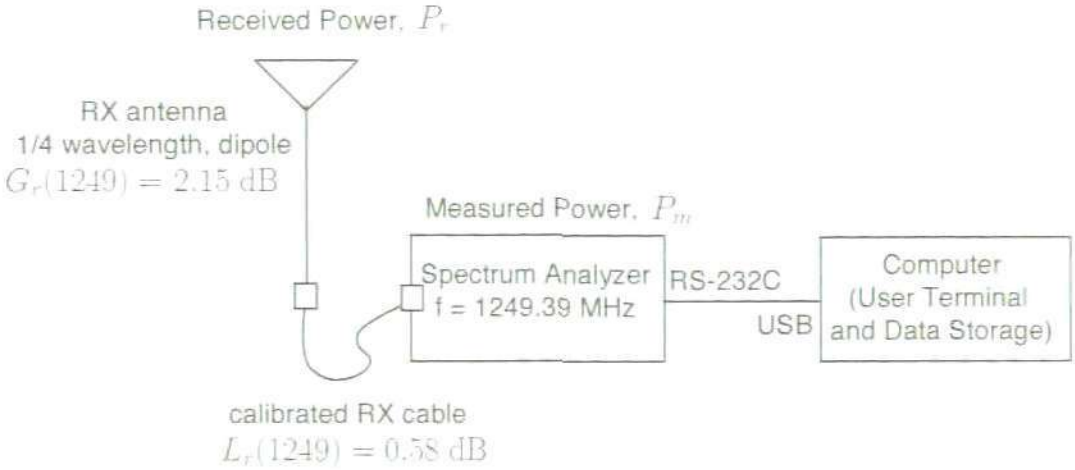


(a) 1249 MHz Receiver block diagram

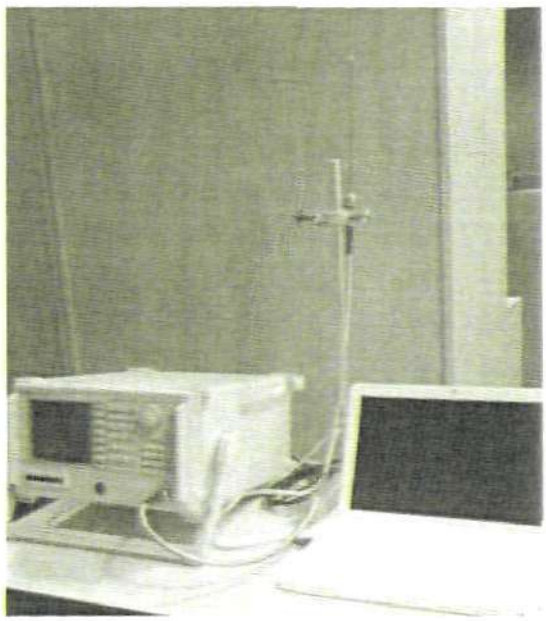

(b) Photo of the 1249 MHz receiver apparatus arrangement on top of a trolley

Figure 7.6: 1249 MHz receiver measurement apparatus

Table 7.1: Details of settings for 433 MHz, 869 MHz and 1249 MHz systems setup. $\lambda$ symbol denotes wavelength.

| Specifications | 433 MHz | 869 MHz | 1249 MHz |
|---|---|---|---|
| Carrier freq., MHz, $f$ | 433.9 | 869.49 | 1249.36 |
| Tx antenna type | 1/4 $\lambda$, whip | Helical | 1/2 $\lambda$, dipole |
| Height of Tx and Rx, m | 1.25 | 1.27 | 1.54 |
| Rx antenna type | Helical | 3/4 $\lambda$, whip | 1/2 $\lambda$, dipole |
| Tx output power, dBm | +21.12 | +24.25 | +31.19 |
| Transmit power, dBm | +21.12 | +24.25 | +28.68 |
| Total of antenna gains in dB, $G_{total}$ | 0.00 | 0.00 | 4.30 |
| Rx dynamic range | 0 to -80 dBm | 0 to -80 dBm | 0 to -80 dBm |
| Path loss limit, dB | 101.12 | 104.25 | 111.19 |
| Resolution Bandwidth, kHz | 30 | 30 | 30 |
| System cable losses in dB, $L_{total}$ | 1.27 | 2.14 | 3.09 |

Figure 7.7: Smeaton Building (SMB) from outside.

### 7.3.1 Smeaton Building (SMB)

The Smeaton Building (SMB) is a four story building that generally accommodates offices, laboratories and workshops. Even though it was built in 1950's, the building interior has been renovated several times since it was built. Therefore, some of interior materials are modern materials. The footprint of the SMB building is a rectangle with the dimensions of 83.5 $\times$ 19.2 meters. Therefore, it is chosen to represent a rectangular building for comparison of footprint shape effects on propagation path loss. Figure 7.7 shows a photo of the SMB Building taken from outside.

Except on the top floor, long and straight corridors connect both ends of the floors

where stairways and lifts are located in the building. The hallways have dimensions of 71.8 × 2.4 meters with a ceiling height of 2.9 meters above the floor.

The ground floor consists of offices and small-size workshops. The first floor and second floor contain computer facilities studios, teaching rooms and offices. The third floor is mainly for electronics laboratories.

The building frames are made of I-shaped steel beams and the floors are made of reinforced concrete.

While measurement activities were in progress, the transmitter (Tx) was located at one end of the second floor's hallway. The same location of Tx was used for measurements of all the choosen frequencies, 433 MHz, 869 MHz and 1249 MHz.

The receiver (Rx) was positioned at various locations within the SMB building. Due to access restrictions in some parts of the building, the whole of the top floor and rooms on the ground floor were excluded from the considered areas.

### 7.3.2 Babbage Building (BBG)

The Babbage Building (BBG) is a 1980's building. The building has five stories and a square shaped footprint. The dimension of the footprint are 39.1 × 39.1 meters. The materials of BBG building are concrete blocks for walls, and reinforced concrete for floors.

The ground floor consists of lecture theaters, teaching rooms and offices. The first floor is mostly allocated for open-access computer facilities halls and the remainder accommodates computer laboratories and teaching rooms. More computer laboratories and teaching rooms are on the second floor. The third floor is allocated for offices and staff training rooms. Several conference rooms, teaching rooms and a refectory are located on the fourth floor.

There is a corridor on each floor. The dimensions of the ground floor corridor is 2.1 meters width and 2.6 m of height; corridors on other floors are 2.1 meters wide and 2.3 meters high. The height of the corridor is the distance from the floor to the ceiling of the corridor.

For the 869 MHz and 1249 MHz measurements, the location of Tx was fixed in the corridor of the BBG fourth floor. The Rx was located at various locations in the corridors on each floor of the building. For the 433 MHz measurements, the location of Tx was fixed located in the third floor corridor. Areas that were covered by the 433 MHz Rx were

all in corridors except for the corridor on the top floor. Note that all measurements in the BBG are done within corridor areas.

### 7.3.3 Roland Levinsky Building (RLV)

The Roland Levinsky Building (RLV) is considered to be a modern building with modern materials and architecture. It was completely developed in 2008. The RLV building consists of two main structures that are attached to each others. The first structure of the building is a three story building and the second is a five story building. It is important to mention that the considered structure of the RLV was actually the three story building. The considered building consists of classrooms, theatres, art studios and offices.

The material that have been used in the RLV building are metals, concrete, wood boards and glass. The floors of RLV are made of reinforced concrete. The internal walls are made of wood boards, concrete blocks and glass.

The existence of an indoor atrium within the RLV building gives it a unique feature compared to the SMB and BBG buildings. At certain locations of the Tx, it is possible to have a Line-of-Sight (LOS) signal propagation path, even though the Rx and Tx are not on the same floor. Since an atrium within a building could sometimes be found in other common multi-floored buildings such as shopping complexes, hotels, airports, cinemas, theatres, etc. Thus, it is interesting to investigate the properties of path loss in such an environment. The indoor atrium of the RLV can be seen in Figure 7.8.

A transmitter location was chosen, and fixed for measurements at all frequencies. At all times, during the measurement activities, the Tx was located close to the atrium perimeter on the second floor. The photo in Figure 7.8 was taken with the photographer standing next to the transmitter. The receiver was located at various points within the building.

## 7.4 Measurement Procedures

At the start of all the measurement activities, the transmitters were located at an fixed position within the building. Locations of the transmitters are discussed in Section 7.3.

While, the Tx was continuously transmitting the signal, straight lines, which are also known as measurement tracks, are stretched on the floor of the area of interest. The length of each of the measurement tracks is varied due to the varying surroundings. Along each

Figure 7.8: The atrium of RLV

of measurement tracks, measurement points are marked, evenly spaced at approximately 0.25 meter intervals. It is important to mention that all measurement tracks, measurement points and the transmitter point are also drawn in an AutoCAD file of corresponding floor plan. This step is important as the drawings are required in order to find the relative coordinates of measurement points with respect to the transmitter point.

Starting at the first point on a track, the receiver measures and records received signal strength values at the measurement points and then moves to the next measurement point. The procedure is repeated until the last point is reached and for all measurement tracks.

At each measurement point, 10 samples of the signal strength reading are taken every 400 ms. Averaged signal strength value are then computed by averaging the sample readings in mW units. The same procedures are repeated for all measurement points.

## 7.5 Post-Measurement Data Processing

### 7.5.1 Spatial Averaging

As defined in [Andersen et al., 1995], path loss is a measure of the average RF attenuation within the measured environment, which is computed by spatially averaging the

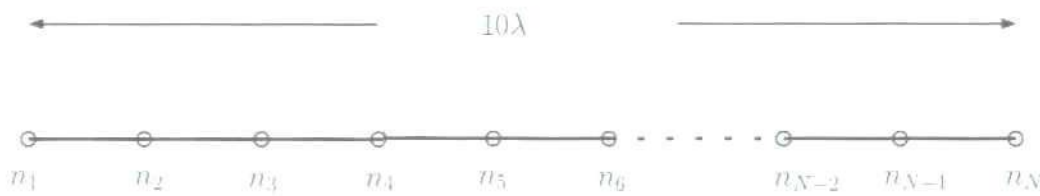


Figure 7.9: Spatial averaging over a $10\lambda$ segment

received signal strength over several wavelengths at the receivers. This procedure is called *spatial averaging* of the signal measurement. The averaging is purposely to eliminate or reduce the effect of small-scale fading, and it is commonly implemented in path loss analysis such as in [Valenzuela et al., 1997, Seidel and Rappaport, 1992, Xu et al., 2007] and others. In [Rappaport, 1996], it is mentioned that a segment length could be $5\lambda$ to $40\lambda$. In [Seidel and Rappaport, 1992, Xu et al., 2007], spatial averaging is done over a $20\lambda$ segmentation. However in [Valenzuela et al., 1997], it is mentioned that $10\lambda$ is the best compromise between removing fast fading effect and retaining the path loss fading pattern when the length is applied in sliding window averaging. Therefore, a segment length of $10\lambda$ is chosen for the spatial averaging procedure in this analysis. The lengths of the segment for 433 MHz, 869 MHz and 1249 MHz measurement tracks are equal to 6.9 meters, 3.45 meters and 2.4 meters respectively.

Local average signal measurement of a segment can be computed by finding the mean or median of the measurements within the segment. Since the median is less sensitive to the outliers [Weisstein, 2010], which in this case are deep fade measurements due to small-scale fading effects, the median is used to represent the local average of signal measurement. Furthermore, most of earlier literature has used median values in the analysis [Seidel and Rappaport, 1992, Phaiboon, 2002]. Therefore, the local average signal measurement of a segment is called *the local median*.

With the length of a segment equal to $10\lambda$ and given $N = n_1, \ldots, n_N$ is the sequence of measurement points within the segment, as shown in Figure 7.9, the local median signal measurement of the segment, $\tilde{X}$, is given as

$$\tilde{X} = \begin{cases} X_{(N+1)/2}, & \text{if} \quad N \text{ is odd} \\ \frac{1}{2}(X_{N/2} + X_{N/2+1}), & \text{if} \quad N \text{ is even} \end{cases} \tag{7.4}$$

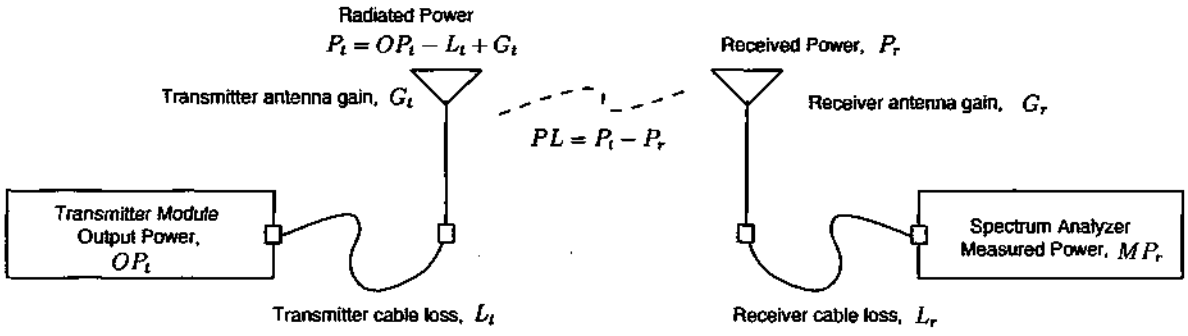


Figure 7.10: Variables of system link budget

where $X$ is the ordered series of $\mathcal{N}$.

Each local median is then assigned as the middle point of the respective segment.

### 7.5.2 Determining local median category: LOS or NLOS

Each local median is also categorised into an LOS or NLOS category. The category of a local median is decided based on the majority vote of measurement points category within the spatial averaging segment. If the majority of the measurement points within the segment are LOS, the local median of the corresponding segment is categorised as a LOS local median. Otherwise, the local median is categorised as a NLOS local median.

The category of the measurement points is decided based on the propagation type between the measurement point and the transmitter which is either LOS or NLOS. The transmitter and measurement point locations are mapped on the AutoCAD building plan; therefore the category of the measurement points could be decided by drawing a straight line from the transmitter point to the corresponding measurement point. If there is no obstruction between the two points, the measurement point is counted as a LOS measurement point. Otherwise, the measurement point is categorised as a NLOS measurement point.

### 7.5.3 Link Budget for Data Measurement

Regardless of the carrier frequency, Figure 7.10 shows variables that have been considered during the system link budget analysis. All variables are assumed in dB units. $OP_t$ is the output power of the transmitter module, $L_t$ and $L_r$ are transmitter cable loss and receiver cable loss respectively, $G_t$ and $G_r$ are the transmitter antenna gain and receiver antenna gain respectively, $P_t$ is the radiated power from the transmitter antenna, $P_r$ is power

received at the receiver antenna, $PL$ is path (propagation) loss and $\tilde{X}$ is local median received power of a segment that has been computed earlier using Equation 7.4.

$PL$ in this analysis refers to local path loss, which is the propagation loss between transmitter antenna and the middle points of a segment. The local path loss of a segment is calculated using

$$\begin{aligned} PL &= P_t - P_r \\ &= OP_t - L_t + G_t - [\tilde{X} + L_r - G_r] \\ &= OP_t - \tilde{X} - (L_t + L_r) + (G_t + G_r) \\ &= OP_t - \tilde{X} - L_{total} + G_{total} \end{aligned} \tag{7.5}$$

Values of $OP_t, L_{total}$ and $G_{total}$ for each measurement configuration are given in Table 7.1.

Along with local path loss values, other information such as transmitter-receiver distance (T-R Distance) and number of obstructed floors between transmitter and receiver are presented.

## 7.6 Path Loss Prediction within multi-floored building at 433 MHz, 869 MHz and 1249 MHz

### 7.6.1 Log-Distance Path Loss Model

A commonly used model to predict mean path loss with known T-R Distance , $d$, for an indoor environment is given by

$$\overline{PL}(d)\,[\text{dB}] = A(d_0)\,[\text{dB}] + 10n\log_{10}\left(\frac{d}{d_0}\right) \tag{7.6}$$

where $d_0$ is the reference distance, $\overline{PL}$ is mean path loss, $A(d_0)$ is path loss when Tx and Rx separation distance is $d_0$ , $n$ is the path loss exponent of the environment and $d$ is the T-R distance. For an indoor environment $d_0$ is commonly equal to 1 meter. The value of $A(d_0)$ can be found either by averaging the radial measurements surrounding the transmitter or using the Free Space Path Loss Model ( Equation 7.3). Equation 7.6 will be shown to be a straight line when it is plotted against $d$ on a log-scale. As an example, Figure 7.11(a) and Figure 7.11(b) show the plot of Equation 7.6 with $d$ on linear scale

and log scale respectively. For both figures, it is assumed that environment type is a free space environment ($n = 2$) with the carrier frequency, $f = 433.9$ MHz.

Note that Equation 7.6 is actually predicts the mean of path loss.However in the real world, actual path loss values vary about the mean. This is due to the shadow effect from the surrounding structures and objects. In [Hashemi, 1993], it has been mentioned that shadowed path loss could be modelled as a Log-Normal random variable about the mean. As implemented in [Seidel and Rappaport, 1992], the previously mentioned mean path loss prediction models could be extended to predict shadowed path loss using

$$PL(d)\,[\text{dB}] = \overline{PL}\,[\text{dB}] + X_\sigma\,[\text{dB}] \tag{7.7}$$

where $PL(d)$ is shadowed path loss at a transmitter and receiver separation distance $d$, and $X$ is a log-normal random variable with standard deviation of $\sigma$; $X$ and $\sigma$ are dB units. If (7.6) is inserted into (7.7), the equation is then written as

$$PL(d)\,[\text{dB}] = A(d_0)\,[\text{dB}] + 10\,n\log_{10}\left(\frac{d}{d_0}\right) + X_\sigma\,[\text{dB}] \tag{7.8}$$

The value of $n$ actually relates to the propagation environment. Variation of $n$ values could be associated with various properties of indoor propagation such as the number of obstructed floors for multi floor propagation, the number of obstructed walls, room and corridor environment for indoor layout scope, etc. As applied in [Seidel and Rappaport, 1992, Phaiboon, 2002], (7.6) with different $n$ values was used to predict the path loss within multi floor buildings. $n$ values are linked to number of obstructed floors between transmitter and receiver. Therefore, the model could be written as

$$PL(d)\,[\text{dB}] = A(d_0)\,[\text{dB}] + 10\,n_F\log_{10}\left(\frac{d}{d_0}\right) \tag{7.9}$$

where $F$ denotes number of obstructed floors between transmitter and receiver. If both transmitter and receiver are on the same floor, which means there is no obstructed floor between Tx and Rx, then $F = 0$. Thus the shadowed path loss model is written as

$$PL(d)\,[\text{dB}] = A(d_0)\,[\text{dB}] + 10\,n_F\log_{10}\left(\frac{d}{d_0}\right) + X_\sigma\,[\text{dB}] \tag{7.10}$$

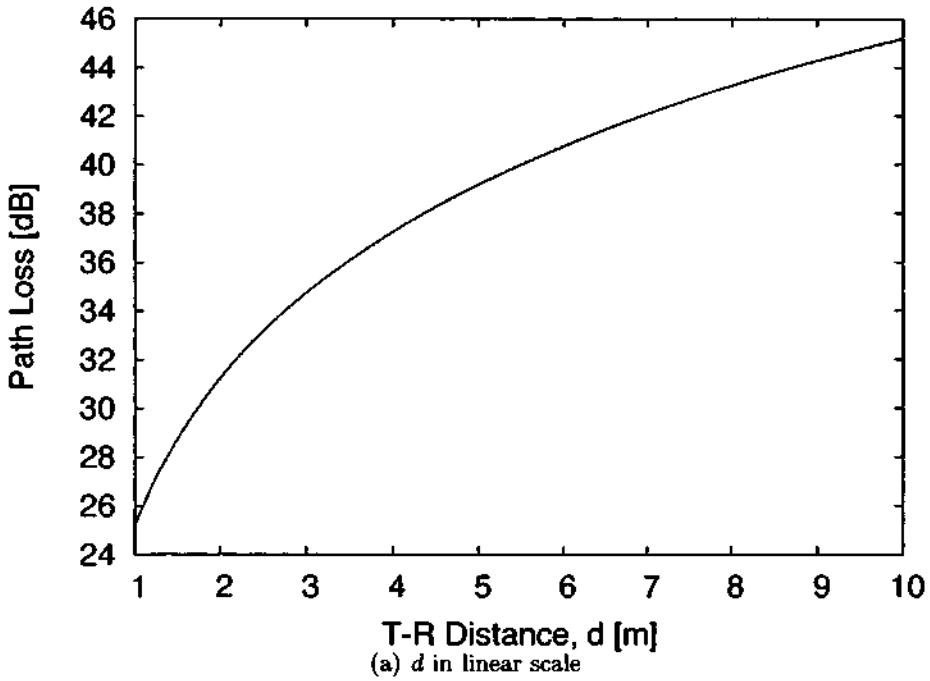


(a) $d$ in linear scale

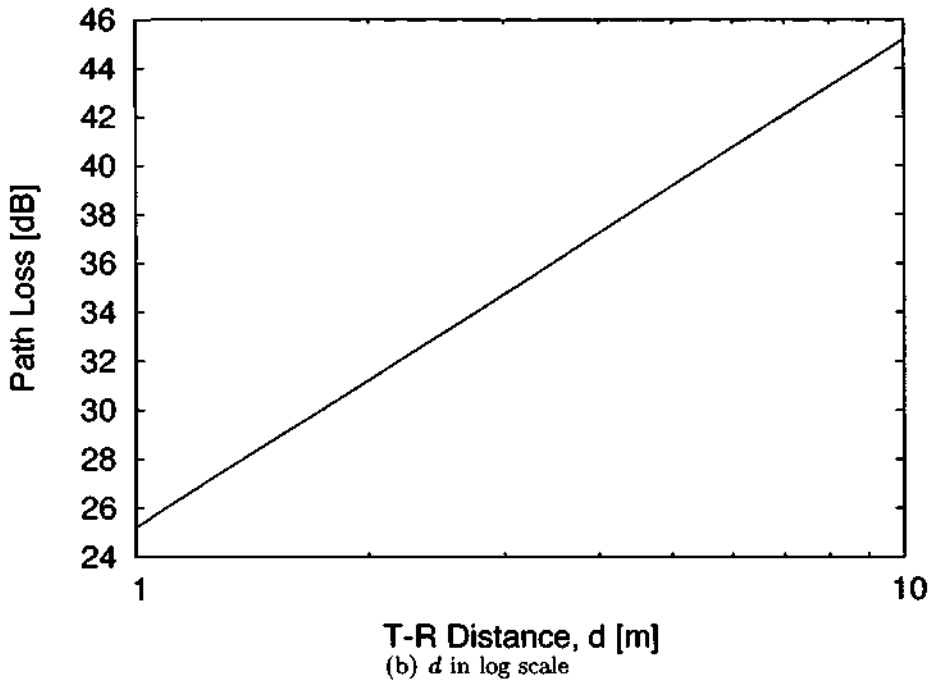


(b) $d$ in log scale

Figure 7.11: Plot of free space path loss at 433.9 MHz on linear-scale and log-scale. $A(d_0) = 25.19$ dB.

Table 7.2: Free Space Path Loss at reference distance, $d_0 = 1$ meter. Note that system losses and gains are assumed to be equal to 1.

| Carrier Frequency, $f$ MHz | $G_t$ | $G_r$ | $L$ | Free Space Path Loss, $PL_0(d_0 = 1)$ dB |
|---|---|---|---|---|
| 433.9 | 1 | 1 | 1 | 25.19 |
| 869.5 | 1 | 1 | 1 | 31.23 |
| 1249.4 | 1 | 1 | 1 | 34.38 |

In order to provide model parameters that are relevant to 433 MHz, 869 MHz and 1249 MHz carrier frequencies, $n$ and $\sigma$ parameters values have to be derived from measurement data. In preparation for that, path losses at the reference distance, $A(d_0)$, for each frequencies are computed with reference distance, $d_0 = 1$ m. Values of $A(d_0)$ are calculated using the Friis free space path loss given by Equation 7.3. It is important to mention that the reference distance of 1 meter is beyond the far-field distance of each systems and only measurement data with Tx and Rx distance higher than $d_0$ are considered in the derivation of parameter values. This means that only measurement data in the far-field region are considered in deriving the parameter values. For a fair comparison between different frequencies, the $A(d_0)$ for all frequencies are calculated with total system loss and total system gains equal to unity ($L = G_t = G_r = 1$). Values of $A(d_0)$ at 433 MHz, 869 MHz and 1249 MHz are equal to 25.19 dB, 31.23 dB and 34.38 dB respectively. These figures are also presented in Table 7.2.

Values of $n$ are found by implementing linear regression analysis using a Least Square Error method. When $A(d_0)$ is the fixed y-intercept for the regression line as implemented in [Seidel and Rappaport, 1992] and [Affandi et al., 1999], the value of $n$, which is the slope of the regression line that fits the measured data points, is found by using the equation below,

$$n = \frac{\sum_{i=1}^{N} x_i PL_i - A(d_0) \sum_{i=1}^{N} x_i}{\sum_{i=1}^{N} x_i^2}. \tag{7.11}$$

where $N$ is the number of data points in the considered dataset, $x_i$ is the logarithm of separation distance between transmitter and $i$-th local path loss point ($x_i = \log_{10} d_i$) and $PL_i$ is the $i$-th local path loss value. The derivation of Equation 7.11 is given in Appendix D.

Since shadowed path loss could be modelled as a Log-Normal random variable with a certain standard deviation, $\sigma$, the same dataset can be used to find the $n$; the value of $\sigma$

is found using

$$\sigma = \sqrt{\frac{1}{N}\sum_{i=1}^{N}(PL(d_i) - \overline{PL}(d_i))^2} \tag{7.12}$$

where $PL(d_i)$ is the $i$-th local path loss and $\overline{PL}(d_i)$ is the predicted mean path loss at transmitter and receiver distance = $d_i$, respectively.

Values of $n$ and $\sigma$ that have been derived from 433 MHz, 869 MHz and 1249 MHz measurement data are presented in Table 7.3, Table 7.4 and Table 7.5, respectively. The last column in each table, shows the number of local path losses that were considered during the derivation of the model parameters; "-" indicates that there is no measurement data collected from the corresponding categories. Derivation of parameter values has been done for two model categories, ie Corridor and Whole-Floor models. Corridor model parameters were derived from datasets that only considered measurement data from corridor areas of the corresponding floor. Whole-floor model parameters were derived from datasets that considered all measurement on the corresponding floor. This included measurement data of corridors and room measurements. In these tables, parameters of the Whole Floor model are written in brackets.

Comparison between Whole-floor and Corridor parameters has found that $n$ for the Whole-floor model is consistently higher than $n$ for the Corridor model. This result is believed to be due to signals propagating within whole floor environment experiencing more obstruction and attenuation from objects within the floor such as pillars, walls and furniture.

Strong correlation is found between $n$ values and number of crossed floors for all buildings and categories. $n$ is found to be proportional to the number of crossed floors. This pattern was expected as similar patterns have been found by other researchers such as in [Seidel and Rappaport, 1992, Phaiboon, 2002].

An interesting environment within the SMB is the corridor area of the second floor. With both transmitter and receiver in the same corridor area, wave propagation between the transmitter and the receiver is categorised as waveguided propagation and LOS. In Table 7.3, Table 7.4 and Table 7.5, the corresponding environment is labelled as SMB(i)-Corridor. In each table, $n$ of the SMB(i)-Corridor environment is always the lowest when compared to the $n$ of other environments. In fact, the $n$ of 869 and 1249 MHz are found to be less than 2 (free space environment). These figures are not surprising results, since

$n < 2$ within a waveguided environments had also been reported in earlier literature such as in [Saleh and Valenzuela, 1987, Rappaport, 1996].

Furthermore, a consistent correlation between values of $n$ and carrier frequency is also observed within the SMB-Corridor(i) environment. As shown in the parameter tables, the path loss exponents of environment SMB(i)-Corridor are 2.32, 1.50 and 1.45 for 433 MHz, 869 MHz and 1249 MHz, respectively. This leads to a conclusion that within a straight corridor where the type of transmission is LOS, the path loss exponent decreases as the frequency increases. In [Yamaguchi et al., 1986], Yamaguchi made a similar observation that supports the above conclusion. Yamaguchi's experiments were done in corridors and in an underground pedestrian street. Yamaguchi found the attenuation constant, which is related to the path loss exponent, as also decreased as the frequency increases (for carrier frequency lower than 2 GHz). As concluded in Yamaguchi's work, it is believed that the decreasing pattern will become an inverse pattern within 2 GHz - 5 GHz frequency range.

Regarding the values of $\sigma$, it is generally found that $\sigma$ values decrease as the number of obstructed floors increases within the SMB and BBG. Most of $\sigma$ values of the Same Floor category, are found to be the highest $\sigma$ compared to $\sigma$ for transmissions being obstructed by floors. As the number of obstructed floors increases, $\sigma$ values gradually decrease. This is true for both Corridor and Whole-floor models. These results seem to agree with the findings in [Turkmani et al., 1987, Turkmani and Parsons, 1988], where the $\sigma$ values of within building propagation were found to be strongly dependant on the nature of its transmission, ie it is either totally NLOS, partially LOS or totally LOS. $\sigma$ were equal to 4 dB, 6.7 dB and 8.9 dB for NLOS, partial LOS and totally LOS, respectively. In contrast for the RLV, $\sigma$ of Same Floor are found to be the lowest and $\sigma$ values of One Floor Obstruction are found to be the highest. This irregular pattern is believed to be due to the existence of the atrium structure within the building.

Values of $\sigma$ and carrier frequency do not show any consistent pattern.

Plots of mean path loss predicted using Equation 7.10 (Log-Distance Path Loss Model) versus measurement data are given in Appendix E.

### Building Footprint and Indoor Path Loss

It is interesting to compare the results shown in Table 7.3, Table 7.4 and Table 7.5 based on the shape of building footprint. Particularly, this comparison is between the SMB

Table 7.3: The mean path loss exponent, $n$, and standard deviation, $\sigma$, for use in Log-Distance Path Loss Model based on a measurement at a carrier frequency of 433 MHz

| | | Corridor (Whole Floor) | | |
|---|---|---|---|---|
| | | $n$ | $\sigma$[dB] | Locations |
| SMB: | | | | |
| i. | Same Floor | 2.32 (2.79) | 3.8 (8.8) | 9 (23) |
| ii. | 1 Floor Obstruction | 3.44 (3.82) | 3.7 (5.4) | 9 (21) |
| iii. | 2 Floors Obstruction | 4.35 (-) | 3.3 (-) | 6 (-) |
| BBG: | | | | |
| i. | Same Floor | 3.51 (-) | 4.6 (-) | 5 (-) |
| ii. | 1 Floor Obstruction | 4.63 (-) | 3.8 (-) | 9 (-) |
| iii. | 2 Floors Obstruction | 5.20(-) | 1.3 (-) | 5 (-) |
| iv. | 3 Floors Obstruction | 5.68(-) | 3.0 (-) | 5 (-) |
| v. | 4 Floors Obstruction | No Data | No Data | No Data |
| RLV: | | | | |
| i. | Same Floor | 2.68 (2.79) | 3.2 (2.7) | 6 (13) |
| ii. | 1 Floor Obstruction | 3.10 (3.51) | 8.4(9.7) | 8(12) |
| iii. | 2 Floors Obstruction | 3.25 (3.54) | 8.2 (7.9) | 12 (22) |

Table 7.4: The mean path loss exponent, $n$, and standard deviation, $\sigma$, for use in Log-Distance Path Loss Model based on a measurement at a carrier frequency of 869 MHz

| | | Corridor (Whole Floor) | | |
|---|---|---|---|---|
| | | $n$ | $\sigma$[dB] | Locations |
| SMB: | | | | |
| i. | Same Floor | 1.50 (2.28) | 4.5 (10.9) | 18 (64) |
| ii. | 1 Floor Obstruction | 3.06 (3.42) | 3.0 (4.7) | 19 (54) |
| iii. | 2 Floors Obstruction | 3.81 (-) | 2.8 (-) | 18 (-) |
| BBG: | | | | |
| i. | Same Floor | 2.85(-) | 3.7 (-) | 11 (-) |
| ii. | 1 Floor Obstruction | 4.17(-) | 4.9 (-) | 12 (-) |
| iii. | 2 Floors Obstruction | 4.93(-) | 3.1 (-) | 18 (-) |
| iv. | 3 Floors Obstruction | 5.33(-) | 2.6 (-) | 12 (-) |
| v. | 4 Floors Obstruction | 5.50(-) | 0.7 (-) | 4 (-) |
| RLV: | | | | |
| i. | Same Floor | 2.32 (2.41) | 3.2 (2.9) | 11 (25) |
| ii. | 1 Floor Obstruction | 2.49 (3.01) | 7.7 (12.0) | 20 (28) |
| iii. | 2 Floors Obstruction | 2.83 (3.18) | 7.9 (8.4) | 27 (50) |

Table 7.5: The mean path loss exponent, $n$, and standard deviation, $\sigma$, for use in Log-Distance Path Loss Model based on a measurement at a carrier frequency of 1249 MHz

| | | Corridor (Whole Floor) | | |
|---|---|---|---|---|
| | | $n$ | $\sigma$[dB] | Locations |
| SMB: | | | | |
| i. | Same Floor | 1.45(2.22) | 3.8 (13.3) | 27 (86) |
| ii. | 1 Floor Obstruction | 3.21 (3.65) | 3.3 (6.3) | 27 (72) |
| iii. | 2 Floors Obstruction | 3.90 (-) | 3.2 (-) | 25 (-) |
| BBG: | | | | |
| i. | Same Floor | 3.07(-) | 7.6 (-) | 18 (-) |
| ii. | 1 Floor Obstruction | 4.45(-) | 4.3 (-) | 18 (-) |
| iii. | 2 Floors Obstruction | 5.30(-) | 4.0 (-) | 26 (-) |
| iv. | 3 Floors Obstruction | 5.73(-) | 3.8 (-) | 20 (-) |
| v. | 4 Floors Obstruction | 5.87(-) | 3.2 (-) | 10(-) |
| RLV: | | | | |
| i. | Same Floor | 2.32 (2.44) | 3.6 (3.9) | 19 (37) |
| ii. | 1 Floor Obstruction | 2.57 (3.05) | 7.4 (11.1) | 29 (41) |
| iii. | 2 Floors Obstruction | 2.87 (3.24) | 10.1 (10.1) | 40 (67) |

and BBG, as the former represents a rectangular footprint office building and the latter represents a square footprint office building. From the $n$ parameters of all frequencies, it is clearly found that the $n$ parameter values of BBG are always higher than the $n$ parameters of SMB. This leads to a conclusion that signals are attenuated at higher rate within a square footprint office building than in a rectangular office building.

For the RLV, it is found that the path loss exponents are always the lowest ones in the context of multi-floor transmission. This behavior is probably best explained by the existence of an atrium within the RLV which can be considered as a vertical wave guide structure allowing the signal to travel between floors. Furthermore, with location of Tx being on the edge of the atrium, direct signal paths between Tx and Rx are possible for multi-floor transmission. This is believed to a cause higher average received power within the RLV as compared to the other considered buildings, even though the Tx and Rx are in a multi-floored environment with the same number of floor differences.

### 7.6.2 Floor Attenuation Factor (FAF) Model

An alternative model that could be used to predict mean path loss within a multifloor building is called the Floor Attenuation Factor (FAF) Model [Seidel and Rappaport, 1992]. With the FAF model, instead of having an independent $n$ associated with the number of obstructed floors, as in (7.10), $n$ of the Same Floor is applied in 7.6 and the result is added

with a factor that relates to the number of crossed floors that exist between transmitter and receiver. The $FAF$ values are found by calculating the average difference between the mean path loss of the Same Floor and the local path loss of corresponding floors. The unit of $FAF$ is Decibles (dB). The $FAF$ requires the path loss prediction model to be written as

$$PL_{FAF}(d)\,[\text{dB}] = A(d_0)\,[\text{dB}] + 10 \times n(SameFloor) \times \log_{10}\left(\frac{d}{d_0}\right) + FAF_i\,[\text{dB}] \quad (7.13)$$

where $FAF_i$ is the floor attenuation factor when number of obstructed floors is equal to $i$, $n(SameFloor)$ is the path loss exponent for the Same Floor category of the building, $A(d_0)$ is the free space path loss at a reference distance and $d$ is the separation distance of transmitter and receiver.

If the shadowed path loss is required to be predicted, Equation 7.13 should be inserted into Equation 7.7. The extended equation is then written as

$$PL_{FAF}(d)\,[\text{dB}] = A(d_0)\,[\text{dB}] + 10 \times n(SameFloor) \times \log_{10}\left(\frac{d}{d_0}\right) + FAF_{MF}\,[\text{dB}] + X_\sigma\,[\text{dB}] \quad (7.14)$$

Values of $FAF$ and $\sigma$ at 433 MHz, 869 MHz and 1249 MHz for use in 7.13 and 7.14 are given in Table 7.6, Table 7.7 and Table 7.8, respectively. Parameters were derived based on two dataset categories: Corridor and Whole Floor datasets. Parameters of the Whole Floor model are presented in brackets. Standard deviations, $\sigma$, are found by calculating the average difference between predicted mean path loss using (7.13) and the local path loss of the corresponding floor.

From the measurement data of SMB corridors, the FAF of 1 Floor Obstruction at 433 MHz, 869 MHz and 1249 MHz are 9.5 dB, 11.2 dB and 14.8 dB respectively. When the number of obstructing floors increases to two floors, the $FAF$ for the same categories increases to 20.5, 22.2 and 24.8 dB, which means the loss caused by the second floor is as much as 11 dB at 433 MHz and 869 MHz, and 10 dB at 1249 MHz.

From the measurement data of the BBG corridors, the losses due to one floor obstructions are equal to 12.1, 12.5 and 13.3 dB at 433 MHz, 869 and 1249 MHz, respectively. With two floor obstructions, the FAF are found to be 17.5, 23.2 and 25.2 dB, with independent losses due to the second floor equal to 5.4, 10.7 and 11.9 dB. Three floor obstruction

*FAFs* are 24.8, 28.1 and 30.4, with independent losses due to the third floor being 7.3, 4.9 and 5.2 dB. For four floor obstruction, the *FAFs* are 31.0 and 33.4 dB for 869 MHz and 1249 MHz respectively. Independent losses of the fourth floor are 2.9 and 3 dB for 869 and 1249 MHz respectively. There is no data for four floor obstruction at 433 MHz. When comparison is made between Corridor *FAF* values of SMB and BBG for first two floor obstructions, generally, it is found that the floor losses of the BBG are slightly higher than floor losses of the SMB building. There is an agreement between the results and the statement in [Andersen et al., 1995] that mentions attenuation between floors within square footprint building being higher than if the building was rectangular.

The *FAF* values of RLV are found to be lower than the *FAF* values of the SMB and BBG. This is especially true for the corridor datasets, which are 5.5, 2.3 and 2.8 dB for 433 MHz, 869 MHz and 1249 MHz respectively. This irregularity is believed to be due to the atrium environment which allows LOS and NLOS propagation between Tx and Rx. The received powers of the LOS paths, which are higher than NLOS paths received powers, contribute to the higher average signal strength and therefore reduce the average path loss experienced within the floor.

Overall, it is found that the values of *FAF* increase as the number of obstructed floor increases for all buildings. The loss for first floor obstructions was found being the highest compared to subsequent floors within the BBG and SMB. Interestingly, it is found that the independent losses of subsequent floors decrease non-linearly as number of floors increases. These observations have been reported in [Seidel and Rappaport, 1992] and [Phaiboon, 2002]. As an example to support the finding, Figure 7.12 shows the plot of predicted mean path loss using the FAF Model at 869 MHz and the corresponding measured local path loss, within the BBG. It is seen that the independent losses of each of the BBG floors are 12.5, 10.7, 4.9 and 2.9 dB for obstructions due to floors one to four respectively.

Another interesting relationship that has been observed from the results is that the FAF values are found to be correlated to the carrier frequency within buildings with no indoor atrium, such as SMB and BBG. Values of FAF are found to increase as the frequency increases within the SMB and BBG. An obvious example can be seen from the comparison of FAF values of 1 Floor Obstruction within SMB corridors for all considered frequencies. The values of FAF at433 MHz, 869 and 1249 MHz are equal to 9.5 dB, 11.2

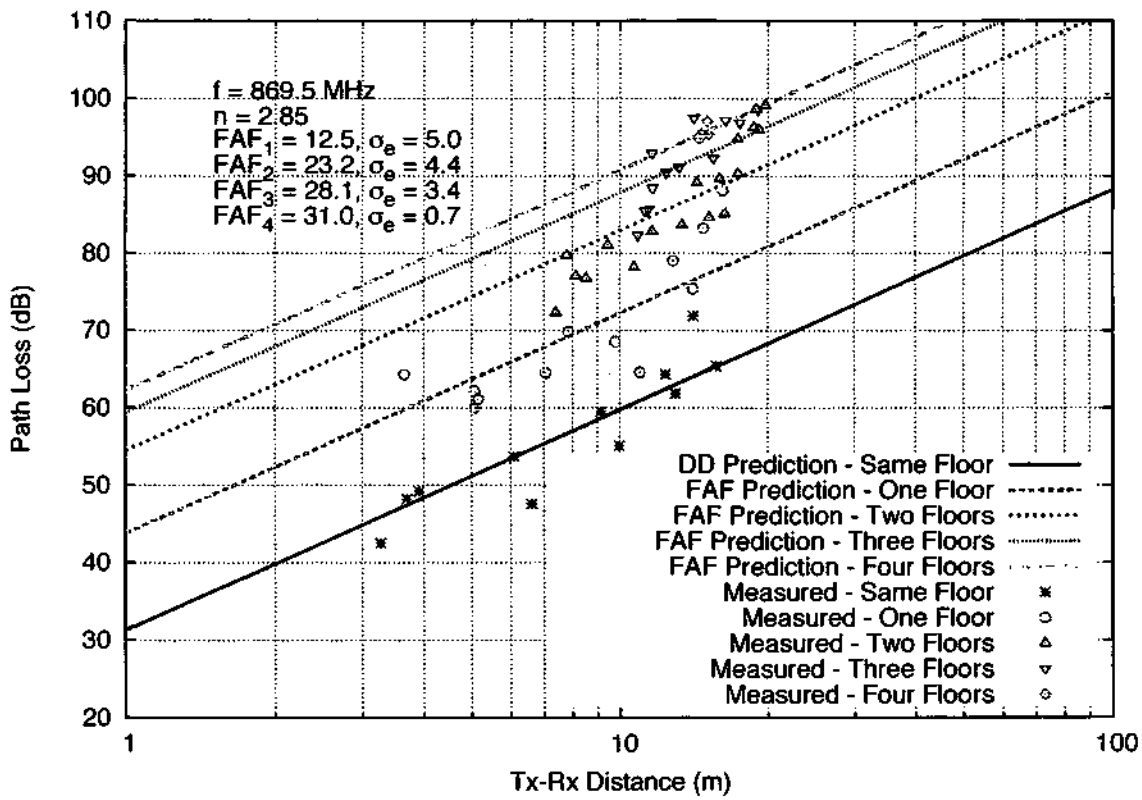


Figure 7.12: Mean path loss of FAF model and measured local path loss of BBG corridors at 869 MHz. Notice that FAF values are a nonlinear function of the number of obstructed floors.

Table 7.6: Parameters to be used in FAF Model at 433 MHz

| | | FAF [dB] Corridor (Whole Floor) | $\sigma$ [dB] |
|---|---|---|---|
| Building 1: | | | |
| | 1 Floor Obstruction | 9.5 (14.3) | 3.0 (5.5) |
| | 2 Floors Obstruction | 20.5 (-) | 0.9 (-) |
| Building 2 : | | | |
| | 1 Floor Obstruction | 12.1 (-) | 3.6 (-) |
| | 2 Floors Obstruction | 17.5 (-) | 1.7 (-) |
| | 3 Floors Obstruction | 24.8 (-) | 2.2 (-) |
| Building 3: | | | |
| | 1 Floor Obstruction | 5.5 (10.0) | 7.5 (9.0) |
| | 2 Floors Obstruction | 6.5 (10.1) | 7.6 (7.4) |

Table 7.7: Parameters to be used in FAF model at 869 MHZ

| | | FAF [dB] Corridor (Whole Floor) | $\sigma$ [dB] |
|---|---|---|---|
| Building 1: | | | |
| | 1 Floor Obstruction | 11.2 (16.5) | 3.5 (5.2) |
| | 2 Floors Obstruction | 22.2 (-) | 3.6 (-) |
| Building 2 : | | | |
| | 1 Floor Obstruction | 12.5 (-) | 5.0 (-) |
| | 2 Floors Obstruction | 23.2 (-) | 4.4 (-) |
| | 3 Floors Obstruction | 28.1 (-) | 3.4 (-) |
| | 4 Floors Obstruction | 31.0 (-) | 0.7 (-) |
| Building 3: | | | |
| | 1 Floor Obstruction | 2.3 ( 8.4) | 7.4 (11.7) |
| | 2 Floors Obstruction | 6.2 (10.6) | 7.4 (8.0) |

dB and 14.8 dB respectively.

In term of $\sigma$ values, there is no strong correlation between $\sigma$ and the number of obstructed floors or carrier frequency. However, values of $\sigma$ seem to be related to the type of transmission being either LOS or NLOS. It is found that $\sigma$ are higher when there is LOS data in the datasets. As shown in Table 7.6, Table 7.7 and Table 7.8, $\sigma$ of the RLV are found to be higher than the $\sigma$ of the other buildings. This finding shows an agreement with the conclusion given in [Turkmani et al., 1987, Turkmani and Parsons, 1988], which found that $\sigma$ values are equal to 4, 6.7 and 8.9 dB for NLOS, partial LOS and totally LOS, respectively.

Table 7.8: Parameters to be used in FAF model at 1249 MHZ

| | | FAF [dB] Corridor (Whole Floor) | $\sigma$ [dB] |
|---|---|---|---|
| Building 1: | | | |
| | 1 Floor Obstruction | 14.8 (20.9) | 2.6 (5.8) |
| | 2 Floors Obstruction | 24.8 (-) | 3.9 (-) |
| Building 2: | | | |
| | 1 Floor Obstruction | 13.3 (-) | 4.5 (-) |
| | 2 Floors Obstruction | 25.2 (-) | 5.8 (-) |
| | 3 Floors Obstruction | 30.4 (-) | 4.8 (-) |
| | 4 Floors Obstruction | 33.4 (-) | 3.5 (-) |
| Building 3: | | | |
| | 1 Floor Obstruction | 2.8 (8.4) | 7.0 (10.8) |
| | 2 Floors Obstruction | 7.1 (11.1) | 9.0 (9.1) |

## 7.7 Prediction of Indoor Path Loss for buildings with atrium

Values of $\sigma$ could be considered to indicate the accuracy of the model. Since $\sigma$ does indicate how widely the prediction values spread from the mean, thus lower values of $\sigma$ mean better accuracy of prediction. As shown in the Log-Distance Model parameter tables (Table 7.3 - 7.5) and Floor Attenuation Model parameter tables (Table 7.6 - 7.8), it is seen that the sigma values of multifloor propagation within the RLV are quite obviously higher than the sigma values of the SMB and BBG, regardless of the carrier frequencies used. This is believed to be due to the layout of the RLV building which has an indoor atrium. Since the locations of Tx within the RLV building are on the edge of the atrium, LOS and NLOS propagation paths are possible between the Tx and some locations of the Rx in multi floor transmission. This is not possible for the other two buildings, BBG and SMB, where all of multifloor propagations are NLOS paths. Thus the received power measured for multifloor propagation within the RLV is actually a combination of LOS and NLOS signal strength measurements. This causes the distribution of measured signal strengths to be widely distributed from its mean, thus affecting the prediction accuracy of the (7.10) and (7.13) models. For example, Figure 7.13 below shows the scattered points of measured signal strength within the RLV at 1249 MHz, with the Tx on the Second Floor and the Rx at various locations within the First Floor. Scattered points of measured signal strength are categorised into LOS and NLOS, as indicated in the figure. Procedures for categorising the data points are described in Section 7.5.2. The straight line indicates the FAF model mean path loss with the corresponding parameters as given in Table 7.8:

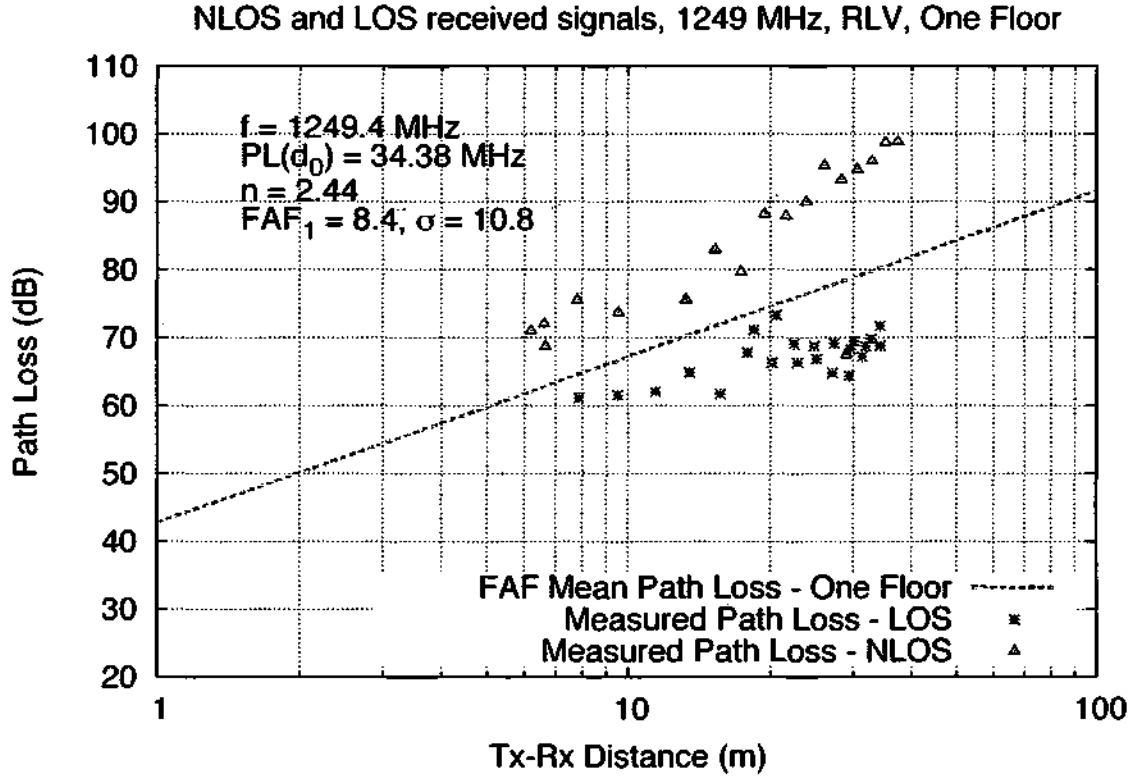


Figure 7.13: NLOS and LOS measured received signal strength at 1249 MHz for RLV One Floor propagation.

$n = 2.44$, $FAF = 8.4$ dB, $PL_{d_0} = 34.38$ dB. It is clearly shown that the data are widely spread with $\sigma = 10.8$ dB from the mean line due to obvious differences between NLOS and LOS received signal strengths. Based on this observation, it is believed that the path loss prediction should be done separately for NLOS and LOS paths within the environment in order to reduce the value of $\sigma$.

Therefore, a model is proposed to improve accuracy of path loss prediction for use in a building with an atrium and a Tx location that allows LOS and NLOS propagation paths between Tx and Rx. Prediction of path loss is done by considering the types of propagation path between Tx and Rx. Prediction of path loss for same floor transmission is retained by using the Log-Distance model with $n$ values of Same Floor that have already been derived from the building. However, for multi-floor transmission, a model to predict mean of path loss is proposed as

$$\overline{PL}(d) = PL_0(d_0) + 10 \times n(\text{Same Floor}) \times \log_{10}\left(\frac{d}{d_0}\right) + \gamma\,(los)\,, \qquad (7.15)$$

with

$$\gamma\,(los) = \left\{ \begin{array}{ll} 0 & \text{if} \quad los = 1 \\ \text{AF(NLOS)} & \text{otherwise} \end{array} \right),$$

where $n$(Same Floor) is the Same Floor mean path loss exponent, $PL_0(d_0)$ is the free space path loss at reference distance $d_0$ and $d$ is distance between Tx and Rx. AF(NLOS) is the attenuation factor in dB. *los* is a binary flag which belongs to a local segment that determines the appropriate $\gamma$ value to be applied in the model. $los = 1$ if the majority of the measurement points in the corresponding segment are LOS, and vice versa. If $los = 1$, $\gamma = 0$ will be applied in the model; otherwise, $\gamma$ = AF(NLOS). AF(NLOS) is the average of difference between the mean of Same Floor predicted path losses and local path loss of NLOS local segments of the corresponding floor. Note that the Whole-Floor dataset is considered in the AF(NLOS) derivation.

Values of AF(NLOS), standard deviation of the difference between predicted path losses and measured local path losses, and the number of local segments used to derive the statistics are given in Table 7.9. AF(NLOS) are found to be higher than FAF for the corresponding floor. This is because the AF(NLOS) are less influenced by LOS path losses, which gives a more realistic attenuation factor caused by the floor. Notice that the AF(NLOS) are more comparable with the FAF parameters of buildings without an atrium. At 433 MHz, the attenuation factors with one floor and two floor obstruction are found to be 18.6 dB and 13.7 dB respectively. The corresponding attenuation factors for 869 MHz are 22.1 dB and 13.5 dB respectively, and, 19.2 dB and 15.0 dB are for 1249 MHz, respectively. It is interesting to find that the average path loss for a one floor obstruction is higher than the average path loss for two floors obstruction within a building with indoor atrium. This is probably due to most of the signal paths that propagate through the atrium being guided and reflected by the atrium structure into the ground floor instead of into the first floor of the RLV.

The last column of Table 7.9 shows that the standard deviations of differences between local path losses and predicted path losses are reduced. This indicates that the proposed model has achieved better prediction accuracy for multi-floor transmission within buildings with an atrium. As an example, Figure 7.14 shows measured local path losses and means of path losses that are predicted using (7.15) at a carrier frequency of 1249 MHz for One Floor Obstruction within RLV. In this environment, $\sigma$ has been reduced to 5.1 dB from

Table 7.9: NLOS Attenuation Factors in Decibels

| Carrier Frequency | | AF(NLOS) (dB) | Number of Locations | $\sigma$ (dB) |
|---|---|---|---|---|
| 433 MHz | 1 Floor Obstruction | 18.6 | 6 | 2.7 |
| | 2 Floors Obstruction | 13.7 | 16 | 4.6 |
| 869 MHz | 1 Floor Obstruction | 22.1 | 11 | 4.0 |
| | 2 Floors Obstruction | 13.5 | 39 | 5.7 |
| 1249 MHz | 1 Floor Obstruction | 19.2 | 18 | 5.1 |
| | 2 Floors Obstruction | 15.0 | 50 | 6.2 |

11.1 dB and 10.8 dB in Log-Distance and Floor Attenuation Factor models respectively.

It is an interesting finding that the LOS path loss is closely predicted with $\gamma = 0$, or equivalently by the Log-Distance Model with $n = n(\text{Same Floor})$. This finding has shown that the Log-Distance with Same Floor path loss exponent is more accurate than the Free Space Path Loss model for predicting the path loss of LOS propagation between transmitter and receiver within a multifloor environment with an indoor atrium.

## 7.8 Summary

In this chapter, large scale propagation characteristics of the indoor environments of multi-floor buildings have been investigated at three different UHF carrier frequencies, 433 MHz, 869 MHz and 1249 MHz. For each frequency, comprehensive received signal strength measurements were made within three different University of Plymouth multifloor office buildings, Smeaton Building (SMB), Babbage Building (BBG) and Roland Levinsky Building (RLV). The SMB and BBG are buildings with a rectangular footprint and square footprint, respectively. The RLV building is a multifloor building with an indoor atrium.

Parameters used in modelling the path loss within various types of propagation environment, such as LOS and waveguided, same floor and multi-floor have been derived from the measurement data.

In addition to providing the parameters from linear best fit analysis, parameters for two common path loss prediction models, the Log-Distance Path Loss Model and the Floor Attenuation Floor Model, were derived independently from the measurement data. Generally, it is found within all buildings and for all considered frequencies, the path loss rate increases as the number of floor obstructions between transmitter and receiver

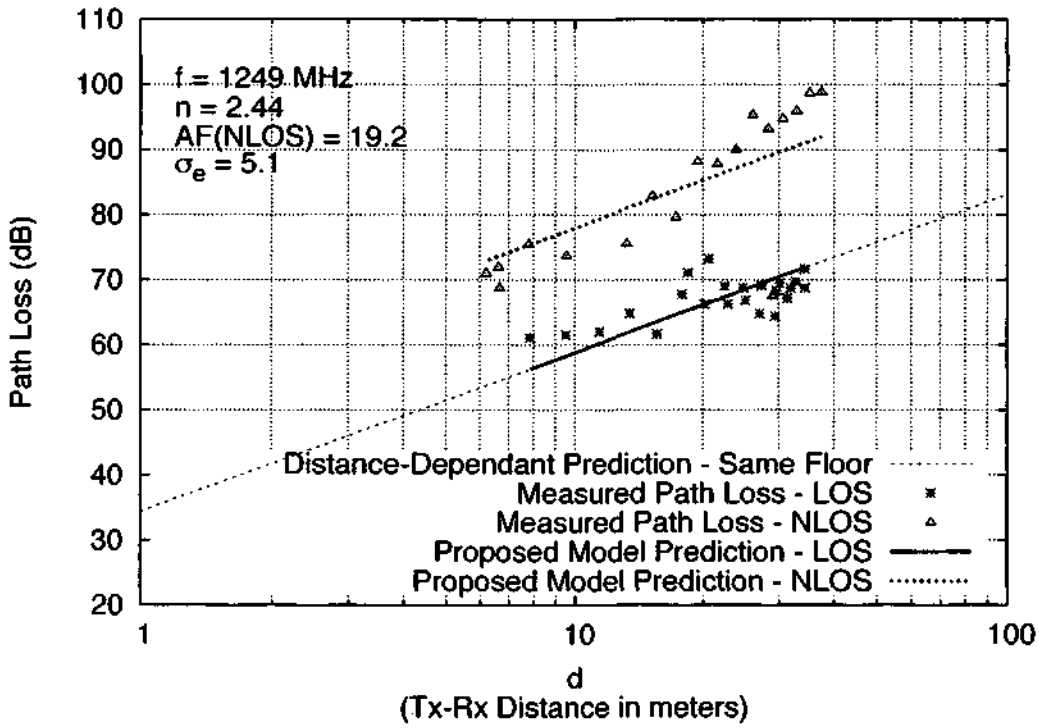


Figure 7.14: Prediction of mean path loss using (7.15) at 1249 MHz for One Floor Obstruction within RLV.

increases. Path loss rates were found to be higher in the square footprint building (BBG) than in the rectangular footprint building (SMB). The RLV building indoor environment, with the presence of an indoor atrium, is found to be less attenuating to the wireless signal compared to the other two buildings for multifloor propagation. Analysis of the FAF model parameters has concluded that the attenuation caused by floors does have a correlation with the carrier frequency used. Higher floor attenuations are observed at higher frequencies.

In the environment where there is a waveguided corridor environment with no obstruction between Tx and Rx, higher frequencies are believed to be an advantage within such an environment. In addition to its higher bandwidth features, it is found that the path loss exponent slightly decreases as the carrier frequencies increase.

A frequency of 433 MHz has better penetration capability than the other higher frequencies. This is seen from its lower path loss level for multi-floor propagation with the number of floor obstructions being greater than two.

Overall, it is found that the 869 MHz frequency is the best among the other two considered frequencies. This is at least true for same floor propagation and up to two floors obstruction for multifloor propagation. Also, the path loss rate at 869 MHz is lower

in most of propagation environments and scenarios with Log-Distance parameter analysis. Supremacy of the 869 MHz frequency over the other considered frequencies is supported by the results of a linear best fit analysis on the measurement data. Even though the levels of path losses at 869 MHz and 433 MHz are at about similar level, 869 MHz is still better than the 433 MHz due to its higher bandwidth properties.

Finally, an extension to the Log-Distance Path Loss model has been proposed that could be used for predicting the path losses around an atrium area within multifloor buildings. Since there are situations where the type of propagation between transmitter and receiver could be a mixture of LOS and NLOS around the atrium area, a new model has been derived by considering the type of propagation in the measurement data. A new attenuation factor, which is called the NLOS attenuation factor, is introduced and derived by categorising measurement data into the two categories, LOS and NLOS. The model shows an improvement in the prediction accuracy compared to both of the considered existing path loss prediction models. It is also found that the Log-Distance path loss model with a path loss exponent of same floor environment is suitable for predicting LOS path losses surrounding the atrium area.

Plots of mean path loss of Log-Distance, Floor Attenuation Factor and proposed models are shown in Appendix E.

# Chapter 8

# Conclusion, Specific Contributions and Future Research Recommendations

## 8.1 Conclusion

From the review in Chapter 2, it is concluded that mobile systems have evolved from hybrid, analogue and digital systems, into totally digital systems. Also, capacity and performance of mobile systems is improved. With improvements of capacity and performance, recent mobile systems are now be able to offer voice and video conversations and web browsing services. These advanced services are now being offered along with improved conventional mobile services such as voice conversation and text messaging services. Greater system requirements in term of system capacity, transmission speed and cost efficiency are some of properties required by next generation mobile systems.

In Chapter 3, the capacity of a Flat Rayleigh fading channel with hard decision decoding has been derived from integration of the Binary Symmetric Channel capacity equation and the probability density function of received SNR per bit of a Flat Rayleigh fading channel. Comparison between the two hard decision channel capacities, AWGN and Flat Rayleigh Fading, has shown that loss due to fading increases exponentially. Analysis of power loss due to hard decision decoding is done for an AWGN channel. The maximum limit of loss due to hard decision decoding is known to be 1.97 dB. Loss due to hard

decision decoding decreases exponentially as SNR per bit increases. From this, it is found that if SNR per bit is above 5 dB, the loss due to hard decision decoding over AWGN channel is less than 1 dB. It is concluded that hard decision is a better choice at high SNR per bit. This is because hard decision decoding is usually less complex than soft decision decoding.

In Chapter 4, a literature study of error performance of general linear block codes is done. Performance of a block code is mainly determined by Hamming distance between codewords. Higher Hamming distance results in lower probability of a given codeword being decoded as another valid codeword. The lower bound of error probability of a linear block code could be calculated if the distribution of Hamming weight of the code is known. For a simpler and looser estimation of error probability of the code, the minimum Hamming distance could be used as the input parameter. This bound is considered as upper bound of error probability of the code.

In Chapter 5, a rule of correlator construction is found to optimize correlator length in wireless channel impulse response measurement. In the environment where maximum excess delay of the channel impulse response is known earlier, a shorter correlator could be constructed by concatenating some parts of the unique word, or CAZAC sequence. Implementation of a shorter correlator could reduce the computation requirement for estimating the channel impulse response by the receiver. This will lead to faster channel estimation and lower power consumption especially for mobile terminals or devices.

The result of simulation in Chapter 6 has shown that performance of a channel coding scheme that consists of [136,68,24] Double Circulant Code encoder and Dorsch List decoder is significantly degraded by multipath fading and ISI effects of the SUI-5 channel. Poor performance of the system over SUI-5 channel is believed to be due to poor performance of the Zero Forcing equalizer that was applied. Application of other types of equalizer is recommended for future investigation.

In Chapter 7, indoor path loss in three multifloor buildings has been investigated at three UHF band frequencies. The considered frequencies are 433 MHz, 869 MHz and 1249 MHz. An extensive series of on-site received signal strength measurements has been done at each of considered frequencies within all three buildings. From the measurement data, parameter values for two existing indoor path loss prediction models, Log-Distance Path Loss Model and Floor Attenuation Factor Path Loss Model, have been derived for

use at 433 MHz, 869 MHz and 1249 MHz. Parameter value comparisons of a square footprint office building and a rectangular footprint building has found that signal power is attenuated at higher rate within the square footprint building as the distance between transmitter and receiver increases. It is also found that floor obstructions increase path loss of indoor signals. This is shown by values of path loss exponent and floor attenuation factor of Log-Distance Path Loss and Floor Attenuation Factor models respectively. Both parameters are found to increase as the number of floor obstructions between transmitter and receiver increases.

It is well known that path loss is distributed about its mean by following a Log-Normal distribution. The degree of its distribution is indicated by the standard deviation of the distribution, $\sigma$. Higher $\sigma$ means path losses are widely distributed from the mean. In [Turkmani et al., 1987] and [Turkmani and Parsons, 1988], $\sigma$ values are found to be related to the type of propagation between transmitter and receiver; either it is LOS, partially NLOS or totally NLOS. Higher $\sigma$ was found if transmitter and receiver in LOS to each other. Lowest $\sigma$ was found if transmitter and receiver are totally NLOS. Similarly, in this study, $\sigma$ values were found to be high within the same floor environment, with $\sigma$ getting smaller as the number of obstructing floors increases. This has drawn a conclusion that the $\sigma$ value is related to level of obstruction and attenuation between transmitter and receiver. It is important to notice that this conclusion is valid for common multifloor buildings which have no indoor atrium. Within the building having an indoor atrium, the standard deviation, of path loss distribution from its mean is higher for multifloor transmission than same floor transmission.

It is also concluded that higher frequency signals tend to attenuate at a lower rate than lower frequency signals if the environment is a waveguided environment and LOS propagation paths occur between transmitter and receiver.

It is also concluded that the accuracy of path loss prediction within a multifloor building and atrium area could be increased by grouping measurement data into LOS and NLOS categories. From this idea, a new path loss prediction formula is proposed in Chapter 7. The formula is useful to estimate indoor path loss within multifloor buildings with the existence of an indoor atrium. Furthermore, it is found Log-Distance with path loss exponent of the Same Floor environment is better suited than the Free Space Path Loss model, to predict LOS path loss. For the case of the NLOS area, it is found that path loss

within middle floor is higher than path loss within ground floors.

## 8.2 Specific Original Contributions

The list below specifies eight specific original contributions to the knowledge and practice made by the thesis.

1. Figure 3.8 and Figure 3.9 present a new way of describing the power loss due to hard decision decoding and fading, respectively.

2. Section 5.3 describes a novel and more efficient method of channel estimation.

3. The performance of a [136,68,24] Double Circulant Code with Dorsch List Decoding has been measured over an SUI-5 channel for the first time in Chapter 6.

4. Table 7.3, Table 7.4 and Table 7.5 present novel parameter values of Log-Distance Path Loss Prediction Model for use during indoor path loss prediction at carrier frequencies of 433 MHz, 869 MHz and 1249 MHz, respectively.

5. Table 7.6, Table 7.7 and Table 7.8 present novel parameter values of Floor Attenuation Factor Path Loss Prediction Model for use during indoor path loss prediction at carrier frequencies of 433 MHz, 869 MHz and 1249 MHz, respectively.

6. In Section 7.7, a new path-loss prediction model has been formulated for indoor environments.

7. In comparing square footprint and rectangular footprint buildings in Chapter 7, it is found that the average signal attenuation was less in the rectangular building.

8. In Chapter 7, for multifloor propagation, the attenuation within the building with the vertical atrium is less than the attenuation within the two more traditional buildings.

## 8.3 Future Research Recommendations

During this study, there are several questions that have not been answered and several potential research direction have been recognised. These are listed below for future and potential research programmes.

1. It is well-known that shadowed path losses are distributed log-normally from the mean with a certain value of standard deviation, $\sigma$. From earlier literature and results of this work, it is concluded that $\sigma$ is related to the level of obstruction and attenuation between transmitter and receiver. It would be useful if there were explanations of the relationship between $\sigma$ values and obstructions from surroundings such as the number of obstructing floors between transmitter and receiver.

2. A rule of correlator construction has been proposed in Chapter 5 to produce a shortened correlator. It would be interesting to measure the performance and efficiency of the shortened correlator if it is applied in on-site experiments in a real environment.

3. It would be useful to find the most suitable equaliser that performs best over the SUI-5 channel by applying different types of equaliser in the simulation model in Chapter 6.

4. In Chapter 7, loss due to first floor obstruction is generally found being the highest, and independent losses due to subsequent floors decrease non-linearly. Explanation of this phenomenon could potentially be used in the derivation of a theoretical path loss prediction model, like a ray-tracing model, that considers path reflections and path penetrations.

# Appendix A

# Approximation of Rayleigh Fading bit error probability

The average error probability of a coded bit, $P_c$, with mean SNR per bit is given as $\frac{E_c}{N_0}$, over Rayleigh Fading channel is given as:

$$P_c = \frac{1}{2}\left(1 - \sqrt{\frac{E_c/N_0}{1+E_c/N_0}}\right) = \frac{1}{2}(1-\alpha) \tag{A.1}$$

where $\alpha = \sqrt{\frac{E_c/N0}{1+E_c/N0}}$. Then, taking the $\alpha$, it can be simplified to

$$\alpha = \sqrt{\frac{E_c/N_0}{1+E_c/N_0}} = \sqrt{\frac{1}{\frac{1}{E_c/N_0}+1}} = \frac{1}{(x+1)^{1/2}} = (1+x)^{-1/2} \tag{A.2}$$

where $x = \frac{1}{E_c/N_0}$ .

Using Binomial Series theorem gives,

$$(1+x)^n = 1 + nx + n(n-1)\frac{x^2}{2!} + n(n-1)(n-2)\frac{x^3}{3!} + \ldots \tag{A.3}$$

with the condition that $x < 1$ in order for the series to converge. Therefore, the condition

in terms of $E_c/N_0$ in dB is given as,

$$\begin{aligned} x &< 1 \\ \frac{1}{E_c/N_0} &< 1 \\ 1 &< E_c/N_0 \\ 10\log_{10}(1) &< 10\log_{10}(E_c/N_0) \\ 0 &< E_c/N_0 \ (dB) \\ E_c/N_0 \ (dB) &> 0 \end{aligned} \tag{A.4}$$

Then using the Binomial series above, $\alpha$ is approximated as below,

$$(1+x)^{-1/2} \approx 1 + \frac{-1}{2}x = 1 + \frac{-x}{2} = 1 - \frac{x}{2} \tag{A.5}$$

Since the approximation of $\alpha$ is done using only the first order of $x$, the approximation is converging at $E_c/N_0 \gg 0$ dB. Therefore, this approximation is true at $E_c/N_0 \gg 0$ dB.

Finally, the error probability of a channel bit over a Rayleigh Fading channel at $E_c/N_0 \gg 0$ dB can be approximated as,

$$\begin{aligned} P_c &= \frac{1}{2}(1-\alpha) \\ &= \frac{1}{2}\left(1-(1+x)^{-1/2}\right) \\ &\approx \frac{1}{2}\left(1-1+\frac{x}{2}\right) = \frac{1}{2}\left(\frac{x}{2}\right) = \frac{1}{4E_c/N_0} \end{aligned} \tag{A.6}$$

# Appendix B

# Error probability of Rayleigh Fading channel with diversity

Assuming that the frequency diversity is used, with L channels of diversity. Instantaneous signal energy on the $k$-th channel, is denoted as $E_k(t)$, and mean signal energy is denoted as $E(E_k(t)) = E$. Instantaneous fading and noise on $k$-th channel are denoted as $\alpha_k(t)$ and $n_k(t)$ respectively. $n_k^2(t) = N_k(t)$ is the instantaneous noise power of $k$-th channel and the mean of the noise power of $k$-th channel is denoted as $E(N_k(t)) = N$. The means of noise powers of each channel are equal. The fading and noise of each channel are statistically independent from each other.

Then, at the receiver side, assume that the channel fading is known and the applied combining technique is Maximal Ratio Combining (MRC). Using MRC, the received signal of each channel will be multiplied by the signal weight $\beta_k(t)$ which is denoted as

$$\beta_k(t) = \frac{\alpha_k^*(t)}{\sum_{x=1}^{L} \alpha_x(t)} \tag{B.1}$$

where $k = 1 \ldots L$ and $\alpha_k^*(t)$ is the complex conjugate of the signal fading $\alpha_k(t)$. The purpose of this multiplication is to weight and correct the phase of the received signal and thus maximize the SNR per bit of the signal.

Therefore, the SNR of received signal in the $k$-th channel is given as,

$$\gamma_k = \frac{E(\alpha_k \beta_k)^2}{N \beta_k^2} \tag{B.2}$$

After weighting, all signals are combined and the mean SNR per bit is given as,

$$\begin{aligned}\gamma_b &= \frac{E(\sum_{k=1}^{L}\alpha_k\beta_k)^2}{N\sum_{k=1}^{L}\beta_k^2} \\ &= \frac{E}{N}\frac{(\sum_{k=1}^{L}\alpha_k\beta_k)^2}{\sum_{k=1}^{L}\beta_k^2}\end{aligned} \tag{B.3}$$

In order to find $P_{bd}$, the bit error probability when diversity is applied as described above, the probability density function of $\gamma_b$ and the bit error probability function with known SNR per bit, $P_b$ can be integrated together as below,

$$P_{bd} = \int_0^\infty P_b(\gamma_b)pdf(\gamma_b)d\gamma_b \tag{B.4}$$

It is well known that, the probability of bit error if BPSK is used with a known SNR per bit, $\gamma_b$, is given as $P_b = \frac{1}{2}\text{erfc}(\sqrt{\gamma_b})$. Also, the pdf of the SNR per bit with L diversity branches over RFC is given by a Chi Square distribution with 2L degrees of freedom [Proakis, 2000].

$$pdf(\gamma_b) = \frac{1}{(L-1)!\bar{\gamma}_k{}^L}\gamma_b^{L-1}e^{-\gamma_b/\bar{\gamma}_k} \tag{B.5}$$

where $\bar{\gamma}_k = E(\alpha_k^2)E/N$ is the mean SNR per diversity channel.

As a result of the integration above, a closed form solution [Proakis, 2000] is found as

$$P_{bd} = \left(\frac{1-\mu}{2}\right)^L \sum_{k=0}^{L-1}\binom{L-1+k}{k}\left(\frac{1+\mu}{2}\right)^k \tag{B.6}$$

where $\mu = \sqrt{\bar{\gamma}_k/(1+\bar{\gamma}_k)}$.

# Appendix C

# Weight Distribution of Well-known Linear Block Codes

| Codeword Weight | Frequency |
|---|---|
| 0 | 1 |
| 7 | 253 |
| 8 | 506 |
| 11 | 1288 |
| 12 | 1288 |
| 15 | 506 |
| 16 | 253 |
| 23 | 1 |

Table C.1: Golay (23,12,7) weight distribution [Proakis, 2000]

| Codeword Weight | Frequency |
|---|---|
| 0 | 1 |
| 8 | 759 |
| 12 | 2576 |
| 16 | 759 |
| 24 | 1 |

Table C.2: Extended Golay (24,12,8) weight distribution [Proakis, 2000]

| Codeword Weight | Frequency |
|---|---|
| 0 | 1 |
| 21 | 41910 |
| 22 | 201930 |
| 23 | 1285494 |
| 24 | 5570474 |
| 25 | 21935186 |
| 26 | 86053422 |
| 27 | 323695568 |
| 28 | 1156055600 |
| 29 | 3886222860 |
| 30 | 12694994676 |
| 31 | 40367970699 |
| 32 | 121103912097 |
| 33 | 343251594420 |
| 34 | 948989702220 |
| 35 | 2561207717808 |
| 36 | 6545308612176 |
| 37 | 15848161044534 |
| 38 | 37535118263370 |
| 39 | 87006465675570 |
| 40 | 191414224486254 |
| 41 | 399875059409826 |
| 42 | 818791788315358 |
| 43 | 1644029128439104 |
| 44 | 3138601063383744 |
| 45 | 5699222325214544 |
| 46 | 10159483275382448 |
| 47 | 17784631560497592 |
| 48 | 29641052600829320 |
| 49 | 47047728573239600 |
| 50 | 73394456574253776 |
| 51 | 112556289078227904 |
| 52 | 164505345575871552 |
| 53 | 229181426369623980 |
| 54 | 314063436136151380 |
| 55 | 423412378312496636 |
| 56 | 544387343544638532 |
| 57 | 667583388554723748 |
| 58 | 805704089635011420 |
| 59 | 957102895925873760 |
| 60 | 1084716615382656928 |
| 61 | 1172938586845599112 |
| 62 | 1248612044061444216 |
| 63 | 1308537943108455059 |
| 64 | 1308537943108455059 |
| 65 | 1248612044061444216 |
| 66 | 1172938586845599112 |
| 67 | 1084716615382656928 |
| 68 | 957102895925873760 |
| 69 | 805704089635011420 |
| 70 | 667583388554723748 |
| 71 | 544387343544638532 |
| 72 | 423412378312496636 |
| 73 | 314063436136151380 |
| 74 | 229181426369623980 |
| 75 | 164505345575871552 |
| 76 | 112556289078227904 |
| 77 | 73394456574253776 |
| 78 | 47047728573239600 |
| 79 | 29641052600829320 |
| 80 | 17784631560497592 |
| 81 | 10159483275382448 |
| 82 | 5699222325214544 |
| 83 | 3138601063383744 |
| 84 | 1644029128439104 |
| 85 | 818791788315358 |
| 86 | 399875059409826 |
| 87 | 191414224486254 |
| 88 | 87006465675570 |
| 89 | 37535118263370 |
| 90 | 15848161044534 |
| 91 | 6545308612176 |
| 92 | 2561207717808 |
| 93 | 948989702220 |
| 94 | 343251594420 |
| 95 | 121103912097 |
| 96 | 40367970699 |
| 97 | 12694994676 |
| 98 | 3886222860 |
| 99 | 1156055600 |
| 100 | 323695568 |
| 101 | 86053422 |
| 102 | 21935186 |
| 103 | 5570474 |
| 104 | 1285494 |
| 105 | 201930 |
| 106 | 41910 |
| 127 | 1 |

Table C.3: BCH (127,64,21) weight distribution [Weight Distribution, ]

| Codeword Weight | Frequency |
|---|---|
| 0 | 1 |
| 22 | 243840 |
| 24 | 6855968 |
| 26 | 107988608 |
| 28 | 1479751168 |
| 30 | 16581217536 |
| 32 | 161471882796 |
| 34 | 1292241296640 |
| 36 | 9106516329984 |
| 38 | 53383279307904 |
| 40 | 278420690161824 |
| 42 | 1218666847725184 |
| 44 | 4782630191822848 |
| 46 | 15858705600596992 |
| 48 | 47425684161326912 |
| 50 | 120442185147493376 |
| 52 | 277061634654099456 |
| 54 | 543244862505775360 |
| 56 | 967799721857135168 |
| 58 | 1473287478189735168 |
| 60 | 2041819511308530688 |
| 62 | 2421550630907043328 |
| 64 | 2617075886216910118 |
| 66 | 2421550630907043328 |
| 68 | 2041819511308530688 |
| 70 | 1473287478189735168 |
| 72 | 967799721857135168 |
| 74 | 543244862505775360 |
| 76 | 277061634654099456 |
| 78 | 120442185147493376 |
| 80 | 47425684161326912 |
| 82 | 15858705600596992 |
| 84 | 4782630191822848 |
| 86 | 1218666847725184 |
| 88 | 278420690161824 |
| 90 | 53383279307904 |
| 92 | 9106516329984 |
| 94 | 1292241296640 |
| 96 | 161471882796 |
| 98 | 16581217536 |
| 100 | 1479751168 |
| 102 | 107988608 |
| 104 | 6855968 |
| 106 | 243840 |
| 128 | 1 |

Table C.4: Extended BCH (128,64,22) weight distribution [Desaki et al., 1997]

# Appendix D

# Derivation of linear regression slope, $m$, with fixed Y-intercept

Given a set of $N$ scattered points $p_{i=1}^{N} = p_1, p_2, \ldots, p_{N-1}, p_N$, where each of the $p_i = (x_i, y_i)$, where $x_i$ and $y_i$ are the x-coordinate and y-coordinate of point $p_i$ respectively. A line that represents the linear regression of the data is a straight line: therefore, it is represented by $\bar{y} = mx + c$, where $m$ is the slope of the linear regression line and $c$ is the interception point of the linear regression line to the y-axis. With the value of $c$ constrained to be a fixed constant, and the linear regression line fulfilling the Minimum Squared Error (MSE) condition, the equation of the linear regression line for the dataset can be found with $m$ values calculated using,

$$m = \frac{\sum_{i=1}^{N} x_i y_i - c\sum_{i=1}^{N} x_i}{\sum_{i=1}^{N} x_i^2}. \tag{D.1}$$

Starting with the definition of Squared Error ($SE$) of the dataset, which is given by:

$$\begin{aligned} SE &= \sum_{i=1}^{N} (y_i - \bar{y_i})^2 \\ &= \sum_{i=1}^{N} (y_i - mx_i - c)^2 \end{aligned}$$

The value of $m$ that fulfills the Minimum Square Error (MSE) fitting criteria is derived

as below,

$$
\begin{aligned}
\frac{\delta SE}{\delta m} &= 0 \\
\frac{\delta}{\delta m}\sum_{i=1}^{N}(y_i - mx_i - c)^2 &= 0 \\
\sum_{i=1}^{N} 2(y_i - mx_i - c) \times -x_i &= 0 \\
2\sum_{i=1}^{N}(-x_i y_i + mx_i^2 + cx_i) &= 0 \\
\sum_{i=1}^{N}(-x_i y_i + mx_i^2 + cx_i) &= 0 \\
\sum_{i=1}^{N} -x_i y_i + \sum_{i=1}^{N} mx_i^2 + \sum_{i=1}^{N} cx_i &= 0 \\
\sum_{i=1}^{N} mx_i^2 &= \sum_{i=1}^{N} x_i y_i - c\sum_{i=1}^{N} x_i \\
m &= \frac{\sum_{i=1}^{N} x_i y_i - c\sum_{i=1}^{N} x_i}{\sum_{i=1}^{N} x_i^2}
\end{aligned}
\tag{D.2}
$$

# Appendix E

# Plots of Measured and Modelled Path Losses

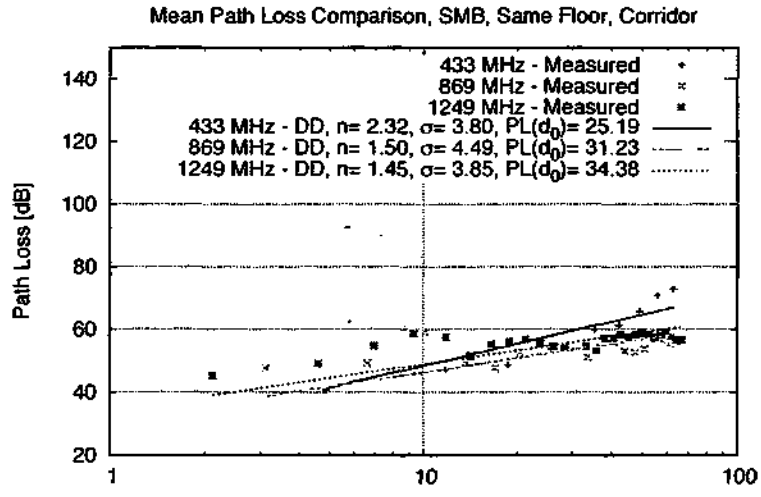


(a) SMB Corridor, Same Floor

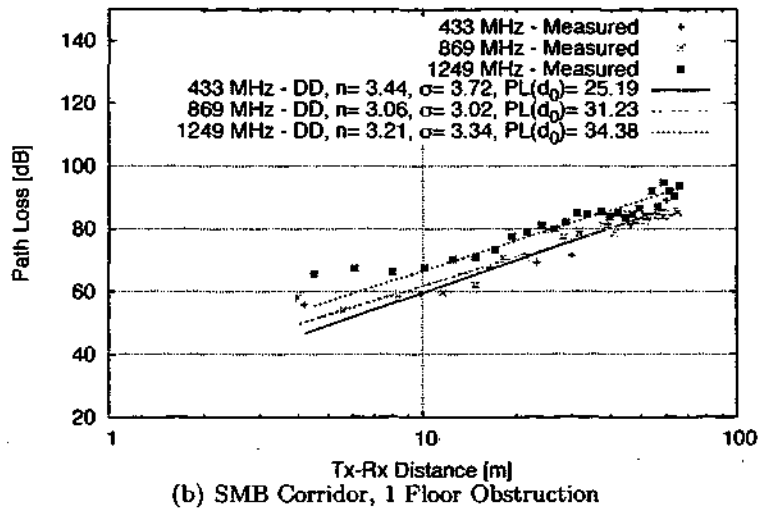


(b) SMB Corridor, 1 Floor Obstruction

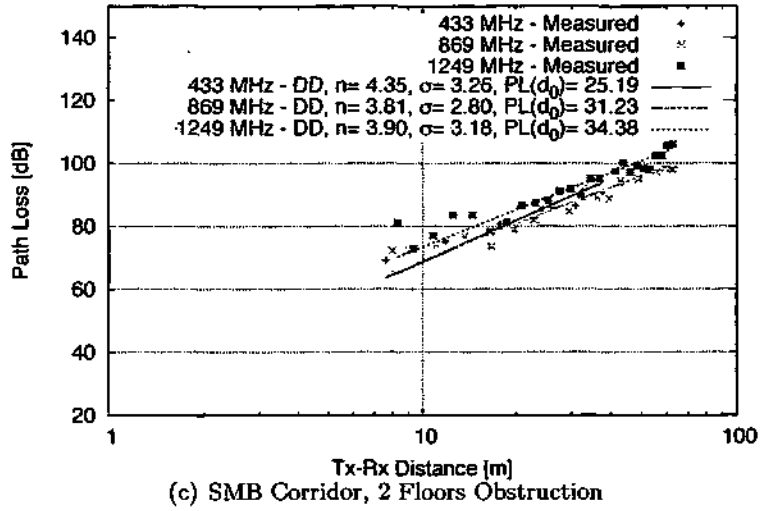


(c) SMB Corridor, 2 Floors Obstruction

Figure E.1: Frequencies Comparison of Log-Distance Model Mean Path Loss for Smeaton Building - Corridors

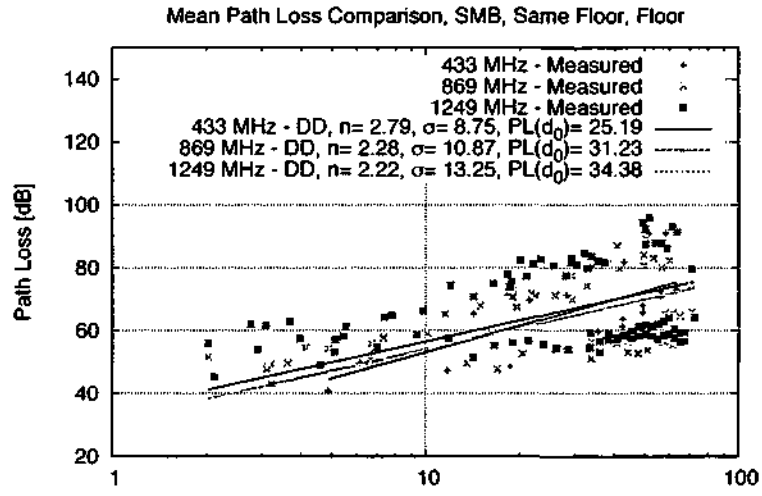


(a) SMB Whole Floor, Same Floor

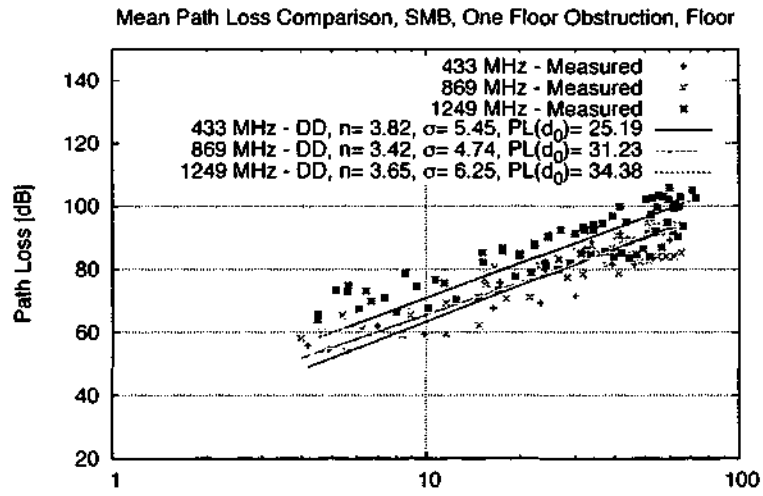


(b) SMB Whole Floor, 1 Floor Obstruction

Figure E.2: Frequencies Comparison of Log-Distance Model Mean Path Loss for Smeaton Building - Corridors and Rooms

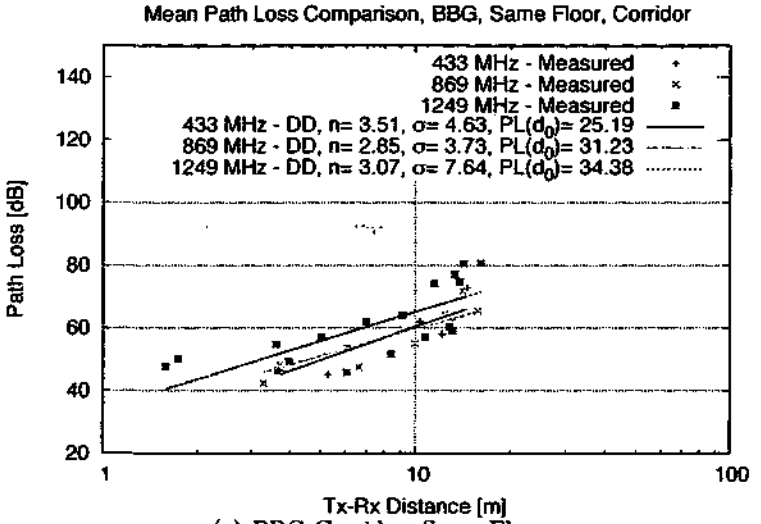


(a) BBG Corridor, Same Floor

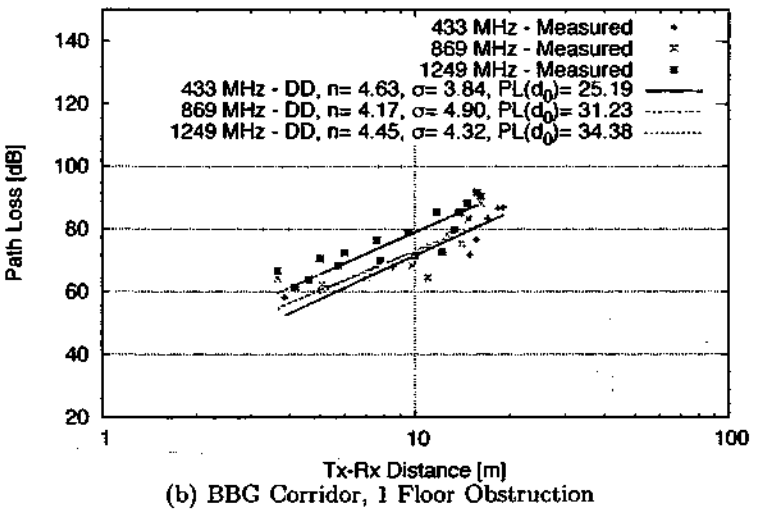


(b) BBG Corridor, 1 Floor Obstruction

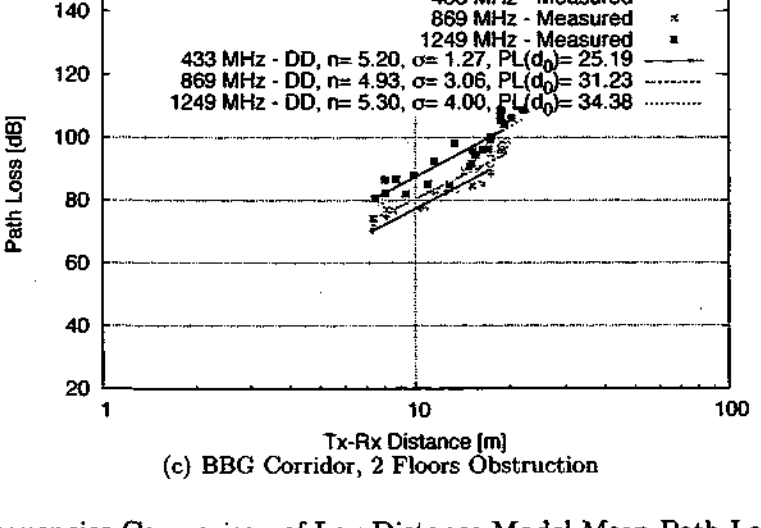


(c) BBG Corridor, 2 Floors Obstruction

Figure E.3: Frequencies Comparison of Log-Distance Model Mean Path Loss for Babbage Building with 0, 1 and 2 floors obstruction

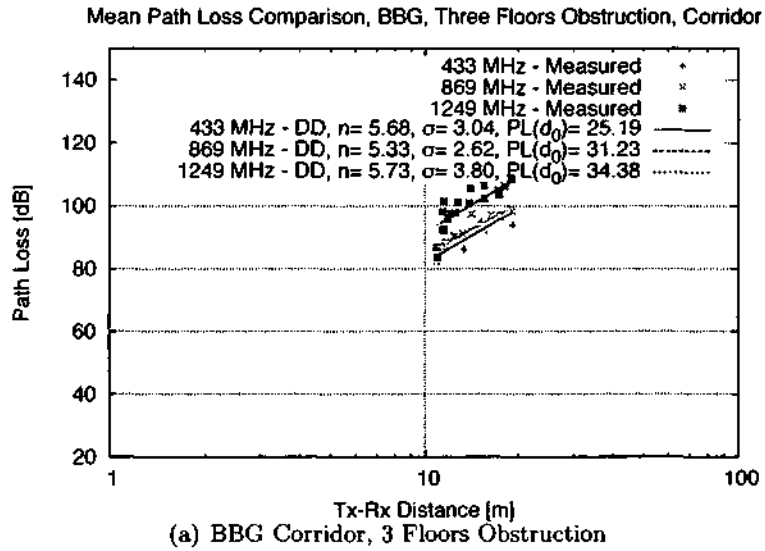


(a) BBG Corridor, 3 Floors Obstruction

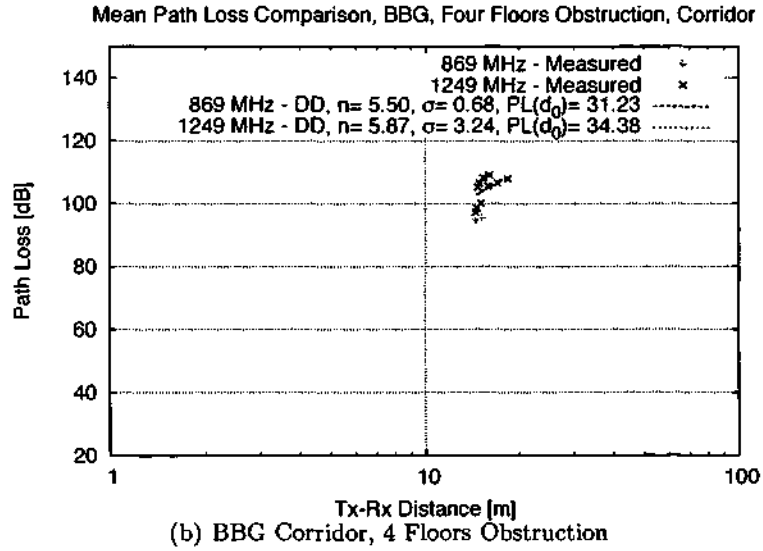


(b) BBG Corridor, 4 Floors Obstruction

Figure E.4: Frequencies Comparison of Log-Distance Model Mean Path Loss for Babbage Building with 3 and 4 floors obstruction

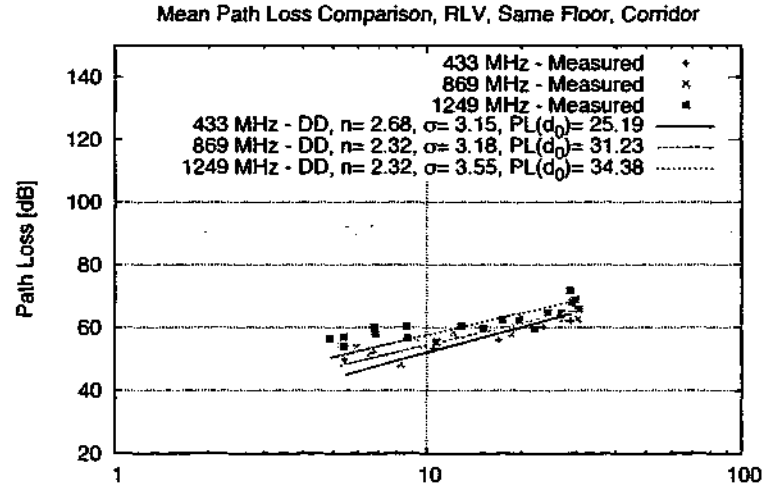


(a) RLV Corridor, Same Floor

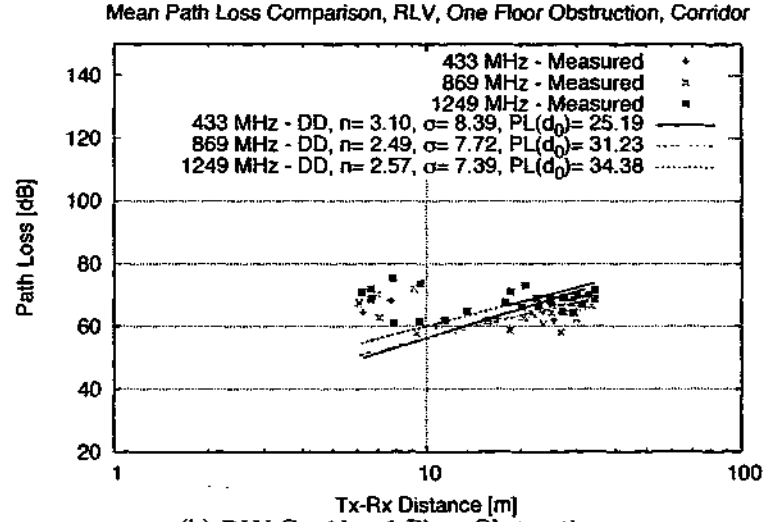


(b) RLV Corridor, 1 Floor Obstruction

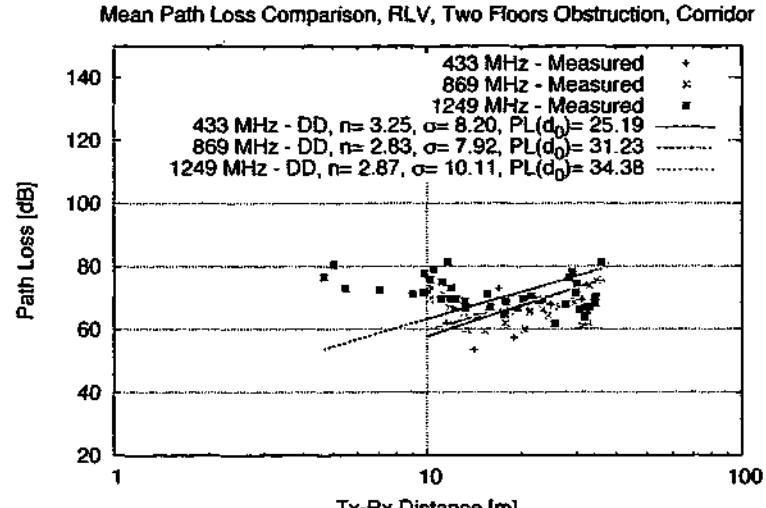


(c) RLV Corridor, 2 Floors Obstruction

Figure E.5: Frequencies Comparison of Log-Distance Model Mean Path Loss for Roland Levinsky Building - Corridors

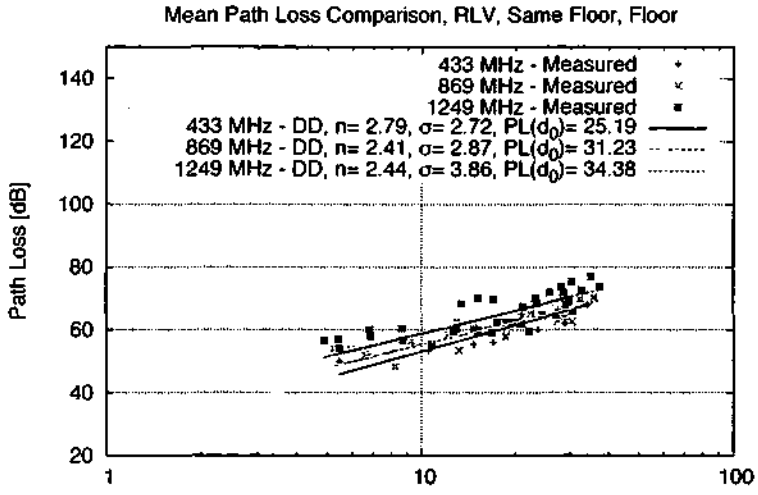


(a) RLV Whole Floor, Same Floor

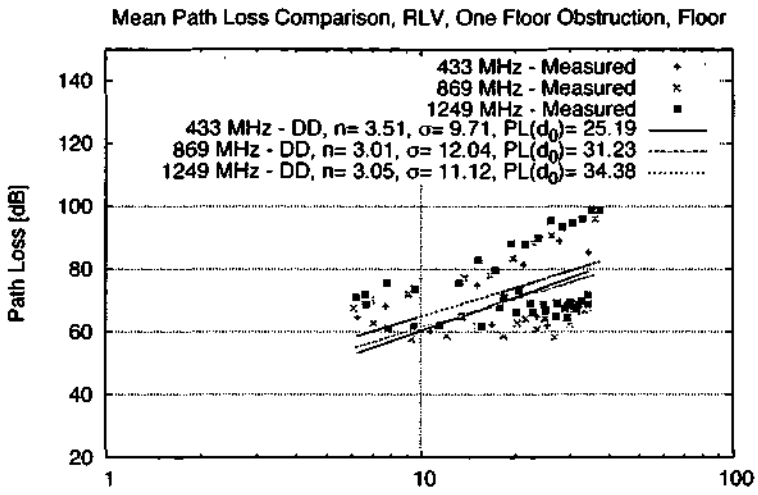


(b) RLV Whole Floor, 1 Floor Obstruction

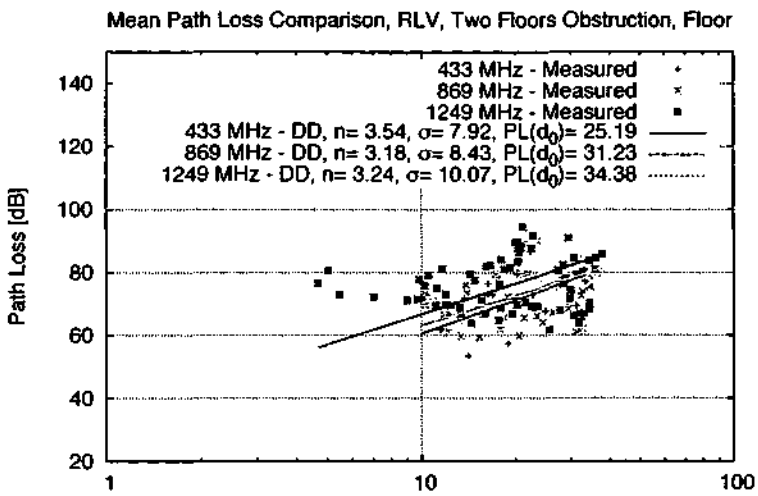


(c) RLV Whole Floor, 2 Floor Obstructions

Figure E.6: Frequencies Comparison of Log-Distance Model Mean Path Loss for Roland Levinsky Building - Corridors and Rooms

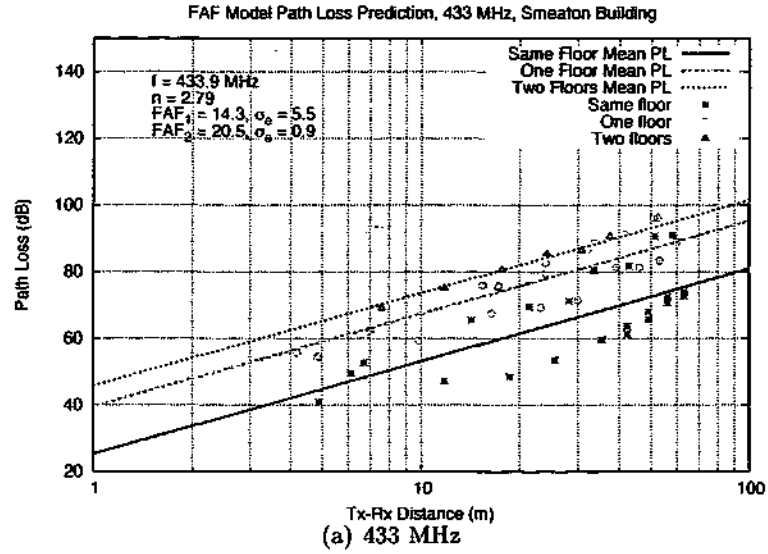


(a) 433 MHz

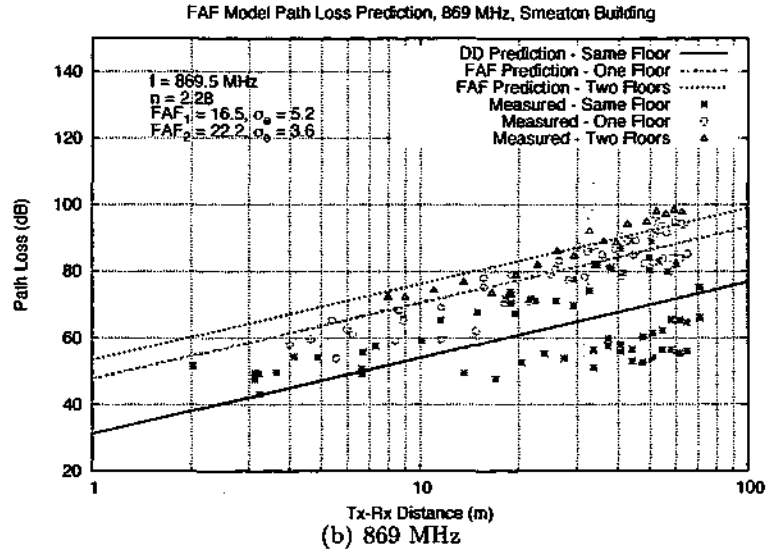


(b) 869 MHz

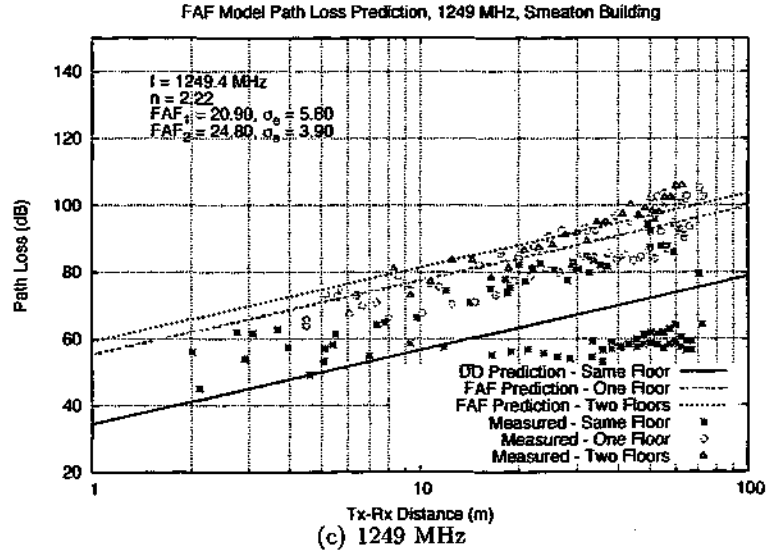


(c) 1249 MHz

Figure E.7: Floor Attenuation Factor Model Mean Path Loss for Smeaton Building at 433 MHz, 869 MHz and 1249 MHz

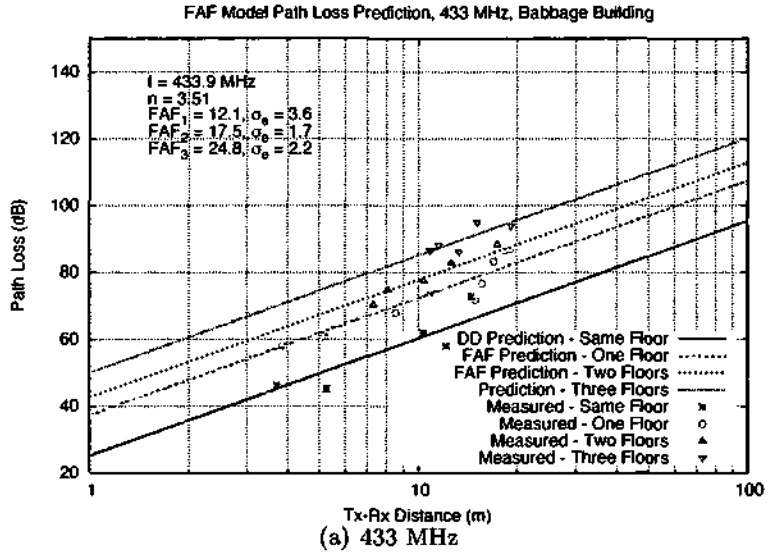


(a) 433 MHz

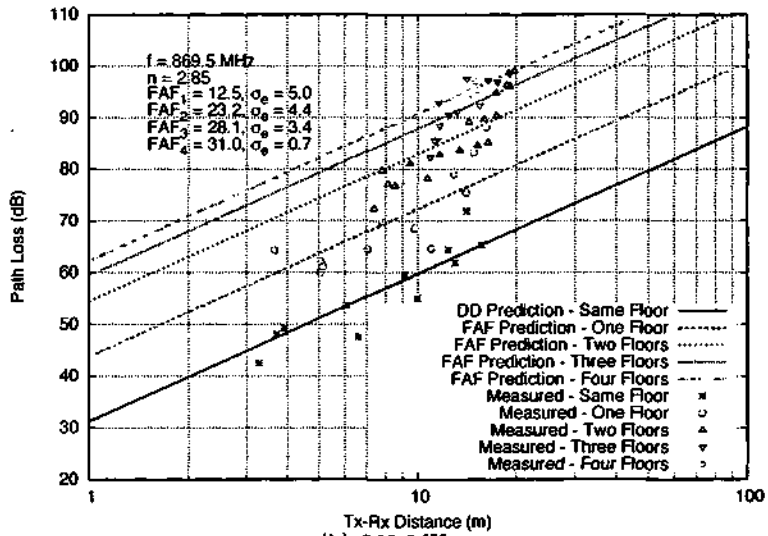


(b) 869 MHz

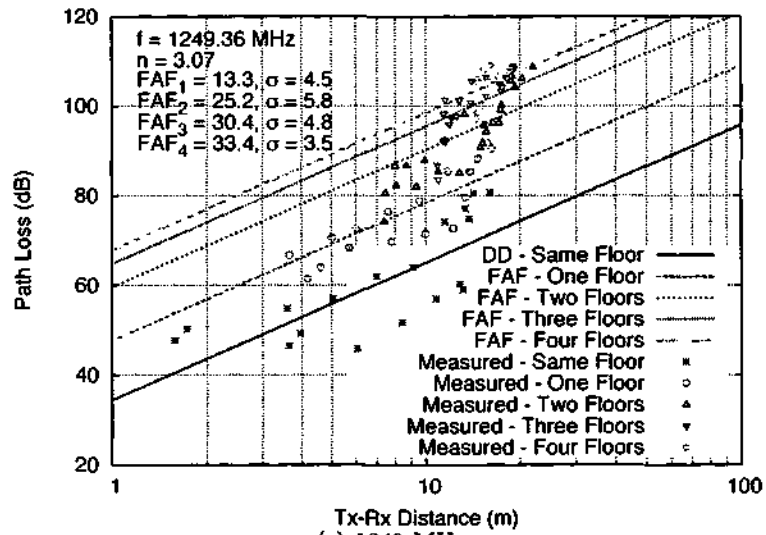


(c) 1249 MHz

Figure E.8: Floor Attenuation Factor Model Mean Path Loss for Babbage Building at 433 MHz, 869 MHz and 1249 MHz

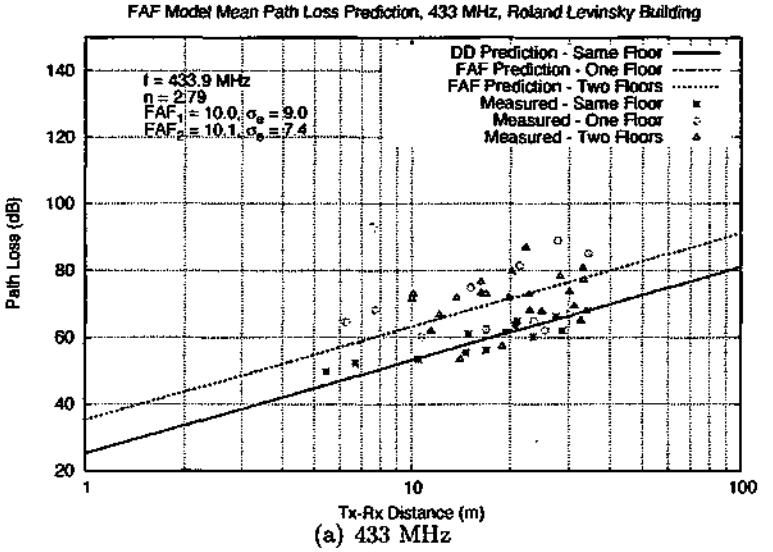


(a) 433 MHz

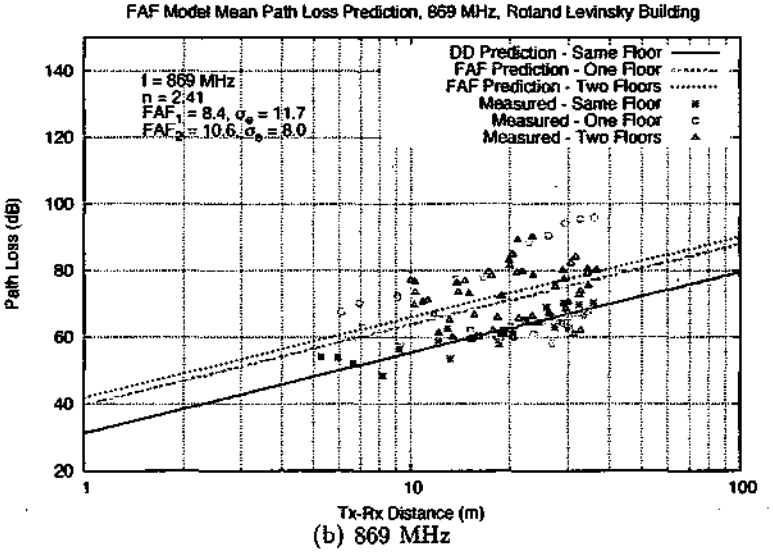


(b) 869 MHz

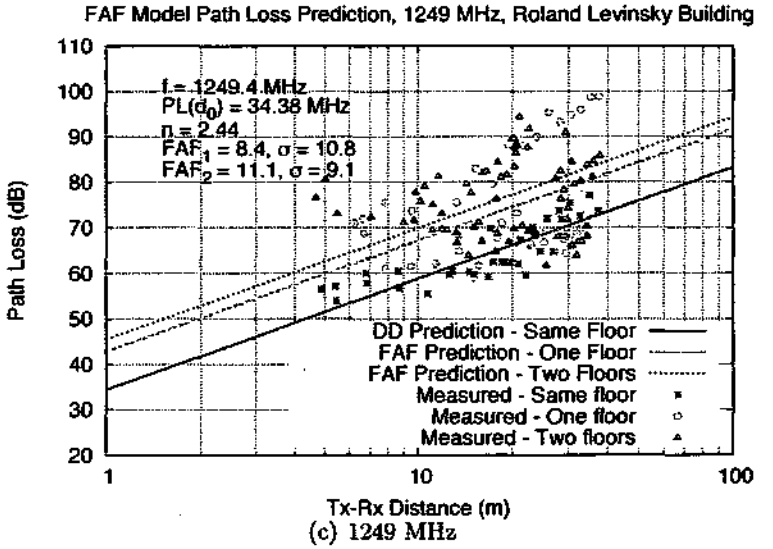


(c) 1249 MHz

Figure E.9: Floor Attenuation Factor Model Mean Path Loss for Roland Levinsky Building at 433 MHz, 869 MHz and 1249 MHz

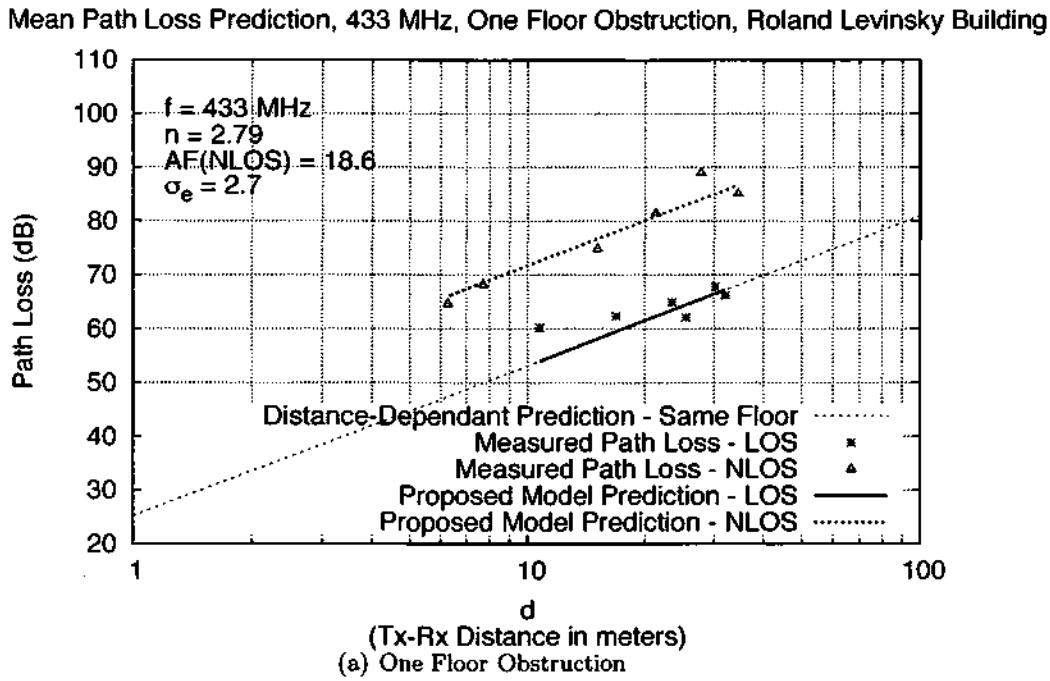


(a) One Floor Obstruction

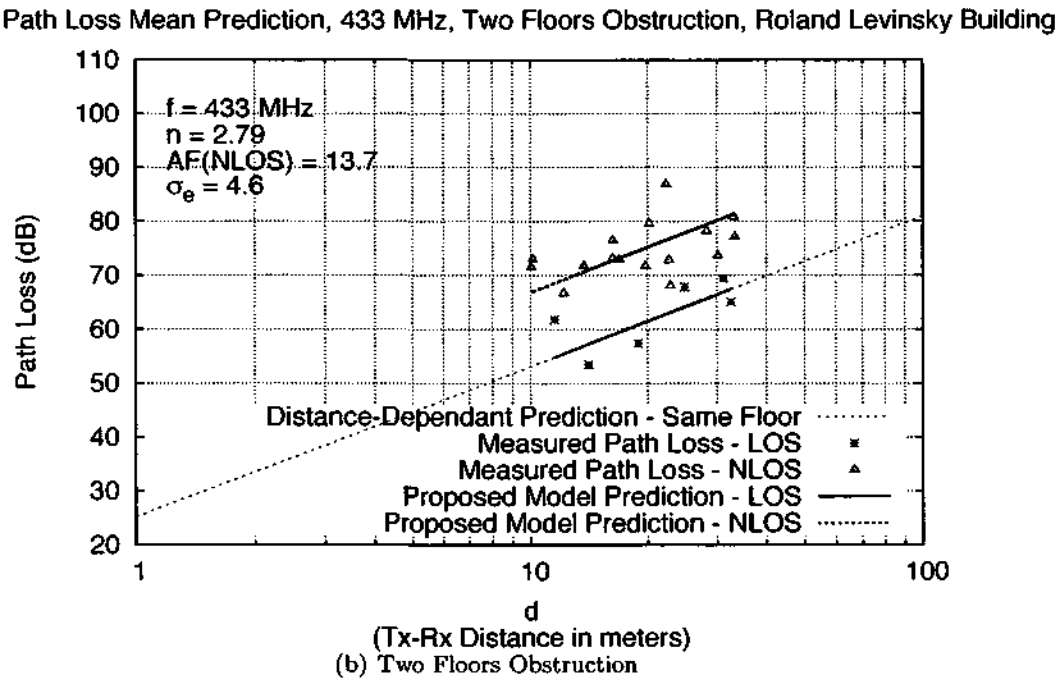


(b) Two Floors Obstruction

Figure E.10: Proposed Model Mean Path Loss for Roland Levinsky Building at 433 MHz

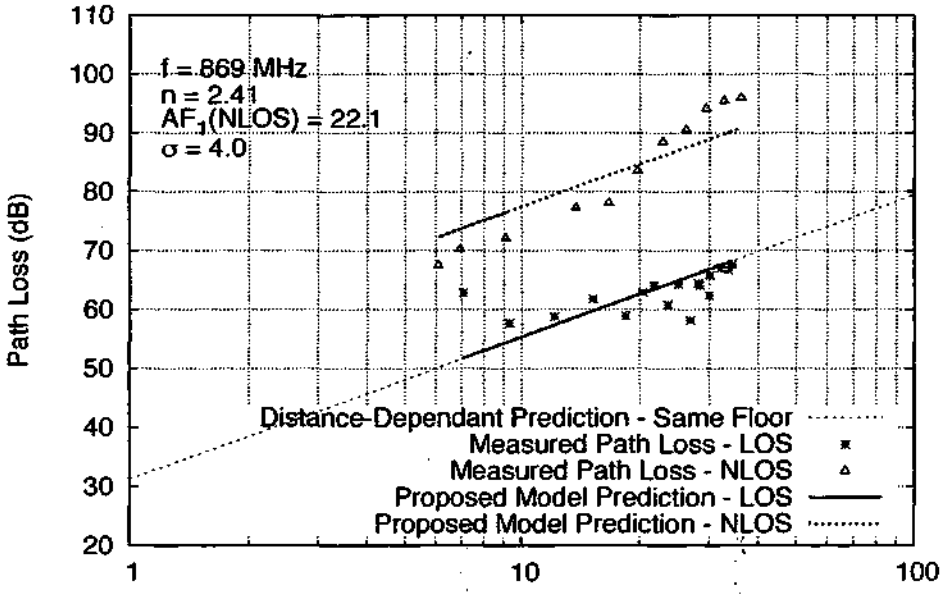


(a) One Floor Obstruction

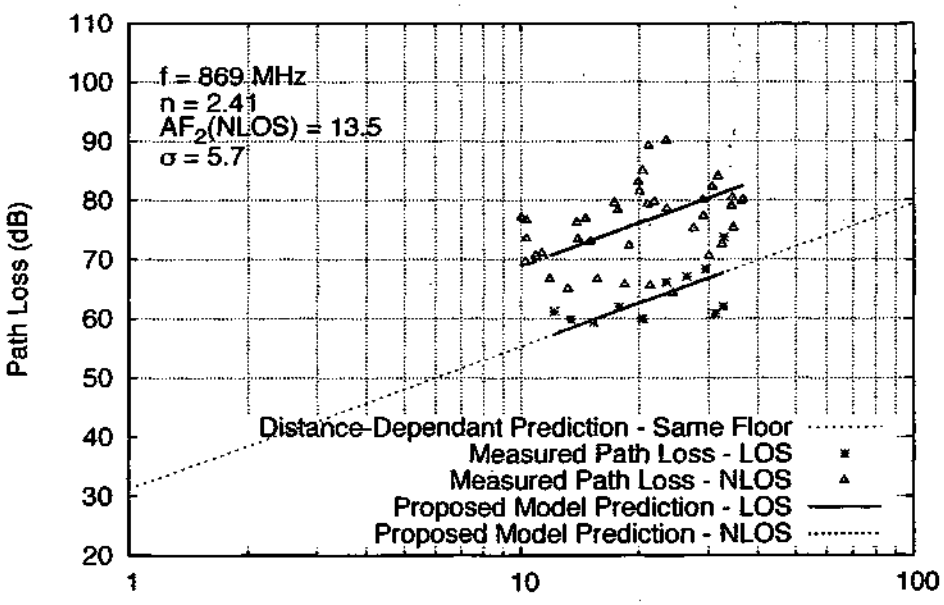


(b) Two Floors Obstruction

Figure E.11: Proposed Model Mean Path Loss for Roland Levinsky Building at 869 MHz

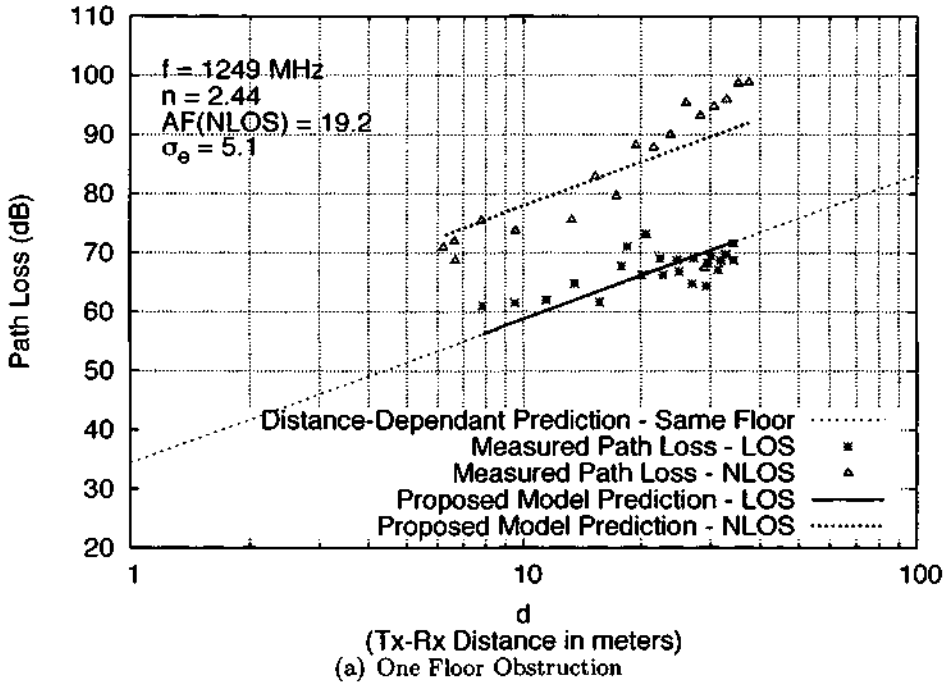


(a) One Floor Obstruction

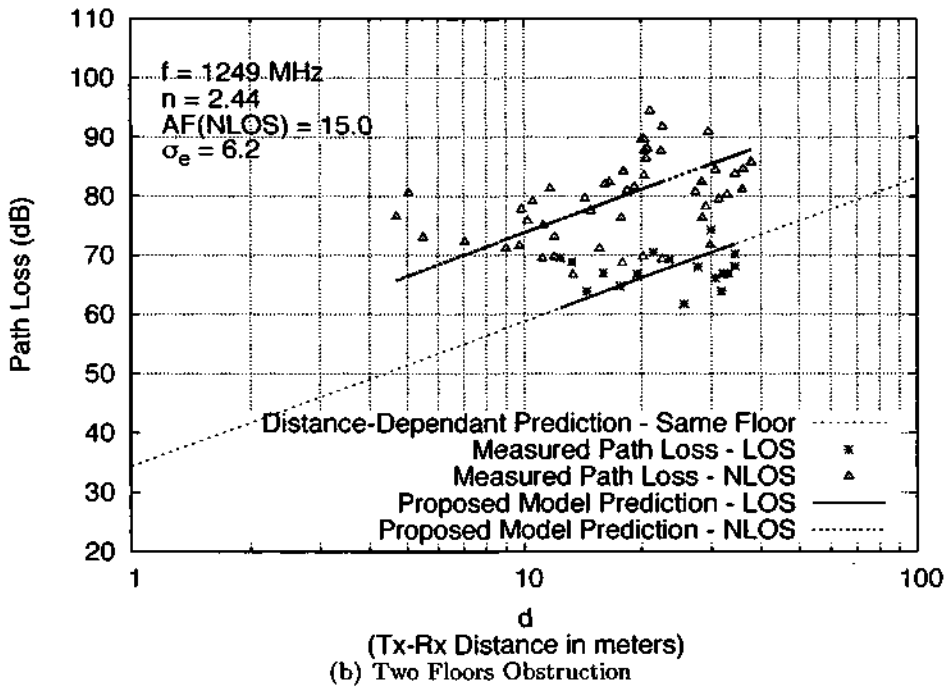


(b) Two Floors Obstruction

Figure E.12: Proposed Model Mean Path Loss for Roland Levinsky Building at 1249 MHz

# Appendix F

# Measurement of cable loss

(a) Calibrate the Reference cable

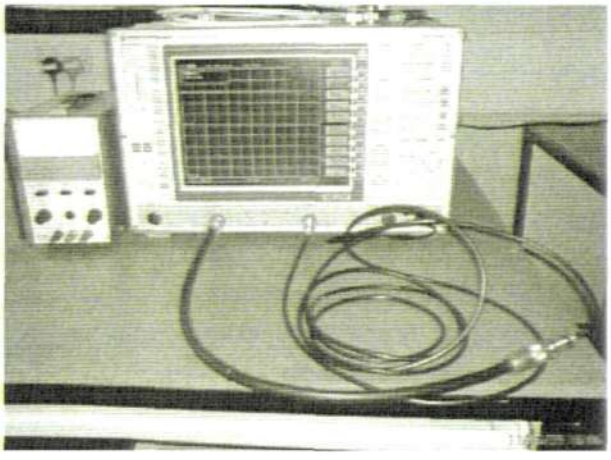

(b) Measuring loss of Cable 1 at 433 MHz and 869 MHz

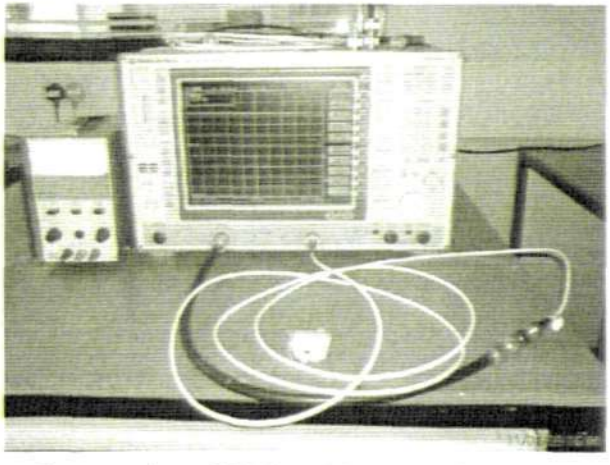

(c) Measuring loss of Cable 2 (Transmitter) at 1249 MHz

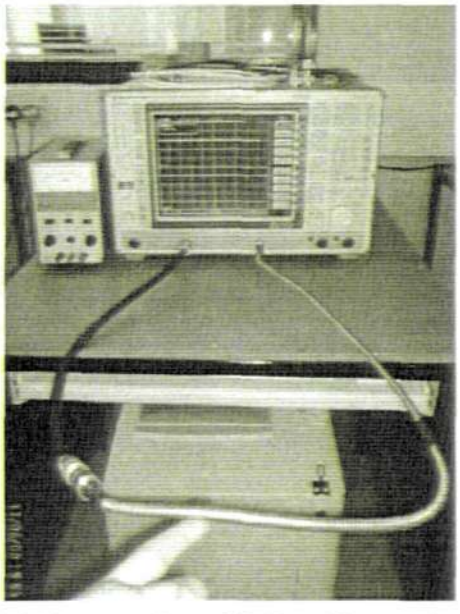

(d) Measuring loss of Cable 3 (Receiver) at 1249 MHz

Figure F.1: Photos of cable losses measurements

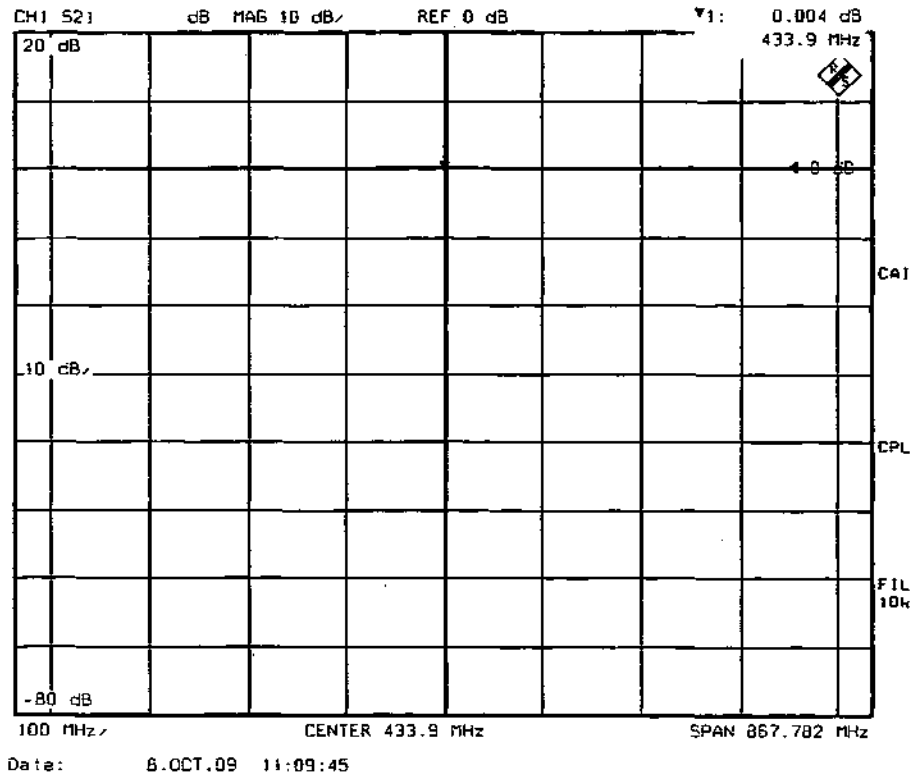


(a) Loss of reference cable at 433.9 MHz

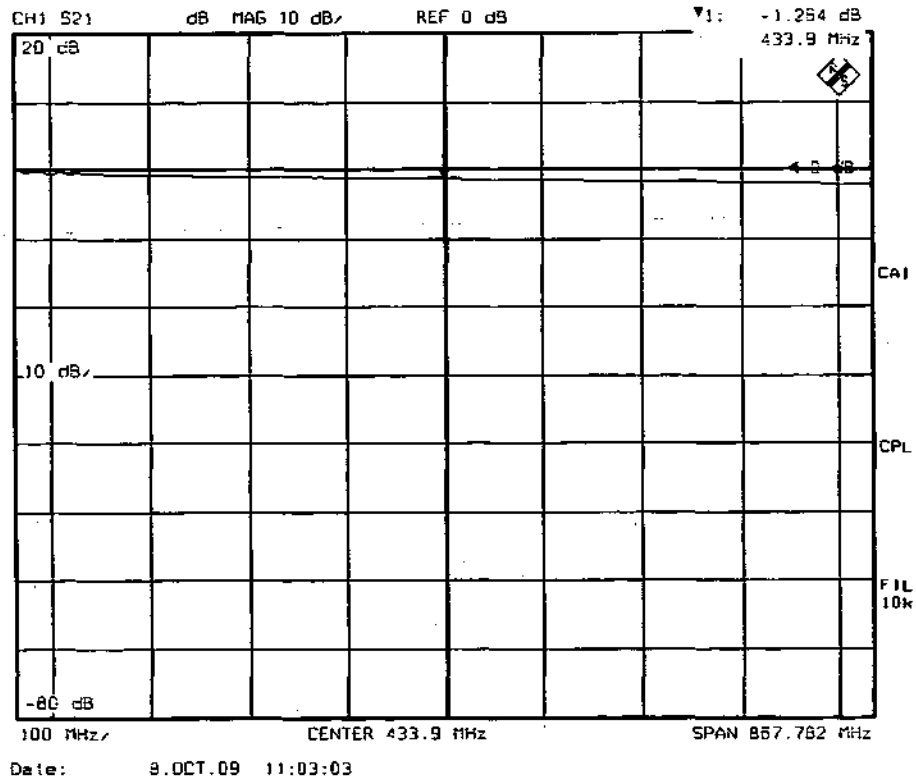


(b) Loss of 433 MHz receiver system connecting cable

Figure F.2: Cable loss of 433 MHz receiver connecting cable is equal to $0.004 - (-1.264) = 1.27$ dB.

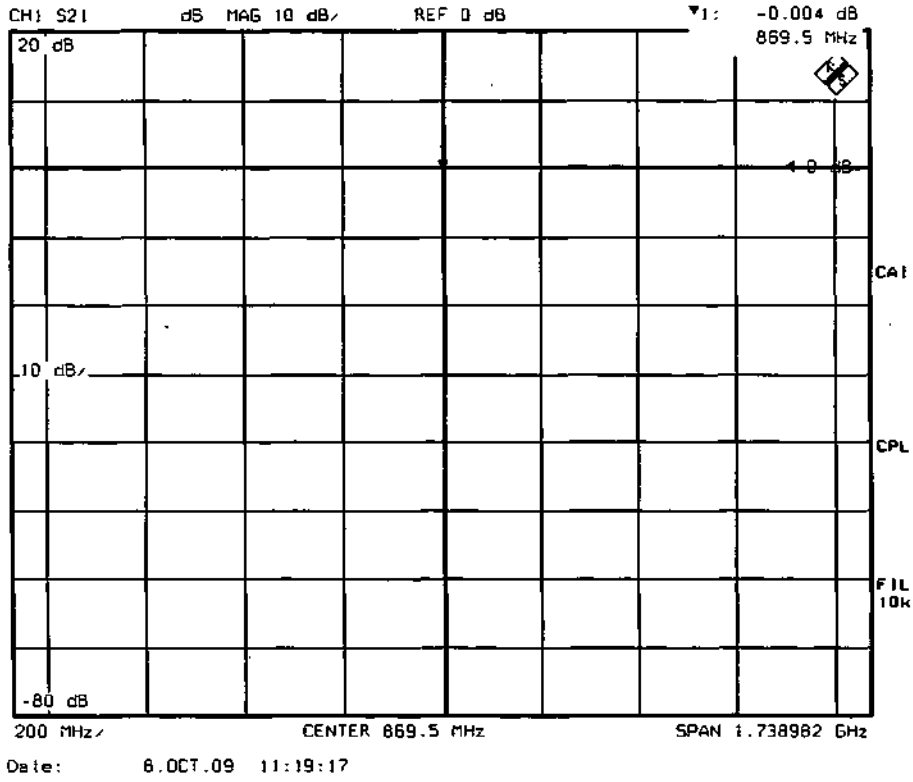


(a) Loss of reference cable at 869.5 MHz

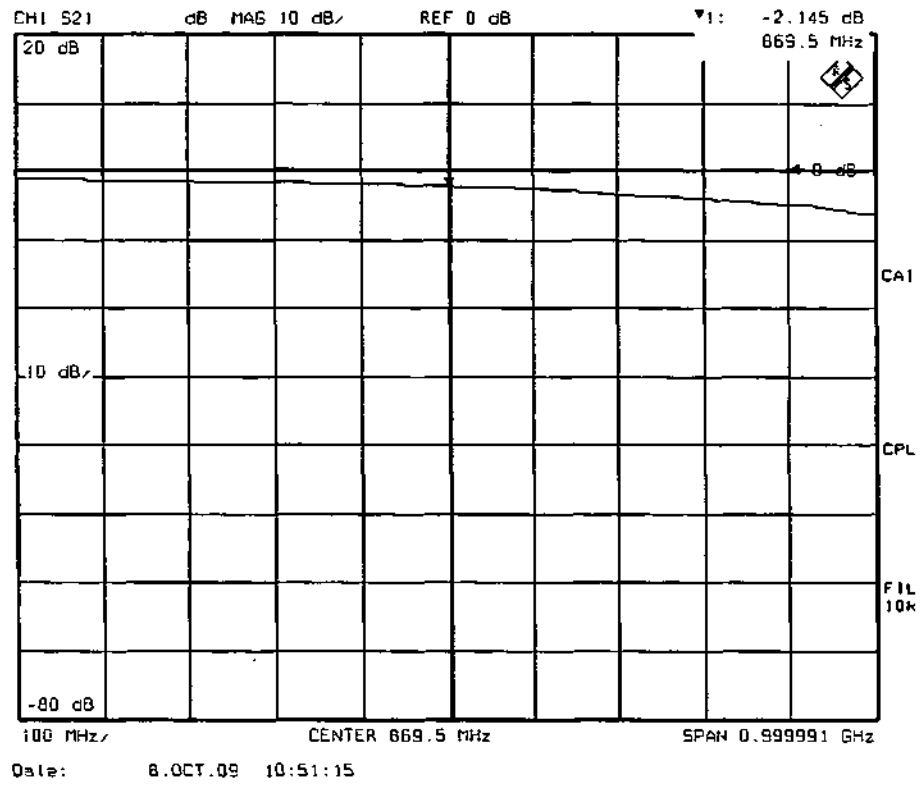


(b) Loss of 869 MHz receiver system connecting cable

Figure F.3: Cable loss of 869 MHz receiver connecting cable is equal to $-0.004-(-2.145) = 2.14$ dB.

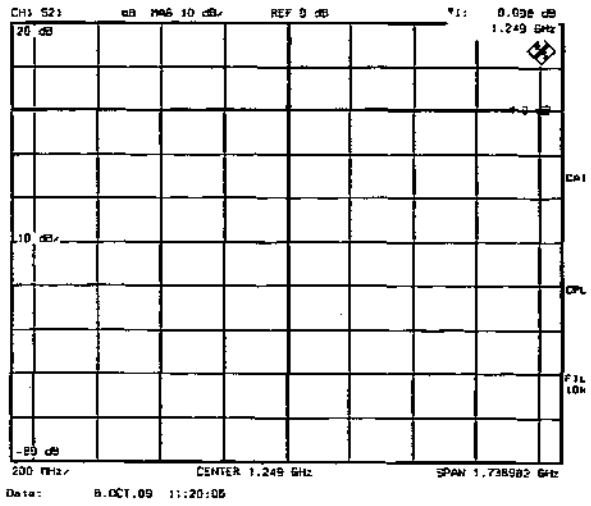


(a) Loss of reference cable at 1249 MHz

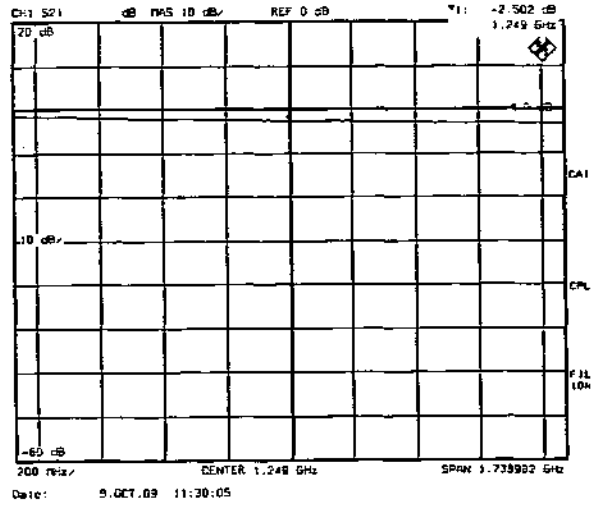


(b) Loss of 1249 MHz transmitter system connecting cable

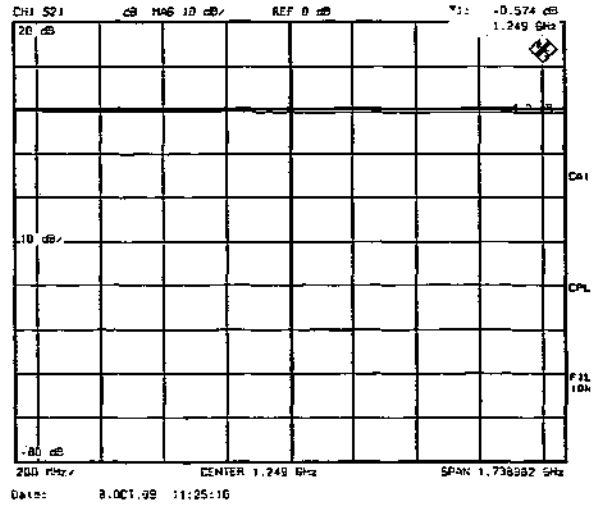


(c) Loss of 1249 MHz receiver system connecting cable

Figure F.4: Cable loss of 1249 MHz transmitter and receiver connecting cables are equal to $0.008 - (-2.502) = 2.51$ dB and $0.008 - (-0.574) = 0.58$ dB, respectively.

# References

[Affandi et al., 1999] Affandi, A., Zein, G. E., and Citerne, J. (1999). Investigation on frequency dependence of indoor radio propagation parameters. *Vehicular Technology Conference, 1999. VTC 1999 - Fall. IEEE VTS 50th*, 4:1988–1992 vol.4.

[Akyildiz et al., 2008] Akyildiz, I. F., Lee, W.-Y., Vuran, M. C., and Mohanty, S. (2008). A survey on spectrum management in cognitive radio networks. *Communications Magazine, IEEE*, 46(4):40–48.

[Andersen et al., 1995] Andersen, J. B., Rappaport, T. S., and Yoshida, S. (1995). Propagation measurements and models for wireless communications channels. *IEEE Communications Magazine*, pages 42–49.

[Brand and Aghvami, 2002] Brand, A. and Aghvami, H. (2002). *Multiple Access Protocols for Mobile Communications: GPRS, UMTS and beyond.* John Wiley & Sons, Ltd. ISBN 0 471 49877 7.

[CDMA Development Group Website, 2007] CDMA Development Group Website (2007). http://www.cdg.org/technology/2g.asp. *Internet Resource.*

[Cover and Thomas, 1991] Cover, T. M. and Thomas, J. A. (1991). *Elements of information theory.* Wiley-Interscience, New York, NY, USA.

[Desaki et al., 1997] Desaki, Y., Fujiwara, T., and Kasami, T. (1997). The weight distribution of extended binary primitive bch code length 128. *IEEE Transactions in Information Theory*, 43(4):1364–1371.

[Erceg et al., 2001] Erceg, V., Hari, K. S., Smith, M., Baum, D., Sheikh, K., Tappenden, C., Costa, J., Bushue, C., Sarajedini, A., Schwartz, R., Branlund, D., Kaitz, T., and Trinkwon, D. (2001). Channel Models for Fixed Wireless Applications.

[Evans and Baughan, 2000] Evans, B. G. and Baughan, K. (2000). Visions of 4g. *IEE Electronic & Communications Engineering Journal.*

[Fan and Darnell, 1995] Fan, P. Z. and Darnell, M. (1995). Aperiodic autocorrelation of Frank sequences. *Communications, IEE Proceedings-*, 142(4):210–215.

[Frank, 1963] Frank, R. (1963). Polyphase codes with good nonperiodic correlation properties. *Information Theory, IEEE Transactions on*, 9(1):43–45.

[Frank and Zadoff, 1962] Frank, R. L. and Zadoff, S. A. (1962). Phase shift codes with good periodic correlation properties. *IRE Transactions in Information Theory*, pages 381–382.

[Hashemi, 1993] Hashemi, H. (1993). The Indoor Radio Propagation Channel. *Proceedings of the IEEE*, 81(7):943–968.

[Hui and Yeung, 2003] Hui, S. Y. and Yeung, K. H. (2003). Challenges in the migration to 4G mobile systems. *IEEE Communications Magazine*, pages 54–59.

[Hwang and Baek, 2007] Hwang, I.-K. and Baek, J.-W. (2007). Wireless access monitoring and control system based on digital door lock. *Consumer Electronics, IEEE Transactions on*, 53(4):1724–1730.

[IEEE-Std-802.16, 2004] IEEE-Std-802.16 (2004). IEEE standard for local and metropolitan area networks part 16: Air interface for fixed broadband wireless access.

[Kaaranen et al., 2005] Kaaranen, H., Ahtiainen, A., Laitinen, L., Naghian, S., and Niemi, V. (2005). *UMTS Networks Architecture, Mobility and Services.* John Wiley & Sons, Ltd., 2 edition. ISBN 0 470 01103 3.

[Kelley, 2007] Kelley, B. (2007). Jointly Optimized Software Radio for Low Power 4G Cellular Systems. In *Signals, Systems and Computers, 2007. ACSSC 2007. Conference Record of the Forty-First Asilomar Conference on*, pages 113–117.

[Phaiboon, 2002] Phaiboon, S. (2002). An empirically based path loss model for indoor wireless channel in laboratory building. *Proceedings of IEEE TENCON 2002*, pages 1020–1023.

[Proakis, 1995] Proakis, J. G. (1995). *Digital Communications.* McGraw-Hill, third edition.

[Proakis, 2000] Proakis, J. G. (2000). *Digital Communications.* McGraw-Hill, fourth edition.

[Radiometrix Ltd, ] Radiometrix Ltd. http://www.radiometrix.co.uk.

[Rappaport, 1996] Rappaport, T. S. (1996). *Wireless Communications : Principles and Practice.* Prentice Hall. ISBN 0 13 461088 1.

[Saleh and Valenzuela, 1987] Saleh, A. A. M. and Valenzuela, R. A. (1987). A Statistical Model for Indoor Multipath Propagation. *Selected Areas in Communications, IEEE Journal on*, SAC-5(2):128–137.

[Seidel and Rappaport, 1992] Seidel, S. Y. and Rappaport, T. S. (1992). 914 Mhz path loss prediction models for indoor wireless communications in multifloored buildings. *IEEE Transactions on Antennas and Propagation*, 40(2):207–217.

[Sklar, 2001] Sklar, B. (2001). *Digital Communications: Fundamentals and Applications.* Pearson Education, 2nd edition. ISBN 81 7808 373 6.

[Tachikawa, 2003] Tachikawa, K. (2003). A perspective on the evolution of mobile communications. *IEEE Communications Magazine*, pages 66–73.

[Take, 2004] Take, S. (2004). Evolution of mobile technology. *Internet Resource.* http://www.buzzle.com/editorials/text7-18-2004-56792.asp.

[Tomlinson et al., 2007] Tomlinson, M., Tjhai, C. J., and Ambroze, M. (2007). Extending the dorsch decoder towards achieving maximum-likelihood decoding for linear codes. *IET Communication*, 1(3):479–488.

[Turkmani and Parsons, 1988] Turkmani, A. M. D. and Parsons, J. D. (1988). Measurement of building penetration loss on radio signal at 441, 900 and 1400 MHz. *Journal of IERE*, 58(6):169–174.

[Turkmani et al., 1987] Turkmani, A. M. D., Parsons, J. D., and Lewis, D. (1987). Radio propagation into buildings at 441, 900 and 1400 MHz. In *Fourth International Conference on Land and Mobile Radio*, pages 129–139, University of Warwick, Coventry.

[Valenzuela et al., 1997] Valenzuela, R. A., Landron, O., and Jacobs, D. L. (1997). Estimating local mean signal strength of indoor multipath propagation. *IEEE Transactions on Vehicular Technology*, 46(1):203–212. printed.

[Vriendt et al., 2002] Vriendt, J. D., Lainé, P., Lerouge, C., and Xu, X. (2002). Mobile network evolution: A revolution on the move. *IEEE Communications Magazine*, pages 104–111.

[Weight Distribution, ] Weight Distribution. http://www.infsys.cne.okayama-u.ac.jp/~koumoto/wd/index.html. Accessed on 1 September 2006.

[Weisstein, 2010] Weisstein, E. W. (2010). "Statistical Median.". From *Math World* - A Wolfram Web Resource. http://mathworld.wolfram.com/StatisticalMedian.html.

[Xu et al., 2007] Xu, D., Zhang, J., Gao, X., Zhang, P., and Wu, Y. (2007). Indoor Office Propagation Measurements and Path Loss Models at 5.25 GHz. In *Vehicular Technology Conference, 2007. VTC-2007 Fall. 2007 IEEE 66th*, pages 844–848.

[Yamaguchi et al., 1986] Yamaguchi, Y., Abe, T., and Sekiguchi, T. (1986). Experimental study of radio propagation characteristics in an underground street and corridors. *IEEE Transactions on Electromagnetic Compatibility*, 28(3):148–155.

[Zheng et al., 2009] Zheng, H., Lei, S., and Hui, T. (2009). A Framework of Access Network Architecture for 4G Systems Based on Cognitive Radio. In *Wireless Communications, Networking and Mobile Computing, 2009. WiCom '09. 5th International Conference on*, pages 1–4.

# Publications

# 1.25 GHz path loss prediction models for multifloored buildings

Ismail Fauzi Isnin[a], Martin Tomlinson[b], Mohammed Zaki Ahmed[c] and Marcel Ambroze[d]

Fixed and Mobile Communications Research
University of Plymouth,
Drake Circus,
PL4 8AA, Plymouth,
United Kingdom

## ABSTRACT

In this paper, parameter statistics of path loss prediction models are presented for 1.25 GHz within multifloored buildings. Parameters are extracted from analyzed data which was collected from measurements within three buildings. Buildings were chosen with specific considerations such as building footprint shapes and internal design.For the consideration of building footprint, a building having rectangular footprint and a building having square footprint were chosen. Because of its internal design, the third building was chosen to represent buildings with an atrium. Results show that, buildings with square footprint caused higher path loss compared to rectangular footprint buildings. It is also found that, buildings with an atrium have the lowest path loss exponent and lowest floor attenuation factor among other considered buildings.

A model for path loss prediction is proposed for multifloor buildings with its internal design allows line-of-sight (LOS) and non line-of-sight (NLOS), even though transmitter and receiver are not on the same floor. The model takes into consideration the factor of transmission type, whether it is LOS or NLOS. The proposed model has reduced the standard deviation of error prediction, which indicates better prediction accuracy is achieved.

**Keywords:** Indoor path loss, multifloor building, atrium or cavity areas, LOS, NLOS

## 1. INTRODUCTION

An undeniable fact nowadays is application of wireless communication technologies within building is becoming popular. Many indoor-use products or in-building systems are using this way of communication such as wireless multimedia systems, wireless security systems and personal communication systems.[1,2] Therefore, investigating the propagation of indoor wireless signal is important. One of properties that is important to be investigated is its path loss characteristic. For example, it is needed in link budget calculation and hardware location planning. There are many research works that have looked on predicting the path loss for indoor wireless transmissions previously, some looked on general indoor environment, some looked on more specific environment such as physical surrounding and areas within the building.[3] Even though this property has been investigated by many researches earlier. It is still relevant to investigate this property for other frequencies since different frequency tent to have different attenuation magnitude.[3-5]

In this paper, path loss characteristic has been investigated for narrow-band wireless signal at center frequency of 1.25 GHz within multifloored buildings. On-site measurements within buildings were first done. The measurement data are analyzed using statistical analysis in order to find the mean path loss exponent and standard deviation of various considerations for path loss prediction within multifloor building. Those

[a] E-mail: ismailfauzi@utm.my
[b] E-mail: mtomlinson@plymouth.ac.uk
[c] E-mail: mahmed@plymouth.ac.uk
[d] E-mail: marcel.ambroze@plymouth.ac.uk

parameters represent the path loss characteristics of 1.25 GHz system with different environment categories, such as same floor and up to four floors penetration categories.

This paper is organized as follows. Section 2 describes the three buildings that were used as measurement sites and also describes procedure of measurement. Section 3 explains the pre-processing procedure applied to measured data Section 4, two relevant path loss prediction models, Distance-Dependant Path Loss Model and Floor Attenuation Factor Path Loss Model are briefly explained and their parameter statistics are presented and discussed. In Section 5, a model is proposed for prediction of path loss within building when both, LOS and NLOS transmission are possible for its multifloor communications. And finally, Section 6 concludes the work and results.

## 2. MEASUREMENT LOCATION AND PROCEDURES

### 2.1 Measurement Locations

*Building 1:* Building 1 is a four stories building which was build in 1950's. However its interior has been renovated in early 2000's. Building 1 has a rectangle footprint with dimensions of 83.5 m × 19.2 m. The ground floor storey contains several offices and several small size machinery workshops. First floor is mostly contained with computer facilities studios and a few teaching rooms and offices. Second floor consists of teaching rooms and offices. While the third floor is equipped with electronics laboratories and offices. Frames of the building are made of I-shaped steel and its floors are made of steel reinforced concrete. The thickness of the floor is about 0.58 m.

Within all floors excepts the third floor, there is a long straight hallway which centrally located on each floor and it acrosses the building. All hallway has dimensions of 71.8 m × 2.4 m and with ceiling at 2.9 m above the floor. At all time during the measurement, the transmitter is located on the west end of second floor hallway. While the receiver was located in rooms and hallways of ground floor, first floor and second floor.

*Building 2:* Building 2 was constructed in 1980's. It has a square footprint. The dimension of its footprint is 39.1 m × 39.1 m. This building has five stories. On the ground floor, there are several lecture theaters, teaching rooms and offices. While the first floor, it is dedicatedly allocated for open-access computer facilities halls and a computer laboratory. This floor contains many computers and networking devices. In the second floor, a mixture of computer laboratories of specialized purpose and teaching rooms are located in this floor. While in the third floor, most of the floor area are allocated for offices and staff training room. And in the fourth floor, there are several conference rooms and teaching rooms. Additionally, a refectory is also located in the fourth floor. Wall structures of the building are made of concrete blocks and its floors are made of reinforce concrete.

Each floors have hallways with 2.1 m wide. And the height of ceiling from the floor is 2.3 m excepts for the ground floor one, which is 2.6 m. In ground floor, second floor and fourth floor, four straight hallways with same dimensions are connected perpendiculárly at each end to form a hall way that circulate within the floor. In first floor, an "L" shape hallway is formed from two straight hallways. And within third floor, the hallway is in "U" shape which is formed by three straight hallways connected. For all measurement, the transmitter is located in fourth floor hallway. And the receiver moved along hallways within the building.

*Building 3:* Building 3 is a building with modern design and architecture. It was completely constructed in 2008. Due to its modern design, it is chosen to be one of experiment sites with a purpose to generally represent a modern building. The building has three stories and has a clear central atrium. Therefore, only the ground floor has full floor area as big as the footprint size. The atrium of the building can be seen from Figure 1. The concept of this design is a considerably similar to some multifloored shopping complexes, cinema halls or theatre halls. Intuitively, this architecture allows direct paths of signal illuminated from transmitter on some area of each floors, even though the receiver is not on the same floor as the transmitter.

Material used for internal walls of this building are combination of concrete walls, wood boards walls and also glass walls. Most of the building consists of classrooms, lecture halls and offices. At all time, the transmitter is located at atrium perimeter on second floor where it is considered as one of potential location

Figure 1. The atrium of Building 3

for transmitter location as if there is a wireless system will be setup in the building. The receiver moved around on corridors, hallways and most of the rooms within these three floors.

### 2.2 Measurement Procedures

At center frequency 1.25 GHz, strength of received signal power was measured within three buildings described in Section 2.1.

With 1 W transmitting power, a narrow-band continuous wave (CW) signal was transmitted from half-wavelength dipole antenna. Height of transmitter antenna is 1.54 m above the floor.

On the receiver side, a similar half-wavelength dipole antenna is used and it is also set to be the same height as the transmitter antenna. Receiver antenna is connected to a spectrum analyzer, and the spectrum analyzer is then connected to a computer which acts as a user input and output terminal and data storage device. All of these devices was set up on top of a trolley for mobility reason. The spectrum analyzer used in the system capable to measure received signal power down to -80 dBm over resolution bandwidth of 30 kHz. And this gives the maximum path loss of the system, is equal to 110 dB since transmitting power is $+30$ dBm.

The transmitter was stationary and its location was fixed for all measurements. Different from the receiver, it was the one that moved around within the buildings. Receiver measures and records received signal power at each point of measurement tracks. Each measurement track is a straight line with marks of measurement points which are distanced evenly at approximately 0.25 meter from each other. Due to varying surroundings, length of a measurement track is varied between 4.98 m to 39 m, whereas for distance between transmitter antenna and receiver antenna, which was measured in three dimensions, is in the range of 1.15 m for the nearest point and 74.4 m for the furthest point.

At each measurement point, 10 samples of signal strength reading were taken at every 400 ms per sample and its average is calculated. The averaging is done in mW. Same procedure was repeated for all points of all measurement tracks.

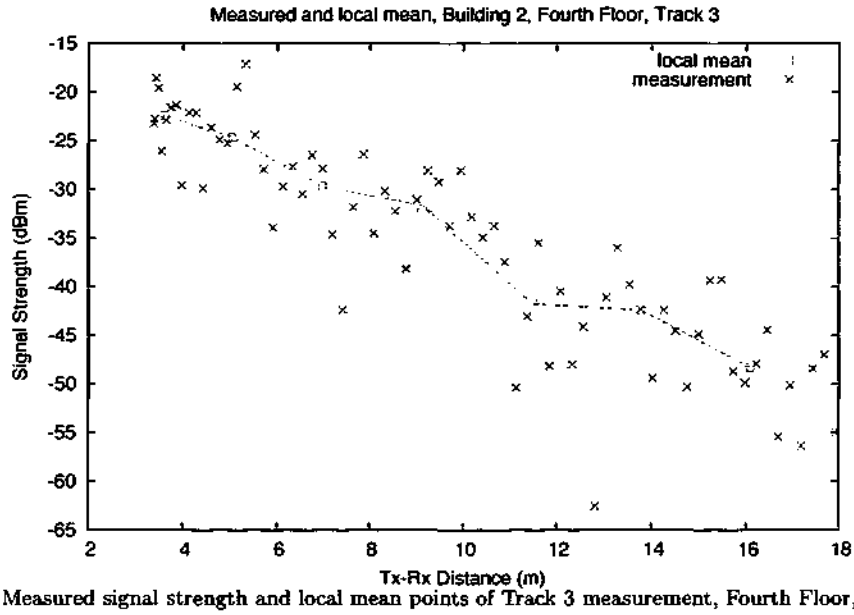

Figure 2. Measured signal strength and local mean points of Track 3 measurement, Fourth Floor, Building 2

## 3. DATA PROCESSING

Signal strength recorded on each measurement tracks are then needed to be averaged over several wavelength for path loss analysis.[6,7] Therefore, all measurement tracks are then segmented with length of 10 $\lambda$ (2.40 m) for each segment. Segment length 10 $\lambda$ was chosen because it was found to be the best compromise between removing fast fading effect and remain the path loss fading pattern.[8] For each segment, a median value is taken to represent the mean signal strength of the segment which is called local mean. Each local mean is assigned to be the middle point of the segment. Figure 2 shows signal strength of measured points and its local mean points for a measurement track from Fourth floor, Building 2 measurements. With a local mean represent signal strength of a segment, path loss of the segment is found by subtracting transmit power with the local mean. Along with each segment path loss value, other informations such as transmitter-receiver distance (T-R Distance) and number of obstructed floors between transmitter and receiver are attached together. These parameters are required in classification of data according to relevant categories and extraction of model parameters as mentioned in Section 4.

## 4. PATH LOSS PREDICTION MODEL

### 4.1 Distance-Dependant Path Loss Model

A general model of predicting mean path loss when the distance between transmitter and receiver, $d$, is known, is given by[6,7,9,10]

$$\overline{PL}(d)[\text{dB}] = PL(d_0)[\text{dB}] + 10 \times n \times \log_{10}\left(\frac{d}{d_0}\right), \tag{1}$$

where $d_0$ denotes the reference distance, $PL(d_0)$ is the path loss of the system when distance between transmitter and receiver is $d_0$ and $n$ indicates the mean path loss exponent an environment.

With $d_0$ is usually chosen to be 1 meter for an indoor environment.$PL(d_0)$ for the system is calculated using Friis free space path loss equation, which gives $PL(d_0) = 30.08$ dB. This calculation is done by assuming system antenna gain is equal to system cable loss.

Since path loss was found to be log-normally distributed about (1).[11,12] Therefore, path loss of known transmitter-receiver distance can be modelled using

$$PL(d)[\text{dB}] = \overline{PL}(d) + X_\sigma[\text{dB}], \tag{2}$$

where $X_\sigma$ is a zero mean log-normally distributed random variable in dB, with distribution standard deviation, $\sigma$. Because of limited data, it is assumed that data is a dataset that fulfill this property.

In order to obtain path loss prediction models for 1.25 GHz system, values of $n$ and $\sigma$ were computed from measured data. $n$ and $\sigma$ values were computed using linear regression method.[6,10,13]

Values of path loss rate and standard deviation for different categories have been computed and shown in Table 1. We have categorized the data of each building into Entire Building category and several categories based on the number of floor crossed between the transmitter and the receiver. Each of path loss rate, $n$ and its standard deviation, $\sigma$ in the table have been computed from data grouped according to relevant categories. While the last column, tells number of local mean considered in each category.

From Table 1, it is found that incrementation pattern is observed for $n$ of Building 1 and 2 as number of crossed floors increased. This obviously shows that existence of each floor, in between transmitter and receiver, contributes some loss on power of signal received at the receiver. Higher the number of obstructed floor between transmitter and receiver, higher the path loss experienced at receiver. Conversely, decremental pattern is found for the standard deviations.

However, pattern shown by $n$ and $\sigma$ for Building 3 are different from others. It seems that $n$ is having inverse pattern compared to pattern observed from Building 1 and 2. Means, $n$ values does decreasing as the number of floor increased. While $\sigma$ values are not always decreasing as number of obstructed floor increases. It is quite surprising to find the fact that the signal strength of floor, where the transmitter is located, experiencing the highest rate of power loss compared to other floors.

It is interesting to analyze model parameters based on shape of building footprint. As Building 1 represent a rectangular footprint building and Building 2 represents a square footprints, it is found that path loss rate for Building 1 is lower than Building 2, which are 1.89 and 6.49 respectively. This shows that, with the same T-R distance, the system will experience less path loss within a rectangular building than a square footprint buildings. For Building 3, we found that the path loss rate is the lowest among these three buildings, which is 1.68. This behavior is probably best explained by atrium of Building 3 which allow direct path of signal even though the transmitter and receiver are not on the same floor. This causes the average received power measured within Building 3 are possible to be higher than the other considered buildings, even though the transmitter and receiver are separated with the same number of floors.

Figure 3 shows the predicted mean path loss over measured signal strength for Building 2 Same Floor category, with $n = 2.88$. Notice that thin lines on the figure act as reference lines that indicate the lines when $n = 2$ to 7.

### 4.2 Floor Attenuation Factor (FAF) Path Loss Model

Model described in Section 4.1 can be alternatively used to predict the path loss for multifloor building by just using the path loss exponent of *same floor*.[6] This is done by adding a constant, which is known as Floor Attenuation Factor (FAF), to the path loss predicted by (1). FAF is a constant in dB that represents attenuation related to a number of crossed floors. FAF is calculated by finding the average of different between predicted mean path loss from *same floor* path loss exponent and local mean of measured data from related category.[6] Thus, equation to predict mean path loss of a multifloor building using FAF path loss model is given as

$$\overline{PL}(d) = PL(d_0) + 10 \times n(samefloor) \times \log_{10}\left(\frac{d}{d_0}\right) + \text{FAF}[\text{dB}], \tag{3}$$

and $n(samefloor)$ is the path loss exponent for same floor, $PL(d_0)$ is path loss at reference distance $d_0$ and $d$ is the shortest distance between transmitter and receiver.

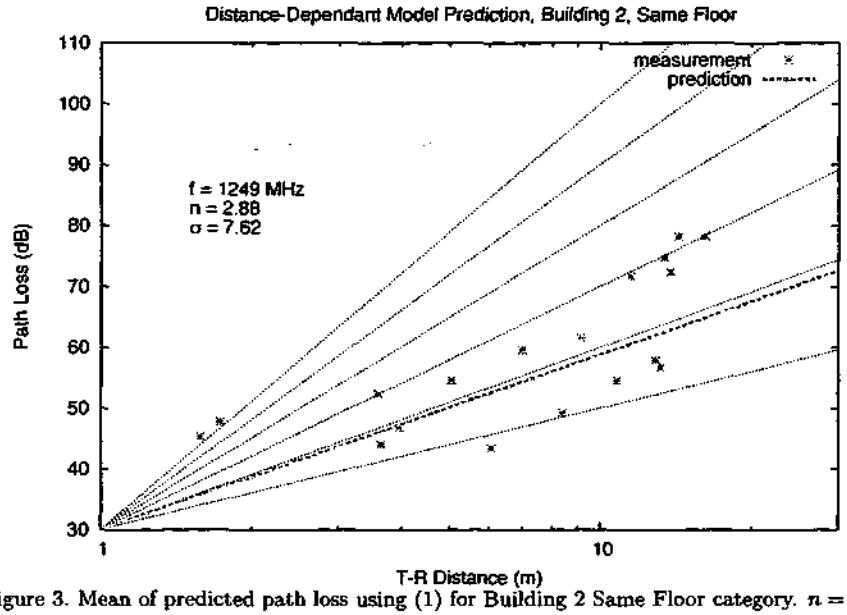


Figure 3. Mean of predicted path loss using (1) for Building 2 Same Floor category. $n = 2.88$

Table 1. The mean path loss exponent, $n$, and standard deviation, $\sigma$, for use in Distance-Dependant Path Loss Model based on a measurement at a carrier frequency of 1.25 GHz

| | | $n$ | $\sigma$[dB] | Number of Locations |
|---|---|---|---|---|
| Building 1: | | | | |
| | (a) Entire Building | 1.89 | 14.15 | 183 |
| | (b) Same Floor | 0.95 | 12.07 | 86 |
| | (c) Crossing 1 floor | 2.79 | 5.43 | 72 |
| | (d) Crossing 2 floors | 3.29 | 2.71 | 25 |
| Building 2: | | | | |
| | (a) Entire Building | 6.49 | 10.38 | 92 |
| | (b) Same Floor | 2.88 | 7.62 | 18 |
| | (c) Crossing 1 floor | 3.88 | 4.14 | 18 |
| | (d) Crossing 2 floors | 6.03 | 3.85 | 26 |
| | (e) Crossing 3 floors | 6.63 | 3.72 | 20 |
| | (f) Crossing 4 floors | 7.91 | 3.18 | 10 |
| Building 3: | | | | |
| | (a) Entire Building | 1.68 | 9.35 | 145 |
| | (b) Same Floor | 2.01 | 3.71 | 37 |
| | (c) Crossing 1 floor | 1.60 | 10.62 | 41 |
| | (d) Crossing 2 floors | 0.47 | 8.07 | 67 |

Table 2. Average Floor Attenuation Factors in Decibels

| | | FAF [dB] | $\sigma$[dB] |
|---|---|---|---|
| Building 1: | | | |
| | (a) Crossing 1 floor | 40.69 | 8.40 |
| | (b) Crossing 2 floors | 45.21 | 6.76 |
| Building 2: | | | |
| | (a) Crossing 1 floor | 17.00 | 4.64 |
| | (b) Crossing 2 floors | 29.23 | 6.03 |
| | (c) Crossing 3 floors | 34.46 | 4.90 |
| | (d) Crossing 4 floors | 37.60 | 3.56 |
| Building 3: | | | |
| | (a) Crossing 1 floor | 15.92 | 10.66 |
| | (b) Crossing 2 floors | 17.98 | 8.49 |

In Table 2, FAF for all three buildings are provided with $\sigma$ indicates the standard deviation for generating a log-normally distributed random variable that distributed about (3). $\sigma$ are extracted from the same dataset used to find the related FAF, which is the standard deviation of different between predicted path loss from *same floor* path loss exponent and local mean of measured data from related category.

Attenuation factors are found to increase as number of obstructed floor increases for each buildings as shown in Table 2. Attenuation caused by a single floor in Building 1 is found to be 40.69 dB, while with two obstructed floors, attenuation factor is found to be 45.21 dB. For Building 2, attenuation caused by the floor are in range between 17.00 to 37.60 dB as number of obstructed floor increases from one to four floors. While for Building 3, floor attenuation seems to be lesser among the other buildings. This phenomenon is explained by the existence of the atrium within the building that allows some direct paths to other floors within the building. The attenuation factor caused by the first floor is equal to 15.92 dB and 19.87 dB for two floors level different.

## 5. SIGHT PATH LOSS MODEL

Within Building 3, the distribution of path loss measured when transmitter and receiver are not on the same floor, has been found to be widely distributed from (2) and (3). This is shown by Table 1 and Table 2, which show the standard deviation of the path loss distribution of Building 3 are higher compared to standard deviation of Building 1 and Building 2 with the same number of floor different. This shows that the existence of the atrium, seems to affect the degree of path loss distribution, measured over the floor. In this environment, LOS and NLOS transmission could occur even though the receiver are not on the same floor as the transmitter. Even though, both transmissions are on the same T-R distance, LOS tend to result the lower path loss and NLOS tend to results to higher path loss. As a result, the floor path loss datasets consists of two subsets of data which isolated from each other at some distance. This phenomenon can be seen from measured data plotted in Figure 4. Data plotted in the figure were categorized into LOS and NLOS at local mean precision, which means each LOS local mean is categorized into LOS dataset and vice versa.

In order to consider the factor of transmission type in path loss prediction, within multifloor buildings with internal design allows both LOS and NLOS transmission during multifloor communications, such as an atrium or cavity, or any similar design to it. Therefore, the FAF model is modified and proposed as

$$\overline{PL}(d) = PL(d_0) + 10 \times n(samefloor) \times \log_{10}\left(\frac{d}{d_0}\right) + \gamma\,(los)\,, \tag{4}$$

which

$$\gamma\,(los) = \begin{cases} \text{AF(LOS)} & \text{if} \quad los = 1 \\ \text{AF(NLOS)} & \text{otherwise} \end{cases} \tag{5}$$

Table 3. SIGHT Attenuation Factors in Decibels

| | AF(LOS) [dB] | Number of Locations | AF(NLOS) [dB] | Number of Locations | $\sigma$ [dB] |
|---|---|---|---|---|---|
| Crossing 1 Floor: | 7.46 | 23 | 26.73 | 18 | 4.70 |
| Crossing 2 Floors: | 9.00 | 25 | 23.32 | 42 | 4.91 |

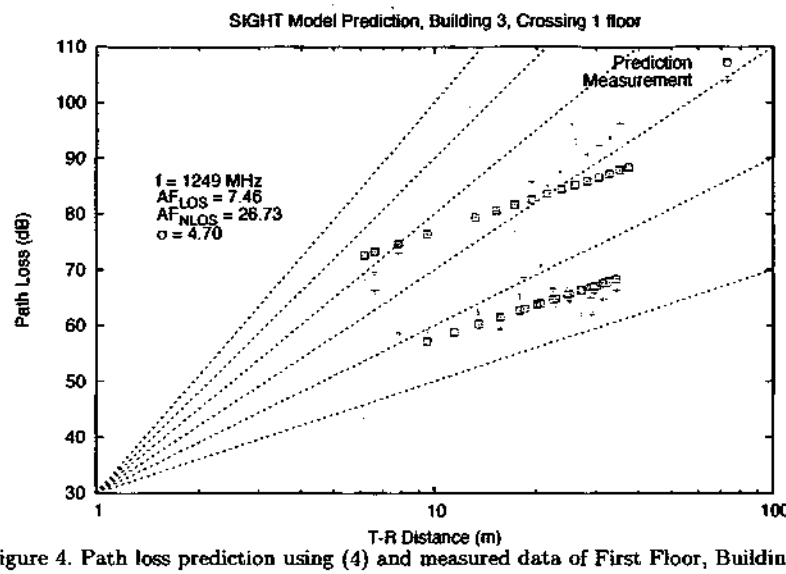

Figure 4. Path loss prediction using (4) and measured data of First Floor, Building 3

and $n(samefloor)$ is the path loss exponent of same floor, $PL(d_0)$ is path loss at reference distance $d_0$ and $d$ is the shortest distance between transmitter and receiver. AF(LOS) is the attenuation factor if transmission between transmitter and receiver is LOS. And AF(NLOS), is the attenuation factor when transmission is NLOS. The variable *los* is a flag that determines the appropriate attenuation factor to be applied in the model. If $los = 1$, which means transmission is LOS, thus AF(LOS) will be applied into the model, otherwise, attenuation factor AF(NLOS) is applied. Note that, the $n(samefloor)$ is still being used, so that the practicality of the FAF model is still remained.

Values of AF(LOS), AF(NLOS), standard deviation of the difference between predicted path loss and measured data, and number of local mean locations used to compute the statistics are given in Table 3. Standard deviation is in decibels. AF(LOS) is found by finding the average of difference between mean of predicted path loss, using (1) with exponent path loss of the same floor, and LOS measured data. AF(NLOS) is found by finding the average of difference between the same mean of predicted path loss and NLOS data set. Note that, since Building 3 is the only building that has both types of transmissions, LOS and NLOS, for multifloor communications, therefore, statistics given in Table 3 were computed by using data measured on the relevant floor of Building 3.

For one floor different of transmitter and receiver location, attenuation factor for LOS transmission is found to be 7.46 dB, and for NLOS, the attenuation factor is 26.73 dB. The distribution of path loss is log-normally distributed about mean with standard deviation of 4.70 dB. While with the different of two floors between transmitter and receiver, the attenuation factor of LOS transmission is 9.00 dB, and 23.32 dB for NLOS transmission. The standard deviation of the path loss is 4.91 dB. Figure 4 shows the measured path loss and mean of path loss predicted using (4) for First Floor of Building 3.

Figure 5 and Figure 6 show scatter plots of measured path loss versus predicted path loss using (3) and (4) respectively, for entire Building 3 environment. It is shown that with proposed model, the standard

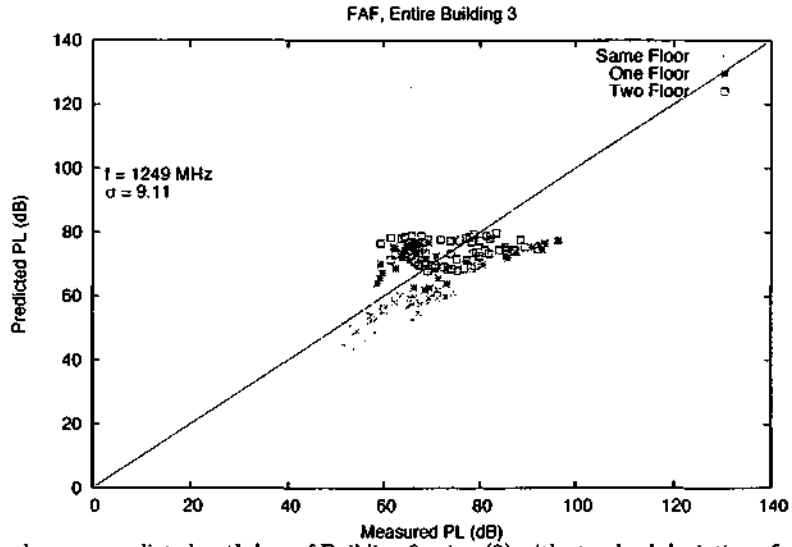


Figure 5. Measured versus predicted path loss of Building 3 using (3) with standard deviation of prediction error of 9.11 dB

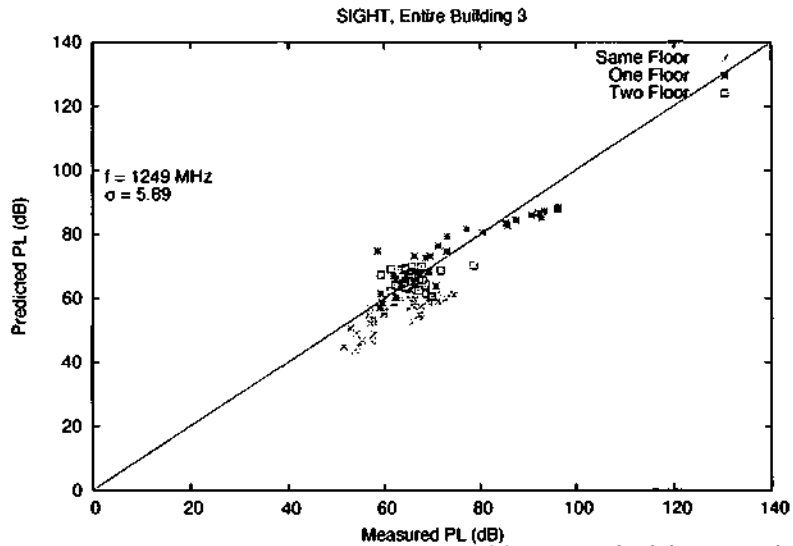


Figure 6. Measured versus predicted path loss of Building 3 using (4) with standard deviation of prediction error of 5.89 dB

deviation of error prediction is reduced from 9.11 dB to 5.89 dB.

## 6. CONCLUSION

In this paper, parameter statistics for use in several path loss prediction models are presented for multi-floored buildings environment and at 1.25 GHz carrier frequency. The statistics were extracted from real experiment data which was collected from three different buildings with different footprint shapes and interior environments. Building 1 and 2 are considered into this work because of their footprint shapes which are rectangular and square respectively. Building 3 is considered because of its modern interior design and materials that represent modern buildings.

Firstly, parameters for the use in Distance-Dependant Path loss model are presented as in Table 1. It is also found that square shaped footprint building is experiencing higher path loss over distance compared to building with rectangular footprint. This is based on the results obtained which show that the path loss exponents for rectangle footprint building are lower than square footprint building with the same number of floor between transmitter and receiver. And for building with an atrium inside the building, as described in Section 2.1, it is found that the mean path loss exponent is less than the other buildings. Secondly, the statistics for the use in Floor Attenuation Factor path loss model are also presented for multifloored buildings for same carrier frequency, as shown in Table 2.

Finally, a model is proposed as in (4), for indoor path loss prediction within buildings, where their environment allows NLOS and NLOS transmission between transmitter and receiver even though both are not on the same floor, such as existence of an atrium or a cavity in the building. This environment or internal design are commonly found within multifloored building such as hotels, shopping complexes, theater halls or cinemas. By considering either LOS or NLOS transmission in place, the statistics for the model were computed and given in Table 3. It is found that standard deviation of error prediction was reduced from 9.11 dB to 5.89 dB from measured data in this work, which shows that the improvement in prediction accuracy is achieved.

## ACKNOWLEDGMENTS

Authors would like to thank Mr. Alan Santillo from Faculty of Technology, the University of Plymouth, for his valuable assistances and suggestions during preparation and set up of system hardwares.

## REFERENCES

[1] He, T., Chan, S.-H. G., and Wong, C.-F., "Homemesh: a low-cost indoor wireless mesh for home networking," *IEEE Communications Magazine* **46**, 79–85 (December 2008).

[2] Hwang, I.-K. and Baek, J.-W., "Wireless access monitoring and control system based on digital door lock," *IEEE Transactions on Consumer Electronics* **53**, 1724–1730 (Nov. 2007).

[3] Molkdar, D., "Review on radio propagation into and within buildings," *Microwaves, Antennas and Propagation, IEE Proceedings H* **138**, 61–73 (Feb 1991).

[4] Motley, A. J. and Keenan, J., "Personal communication radio coverage in buildings at 900 MHz and 1700 MHz," *Electronics Letters* **24**, 763–764 (Jun 1988).

[5] Yamaguchi, Y., Abe, T., and Sekiguchi, T., "Experimental study of radio propagation characteristics in an underground street and corridors," *IEEE Transactions on Electromagnetic Compatibility* **28**, 148–155 (August 1986).

[6] Seidel, S. Y. and Rappaport, T. S., "914 MHz path loss prediction models for indoor wireless communications in multifloored buildings," *IEEE Transactions on Antennas and Propagation* **40**, 207–217 (February 1992).

[7] Andersen, J. B., Rappaport, T. S., and Yoshida, S., "Propagation measurements and models for wireless communications channels," *IEEE Communications Magazine* , 42–49 (January 1995).

[8] Valenzuela, R. A., Landron, O., and Jacobs, D. L., "Estimating local mean signal strength of indoor multipath propagation," *IEEE Transactions on Vehicular Technology* **46**, 203–212 (February 1997).

[9] Gibson, J. D., [*The Mobile Communications Handbook*], CRC Press Inc (1996). ISBN 0 849 38573 3.

[10] Affandi, A., Zein, G. E., and Citerne, J., "Investigation on frequency dependence of indoor radio propagation parameters," *Vehicular Technology Conference, 1999. VTC 1999 - Fall. IEEE VTS 50th* **4**, 1988–1992 vol.4 (1999).

[11] Cox, D. C., Murray, R. R., and Norris, A. W., "800 MHz attenuation measured in and around suburban houses," *AT&T Bell Lab Tech Journal* **63**, 921–954 (July/August 1984).

[12] Rappaport, T. S., "Characterization of uhf multipath radio channels in factory buildings," *IEEE Transactions on Antennas and Propagation* **37**, 1058–1069 (August 1989).

[13] Lafortune, J.-F. and Lecours, M., "Measurement and modelling of propagation losses in a building at 900 MHz," *IEEE Transactions on Vehicular Technology* **39**, 101–108 (May 1990).

# Path loss measurements and comparisons of 433 MHz, 869 MHz and 1249 MHz within multi-floored buildings

Ismail Fauzi Isnin*°, Martin Tomlinson*, Mohammed Zaki Ahmed* and Marcel Ambroze*

## ABSTRACT

In this paper, an extensive set of propagation path loss measurements within multi-floored buildings at 433 MHz, 869 MHz and 1249 MHz are presented. Parameter for use in two indoor path loss prediction models, Distance-Dependant Model (DD) and Floor Attenuation Floor Model (FAF), are derived from measurement data of three multi-floored buildings. Buildings were chosen with typical features such as rectangle footprint, square footprint and existence of an atrium within the building, respectively.

Comparison of model parameters has concluded that higher attenuation is experienced by the signal within a square footprint building than rectangle footprint. Building with an indoor atrium is found to have lower path losses than buildings without atrium, when considering multi-floor transmission. 869 MHz signal attenuated at slowest rate in most of the considered environments. 433 MHz signal is found to have better floor penetration compared to other frequencies. 1249 MHz is found to attenuate at slowest rate within a straight corridor with waveguiding and line-of-sight propagation path between the transmitter and the receiver.

Path loss prediction within multi-floored buildings with indoor atrium is refined by considering type of propagation path between trnamsitter and receiver. It is found that path loss of areas with line-of-sight propagation path could be modelled using parameters of same floor environment. An attenuation factor is derived and added for areas with non line-of-sight propagation path. It is shown that using this refinement, better prediction accuracy is obtained. Standard deviations of path loss prediction error are reduced as a result.

**Keywords:** Indoor path loss prediction, multi floored building, atrium or cavity areas, LOS, NLOS, building footprint

## 1. INTRODUCTION

Good knowledge on wireless propagation of an environment is important for the design, installation and operation of efficient and cost effective wireless systems. One of important wireless propagation characteristics is the path loss. Good path loss prediction models are useful during coverage planning and hardware location planning. As wireless solutions are becoming popular for indoor systems (multimedia, security monitoring and etc), therefore, works on various frequencies are useful to support wireless solutions for future deployments or implementations.

*Fixed and Mobile Communications Research
University of Plymouth,
Drake Circus,
PL4 8AA, Plymouth,
United Kingdom
e-mail: {ismail.isnin,mtomlinson,mahmed,marcel.ambroze}@plymouth.ac.uk

°Department of Computer System and Communication
Faculty of Computer Science and Information Systems
Universiti Teknologi Malaysia,
81310, Skudai, Johor,
Malaysia
e-mail: ismailfauzi@utm.my

In this paper, path loss characteristic has been investigated within three multi-floored buildings at 433 MHz, 869 MHz and 1249 MHz. Each building represents a typical features of a building. The first building is a building with a rectangle shape footprint. The second building is a building with a square shape footprint. Comparison of path loss models parameters between these two buildings is done to find out the influences of building footprint shape to indoor path loss of a building. Path loss characteristics from the third building are related to a building with an indoor atrium.

This paper is organized as follows. Section 2 describes the three buildings that were used as measurement sites and also describes procedure of measurement. Section 3 mentions the pre-processing procedures applied to measured data. In Section 4, two relevant path loss prediction models, Distance-Dependant Path Loss Model and Floor Attenuation Factor Path Loss Model are briefly explained and their parameter statistics are presented and discussed. In Section 5, a model is proposed for prediction of path loss within multi-floored buildings when both, line-of-sight (LOS) and non line-of-sight (NLOS) propagation paths are possible during multi floor communications. Section 6 finally concludes the work and results.

## 2. MEASUREMENT LOCATION AND PROCEDURES

### 2.1 Measurement Locations

#### 2.1.1 Building 1 (B1)

B1 is a four stories building that generally accommodates offices, laboratories and workshops. Even though it was build in 1950's, the building interior has been renovated for several times. Therefore, some of interior materials are from recent years materials. Footprint of B1 building is a rectangle shape with dimensions of 83.5 m $\times$ 19.2 m. Therefore, B1 is chosen to represent a rectangle building regarding the comparison of footprint shape effect on transmission path loss.

Except in the top floor, there is a long and straight corridor in each floors that links two stairway areas which are located at each end of the building. The corridors have dimensions of 71.8 m $\times$ 2.4 m and with ceiling height of 2.9 m above the floor.

Ground floor consists of offices and small-size workshops. First floor and second floor contain computer facilities studios, teaching rooms and offices. And the third floor is mainly for electronic laboratories.

Building frames are made of I-shaped steel and floors are made of reinforced concrete.

During measurement activities, the transmitter (Tx) was located at one end of the second floor corridor.

The same location of Tx was used for measurements of all considered frequencies, 433 MHz, 869 MHz and 1249 MHz. The receiver (Rx) was the one that had been positioned at various location within the B1 building. Due to access restrictions on some parts of the building, the top floor and rooms of ground floor were excluded from considered areas.

#### 2.1.2 Building 2 (B2)

B2 was constructed in 1980's and it is a five stories building. It is a square footprint building. The dimension of the footprint is 39.1 m $\times$ 39.1 m. Material of B2 building are concrete blocks for walls, and reinforced concrete for floors.

The ground floor consists of lecture theaters, teaching rooms and offices. The first floor is mostly allocated for open-access computer facilities halls and the rest of the floor accomodates computer laboratories and teaching rooms. More computer laboratories and teaching rooms in the second floor. The third floor is allocated for offices and staff training rooms. Several conference rooms, teaching rooms and a refectory are located in the fourth floor.

There is a corridor on each floor. Dimension of ground floor corridor is 2.1 m of wide and 2.6 m of height. Corridors on other floors are 2.1 m of wide and 2.3 m of height. Height of the corridor is the distance from the floor to the ceiling of the corridor.

Figure 1. The atrium of Building 3

For 869 MHz and 1249 MHz measurements, location of Tx was stationary in the corridor of B2 fourth floor. Rx was located at various locations in corridors of each floors of the building. For 433 MHz measurements, location of Tx was stationary located in the third floor corridor. Areas that were canvassed by 433 MHz Rx were all corridors except the corridor in the top floor. Note that all measurements in B2 were done within corridors area.

#### 2.1.3 Building 3 (B3)

B3 is a part of a building with modern materials and architectures which was completely developed in 2008. It is a three stories building. The building consists of classrooms, theatres, art studios and offices.

Materials that have been used for B2 are metals, concretes, wood boards and glasses. Floors of B3 are made of reinforced concrete.Internal walls are made of wood boards, concrete blocks and glasses.

B3 is not in the comparison of the footprint shape effect on path loss. With existence of an indoor atrium in the building, it gives a unique feature to the building compared to other two buildings. At some Tx locations within the building, it is possible to have line-of-sight (LOS) propagation path between Tx and Rx, even though the receiver is not in the same floor as the transmitter is. Since atrium within a building could sometimes be found in other common multi-floored buildings such as shopping complexes, hotels, airports, cinemas, theatres and etc. Thus, it is interesting to investigate properties of path loss in this environment. The atrium of B3 can be seen in Figure 1.

Transmitter location was fixed for measurements of all frequencies. At all time, during measurement activities, Tx was located nearby the atrium perimeter in the second floor. The receiver was located at various locations within the building.

### 2.2 Measurement Setup and Procedures

Table 1 gives the specifications that was applied in measurement activities.

#### 2.2.1 433 MHz Equipments Setup

On the transmitter side, the transmitter unit was transmitting a narrow-band continuous wave (CW) signal which was emitted by a 1/4 wavelength monopole whip antenna. Transmit power of the Tx is +21.12 dBm. Height of the Tx antenna was set to be 1.25 meters above the floor. All of these equipments were arranged on top of a trolley.

On the receiver side, a helical antenna was used as the receiving antenna. The antenna was also set to be at the same height as the Tx antenna, which is 1.25 meters above the floor. The antenna was then

Table 1. Settings of 433 MHz, 869 MHz and 1249 MHz systems in measurement activities. $\lambda$ symbol denotes wavelength.

| Specifications | 433 MHz | 869 MHz | 1249 MHz |
|---|---|---|---|
| Carrier frequency, MHz, $f$ | 433.9 | 869.49 | 1249.36 |
| Tx antenna type | 1/4 $\lambda$, monopole (whip) | Helical | 1/2 $\lambda$, dipole |
| Height of Tx and Rx, m | 1.25 | 1.27 | 1.54 |
| Rx antenna type | Helical | 3/4 $\lambda$, monopole (whip) | 1/2 $\lambda$, dipole |
| Tx power, dBm | +21.12 | +24.25 | +31.19 |
| System antenna gain in dB | 0.00 | 0.00 | 4.30 |
| Rx dynamic range | 0 to -80 dBm | 0 to -80 dBm | 0 to -80 dBm |
| System maximum path loss, dB | 101.12 | 104.25 | 111.19 |
| Resolution Bandwidth, kHz | 30 | 30 | 30 |
| System cables loss, dB | 1.27 | 2.14 | 3.09 |

connected to a spectrum analyser which functioning to measure relative signal strength of received signal. The spectrum analyzer capables to measure relative received signal power of 0 to -80 dBm over resolution bandwidth of 30 kHz. Thus, maximum path loss of the system was equal to 101.12 dB. A computer was connected to the spectrum analyser as user terminal that controls spectrum analyser during measurement process and as a data storage terminal. These equipments were setup on top of a another trolley.

### 2.2.2 869 MHz Equipments Setup

A continuous wave signal was generated from the Tx with power of +24.25 dBm. Signal was illuminated by a helical antenna which was set to be 1.27 meters above the floor.

For the Rx, a 3/4 wavelength whip antenna was used and set to be at 1.27 meters above the floor. The rest of the equipment setup were similar as 433 MHz system setup. With the spectrum analyser dynamic range is 0 to -80 dBm and transmit power was +24.25 dBm, thus the maximum path loss of 869 MHz system was 104.25 dB.

### 2.2.3 1249 MHz Equipments Setup

With +31.19 dBm transmitting power, a narrow-band continuous wave (CW) signal was transmitted from half-wavelength dipole antenna at 1.54 m above the floor.

On the receiver side, a similar half-wavelength dipole antenna was used as the receiver antenna. The rest of the equipment setup were similar as 433 MHz system. The maximum path loss of the system was equal to 111.19 dB.

### 2.2.4 Measurement Procedures

While, the transmitter was transmitting the continuous signal. Straight lines were stretched on the floor of the interest area to represent measurement tracks. Each measurement tracks were marked with evenly distanced points that indicate measurement points. Each points were distanced at approximately 0.25 meter from neighbouring points. Length of each measurement tracks were varies, due to the varying surroundings. Beginning from the first point on a track, the receiver measured and recorded received signal strength value at the measurement points and then moved to next measurement point. The procedure were repeated till the last point was reached and for all measurement tracks.

10 samples of signal strength reading were recorded at every 400 ms at each measurement point. Readings were then averaged in mW unit. Same procedure were repeated for all measurement points.

## 3. DATA PROCESSING

Recorded values was then spatially averaged over several wavelength for path loss analysis.[1,2] Segment length of $10\lambda$ was chosen as it was found to be the best compromise between removing fast fading effect and retaining the path loss fading pattern.[3] Thus, measurement tracks were segmented by segments with length of $10\lambda$ per segment. Length of a segment were 6.9 meters, 3.45 meters and 2.4 meters for 433 MHz, 869 MHz and 1249 MHz measurement tracks, respectively. A median values of each segments was taken to represent the spatially averaged signal strength of the segment which is called local median. Each local median was assigned to middle point of the segment. Distance between the transmitter antenna and a local median point, which was measured in three dimensions, were in range of 1.58 m for the nearest point and 72.98 m for the farthest point.

Local path loss of a segment was calculated by subtracting the transmit power with local median of the corresponding segment. All local path loss values were normalised by subtracting system antenna gains and adding the system cable losses. Transmit power, antennas gain and cable losses values are given in Table 1. Along with normalised local path loss values, other informations such as transmitter-receiver distance (T-R Distance) and number of obstructed floors between transmitter and receiver were attached together. These parameters were required in classification of data according to relevant categories and derivation of model parameters as described in Section 4.

## 4. PATH LOSS PREDICTION MODEL

### 4.1 Distance-Dependant Path Loss Model

A classic model of predicting mean path loss with known distance between transmitter and receiver, $d$, is given by[1,2,4,5]

$$\overline{PL}(d)[\text{dB}] = PL_0(d_0)[\text{dB}] + 10 \times n \times \log_{10}\left(\frac{d}{d_0}\right), \tag{1}$$

where $d_0$ denotes the reference distance, $PL_0(d_0)$ is free space path loss of the system when distance between transmitter and receiver is $d_0$ and $n$ indicates the mean path loss exponent of the environment. It is well known that $n = 2$ is for free space environment and $d_0$ is chosen as 1 meter for indoor environments. With $PL_0(d_0)$ is calculated using Friis free space path loss formula, path loss of the 433 MHz, 869 MHz and 1249 MHz systems at $d_0 = 1.0$ are equal to 25.19 dB, 31.23 dB and 34.38 dB respectively. Note that computation of $PL_0(d_0)$ considered system gains and system losses were equal to unity.

Path loss of known transmitter-receiver distance, with shadowing effect, could be modelled using[1]

$$PL(d)[\text{dB}] = \overline{PL}(d) + X_\sigma[\text{dB}], \tag{2}$$

where $\overline{PL}(d)$ is the mean of path loss, $X_\sigma$ is a zero mean log-normally distributed random variable in dB, with standard deviation equal to $\sigma$.[6–8] Because of limited data, it is assumed that measurement data fulfill this property.

To obtain parameters of path loss prediction models for the systems, values of $n$ and $\sigma$ were derived from measured data using linear regression with Least Squared Error method.[1,5,9] Values of $n$ and $\sigma$ for 433 MHz, 869 MHz and 1249 MHz measurement data are given in Table 2, Table 3 and Table 4, respectively. The last column in each tables, shows number of local path loss that were considered during derivation of model parameters. "No Data" indicates no measurement data collected from the corresponding categories. Derivation of Distance-Dependant path loss model parameters were done for two categories, Corridor and Whole Floor models. Corridor model parameters were derived by considering only data from corridor areas of the corresponding floor. Whole Floor model parameters were derived by considering all measurement data that were collected from the corresponding floor. This included data from corridors and rooms measurements.

Generally, values of $n$ are found to be proportional to the number of crossed floor for all buildings and for both models, Corridor and Whole-Floor. This pattern is expected to be found as the same pattern have

Table 2. The mean path loss exponent, $n$, and standard deviation, $\sigma$, for use in Distance-Dependant Path Loss Model based on a measurement at a carrier frequency of 433 MHz

| | Corridor | | | Whole Floor | | |
|---|---|---|---|---|---|---|
| | $n$ | $\sigma$[dB] | Locations | $n$ | $\sigma$[dB] | Locations |
| Building 1: | | | | | | |
| Same Floor | 2.32 | 3.8 | 9 | 2.79 | 8.8 | 23 |
| 1 Floor Obstruction | 3.44 | 3.7 | 9 | 3.82 | 5.4 | 21 |
| 2 Floors Obstruction | 4.35 | 3.3 | 6 | No Data | No Data | No Data |
| Building 2: | | | | | | |
| Same Floor | 3.51 | 4.6 | 5 | No Data | No Data | No Data |
| 1 Floor Obstruction | 4.63 | 3.8 | 9 | No Data | No Data | No Data |
| 2 Floors Obstruction | 5.20 | 1.3 | 5 | No Data | No Data | No Data |
| 3 Floors Obstruction | 5.68 | 3.0 | 5 | No Data | No Data | No Data |
| Building 3: | | | | | | |
| Same Floor | 2.68 | 3.2 | 6 | 2.79 | 2.7 | 13 |
| 1 Floor Obstruction | 3.10 | 8.4 | 8 | 3.51 | 9.7 | 12 |
| 2 Floors Obstruction | 3.25 | 8.2 | 12 | 3.54 | 7.9 | 22 |

Table 3. The mean path loss exponent, $n$, and standard deviation, $\sigma$, for use in Distance-Dependant Path Loss Model based on a measurement at a carrier frequency of 869 MHz

| | Corridor | | | Whole Floor | | |
|---|---|---|---|---|---|---|
| | $n$ | $\sigma$[dB] | Locations | $n$ | $\sigma$[dB] | Locations |
| Building 1: | | | | | | |
| Same Floor | 1.50 | 4.5 | 18 | 2.28 | 10.9 | 64 |
| 1 Floor Obstruction | 3.06 | 3.0 | 19 | 3.42 | 4.7 | 54 |
| 2 Floors Obstruction | 3.81 | 2.8 | 18 | No Data | No Data | No Data |
| Building 2: | | | | | | |
| Same Floor | 2.85 | 3.7 | 11 | No Data | No Data | No Data |
| 1 Floor Obstruction | 4.17 | 4.9 | 12 | No Data | No Data | No Data |
| 2 Floors Obstruction | 4.93 | 3.1 | 18 | No Data | No Data | No Data |
| 3 Floors Obstruction | 5.33 | 2.6 | 12 | No Data | No Data | No Data |
| 4 Floors Obstruction | 5.50 | 0.7 | 4 | No Data | No Data | No Data |
| Building 3: | | | | | | |
| Same Floor | 2.32 | 3.2 | 11 | 2.41 | 2.9 | 25 |
| 1 Floor Obstruction | 2.49 | 7.7 | 20 | 3.01 | 12.0 | 28 |
| 2 Floors Obstruction | 2.83 | 7.9 | 27 | 3.18 | 8.4 | 50 |

been reported in earlier works.[1,10,11] Pattern of $\sigma$ are found not being consistent. However, in buildings which have no indoor atrium, $\sigma$ are generally found to decrease as number of obstructed floor increases.

$n$ of 869 MHz and 1249 MHz corridor models at Same Floor of B1 environment are found to be less than 2. The environment was a long rectangle waveguided environment and propagation path were LOS between Tx and Rx. It is not a surprising result since $n < 2$ had been reported within similar environments by others.[8,12,13]

Comparison between Whole-Floor model parameters and Corridor model parameters has found that $n$ of Whole-Floor are higher than $n$ of Corridor models. This is believed due to the signal propagation in whole floor environment experienced more obstructions and attenuations from objects within the floor such as walls, pillars and furnitures.

Table 4. The mean path loss exponent, $n$, and standard deviation, $\sigma$, for use in Distance-Dependant Path Loss Model based on a measurement at a carrier frequency of 1249 MHz

| | | Corridor | | | Whole Floor | | |
|---|---|---|---|---|---|---|---|
| | | $n$ | $\sigma$[dB] | Locations | $n$ | $\sigma$[dB] | Locations |
| Building 1: | | | | | | | |
| | Same Floor | 1.45 | 3.8 | 27 | 2.22 | 13.3 | 86 |
| | 1 Floor Obstruction | 3.21 | 3.3 | 27 | 3.65 | 6.3 | 72 |
| | 2 Floors Obstruction | 3.90 | 3.2 | 25 | No Data | No Data | No Data |
| Building 2: | | | | | | | |
| | Same Floor | 3.07 | 7.6 | 18 | No Data | No Data | No Data |
| | 1 Floor Obstruction | 4.45 | 4.3 | 18 | No Data | No Data | No Data |
| | 2 Floors Obstruction | 5.30 | 4.0 | 26 | No Data | No Data | No Data |
| | 3 Floors Obstruction | 5.73 | 3.8 | 20 | No Data | No Data | No Data |
| | 4 Floors Obstruction | 5.87 | 3.2 | 10 | No Data | No Data | No Data |
| Building 3: | | | | | | | |
| | Same Floor | 2.32 | 3.6 | 19 | 2.44 | 3.9 | 37 |
| | 1 Floor Obstruction | 2.57 | 7.4 | 29 | 3.05 | 11.1 | 41 |
| | 2 Floors Obstruction | 2.87 | 10.1 | 40 | 3.24 | 10.1 | 67 |

#### 4.1.1 Relation between footprint shape and path loss rate

It is interesting to discuss the results based on shape of building footprint. Particularly, the comparison is between B1 and B2 as the former represent a rectangular footprint building and the latter represents a square footprint building respectively. From $n$ parameters of all frequencies, it is clearly found that $n$ values of B2 are higher than the $n$ parameters of B1. This shows that loss within a square footprint building is higher than in a rectangle footprint building.

For B3, it is found that the path loss exponents are the lowest one when it comes to multi-floor propagation. This behavior is probably best explained by existence of an atrium within B3 which could be considered as a vertically waveguiding structure for the signal to propagate between floors. With location of Tx being on the edge of the atrium, LOS propagation paths between Tx and Rx are possible for multi-floor propagation. This is believed to result in higher average received power being measured within B3 compared to other buildings.

### 4.2 Floor Attenuation Factor (FAF) Path Loss Model

Model (1) and (2) with its $n = n(SameFloor)$ can be alternatively used to predict path loss within multi-floored buildings by adding a constant, which is known as Floor Attenuation Factor (FAF). FAF is a constant in dB that represents attenuation related to a number of crossed floors. FAF is calculated by finding the average of difference between predicted mean path loss with Same Floor path loss exponent and measured local path loss of the corresponding category. Thus, equation to predict mean path loss of a multi floor building using FAF path loss model is given as

$$\overline{PL}(d) = PL_0(d_0) + 10 \times n(SameFloor) \times \log_{10}\left(\frac{d}{d_0}\right) + \text{FAF[dB]}, \tag{3}$$

with $n(SameFloor)$ is the path loss exponent for Same Floor environment, $PL_0(d_0)$ is free space path loss at reference distance $d_0$ and $d$ is distance between Tx and Rx.

FAF model parameters are given in Table 5, Table 6 and Table 7, respectively for 433 MHz, 869 MHz and 1249 MHz. $\sigma$ is the standard deviation of difference between predicted mean path loss by (3) with local path loss of the corresponding floor. FAF and $\sigma$ for B1 and B3 were extracted from Whole Floor dataset. Due to data unavailability, Corridor dataset was used for B2.

Table 5. Average Floor Attenuation Factors in Decibels based on a measurement at a carrier frequency of 433 MHz

| | | FAF [dB] | $\sigma$[dB] |
|---|---|---|---|
| Building 1: | | | |
| | 1 Floor Obstruction | 14.3 | 5.5 |
| | 2 Floors Obstruction | 20.5 | 0.9 |
| Building 2 (Corridor) : | | | |
| | 1 Floor Obstruction | 12.1 | 3.6 |
| | 2 Floors Obstruction | 17.5 | 1.7 |
| | 3 Floors Obstruction | 24.8 | 2.2 |
| Building 3: | | | |
| | 1 Floor Obstruction | 10.0 | 9.0 |
| | 2 Floors Obstruction | 10.1 | 7.4 |

Table 6. Average Floor Attenuation Factors in Decibels based on a measurement at a carrier frequency of 869 MHz

| | | FAF [dB] | $\sigma$[dB] |
|---|---|---|---|
| Building 1: | | | |
| | 1 Floor Obstruction | 16.5 | 5.2 |
| | 2 Floors Obstruction | 22.3 | 3.6 |
| Building 2 (Corridor) : | | | |
| | 1 Floor Obstruction | 12.5 | 5.0 |
| | 2 Floors Obstruction | 23.2 | 4.4 |
| | 3 Floors Obstruction | 28.1 | 3.4 |
| | 4 Floors Obstruction | 31.0 | 0.7 |
| Building 3: | | | |
| | 1 Floor Obstruction | 8.4 | 11.7 |
| | 2 Floors Obstruction | 10.6 | 8.0 |

Table 7. Average Floor Attenuation Factors in Decibels based on a measurement at a carrier frequency of 1249 MHz

| | | FAF [dB] | $\sigma$[dB] |
|---|---|---|---|
| Building 1: | | | |
| | 1 Floor Obstruction | 20.9 | 5.8 |
| | 2 Floors Obstruction | 24.8 | 3.9 |
| Building 2 (Corridor): | | | |
| | 1 Floor Obstruction | 13.3 | 4.5 |
| | 2 Floors Obstruction | 25.2 | 5.8 |
| | 3 Floors Obstruction | 30.4 | 4.8 |
| | 4 Floors Obstruction | 33.4 | 3.5 |
| Building 3: | | | |
| | 1 Floor Obstruction | 8.4 | 10.8 |
| | 2 Floors Obstruction | 11.1 | 9.1 |

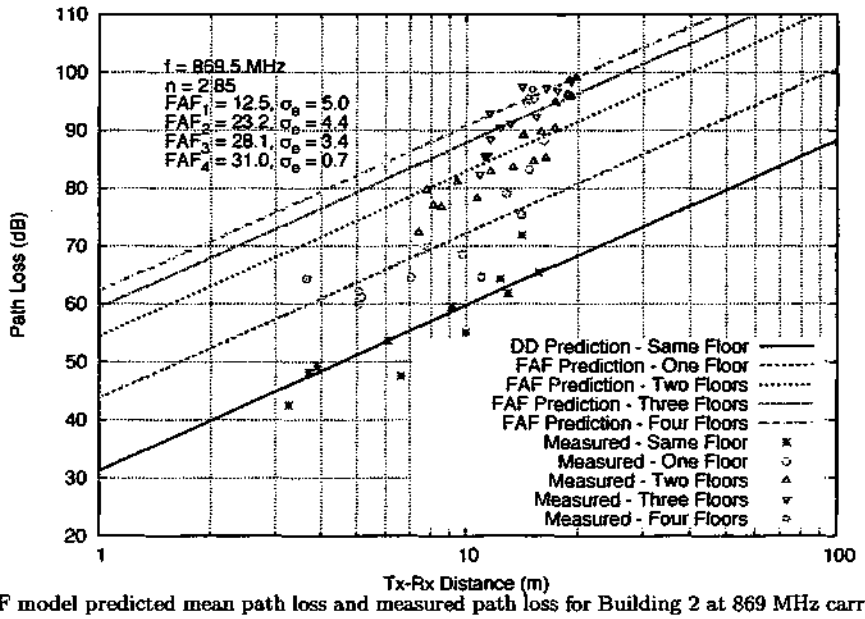


Figure 2. FAF model predicted mean path loss and measured path loss for Building 2 at 869 MHz carrier frequency.

Within B1, attenuation caused by one floor and two floors obstructions are respectively 14.2 dB and 20.3 dB for 433 MHz, 16.6 dB and 22.3 dB for 869 MHz and 20.8 dB and 24.7 dB for 1249 MHz.

Within B2, attenuation caused by up to three floors are in the range of 12.2 dB and 25.0 dB for 433 MHz, 12.6 dB and 27.7 dB for 869 MHz and 13.3 dB and 30.7 dB for 1249 MHz. Floor attenuation factors are found to non linearly increase as number of obstructed floor between Tx and Rx increases. It is obviously seen from Figure 2 which shows predicted mean path loss using (3) within B2 at 869 MHz. Similar observations had also been reported by other researchers.[1,10]

Within B3, which is a building with an atrium, FAF values are significantly smaller compared to the FAF of corresponding category from B1 and B2. Difference between FAF values of 1 Floor Obstruction and 2 Floors Obstruction are insignificant. These results are believed due to the same reason that has been discussed in Section 4.1.

From the comparison of FAF values among different frequencies, FAF is proportional to signal frequency. 1249 MHz signal attenuates the most, followed by 869 MHz signal and 433 MHz signal, with same number of obstructed floor between Tx and Rx.

## 5. CONSIDERATION OF LINE-OF-SIGHT AND NON-LINE-OF-SIGHT FOR BETTER PATH LOSS PREDICTION WITHIN MULTI-FLOOR BUILDINGS WITH ATRIUM

Some locations of Tx within a building with atrium could have both, LOS and NLOS propagation paths, between Tx and Rx even for multi-floor transmission. This situation is found to affect the prediction accuracy of (1) and (3). This is shown by higher $\sigma$ values of B3 compared to $\sigma$ of other buildings as shown in Tables 2 to 7.

Therefore, a model is proposed to improve accuracy of path loss prediction for use in a building with atrium, provided Tx location is where LOS and NLOS propagation paths between Tx and Rx are possible in multi-floor transmission. Prediction of path loss is done by considering types of propagation path between Tx and Rx. Prediction of path loss for same floor transmission is done by using the Distance-Dependant

Table 8. NLOS Attenuation Factors in Decibels

| Carrier Frequency | | AF(NLOS) (dB) | Number of Locations | $\sigma$ (dB) |
|---|---|---|---|---|
| 433 MHz | 1 Floor Obstruction | 18.6 | 6 | 2.7 |
| | 2 Floors Obstruction | 13.7 | 16 | 4.6 |
| 869 MHz | 1 Floor Obstruction | 22.1 | 11 | 4.0 |
| | 2 Floors Obstruction | 13.5 | 39 | 5.7 |
| 1249 MHz | 1 Floor Obstruction | 19.2 | 18 | 5.1 |
| | 2 Floors Obstruction | 15.0 | 50 | 6.2 |

model with $n$(Same Floor). But for multi-floor transmission, the model to predict mean of path loss is proposed as

$$\overline{PL}(d) = PL_0(d_0) + 10 \times n(\text{Same Floor}) \times \log_{10}\left(\frac{d}{d_0}\right) + \gamma\,(los)\,, \tag{4}$$

with

$$\gamma\,(los) = \left\{ \begin{array}{ll} 0 & \text{if} \quad los = 1 \\ \text{AF(NLOS)} & \text{otherwise} \end{array} \right), \tag{5}$$

where $n$(Same Floor) is the Same Floor mean path loss exponent, $PL_0(d_0)$ is free space path loss at reference distance $d_0$ and $d$ is distance between Tx and Rx. AF(NLOS) is the attenuation factor in dB. $los$ is a binary flag which belongs to a local segment. $los = 1$, if majority of the measurement points in the corresponding segment are LOS, and vice versa. If $los = 1$, then $\gamma = 0$ is applied into the model, otherwise, $\gamma =$ AF(NLOS). AF(NLOS) is the average of difference between mean path loss of Same Floor with local path loss of the corresponding floor. Note that Whole-Floor dataset were used in AF(NLOS) derivation.

Values of AF(NLOS), standard deviation of the difference between predicted path losses and measured local path losses, and number of local segments used to derive the statistics are given in Table 8. Notice, the AF(NLOS) are comparable with the FAF parameters of buildings without atrium. At 433 MHz, attenuation factors with one floor and two floor obstruction are found to be 18.6 dB and 13.7 dB respectively. The corresponding attenuation factors for 869 MHz are 22.1 dB and 13.5 dB respectively. And, 19.2 dB and 15.0 dB for 1249 MHz, respectively. It is interesting to find that average path loss of one floor obstruction is higher than the average path loss of two floors obstruction within a building with indoor atrium. Perhaps this is due to most of signal paths that propagated through the atrium were guided and reflected by the atrium structure into the ground floor instead of into the first floor of B3.

Last column of Table 8 shows standard deviations of predicted path losses to local path losses are reduced. This indicates that the proposed model has gained better prediction accuracy for multi-floor propagation within buildings with atrium. As an example, Figure 3 shows measured local path losses and predicted mean of path loss using (4) at carrier frequency 1249 MHz for One Floor Obstruction within Building 3. In this environment, $\sigma$ has been reduced to 5.1 dB from 11.1 dB and 10.8 dB with (1) and (3) respectively.

## 6. CONCLUSION

In this paper, parameter statistics for use in Distance-Dependant and Floor Attenuation Factor path loss prediction models are presented for multi-floored buildings at 433 MHz, 869 MHz and 1249 MHz. Parameter values were derived from site measurement data which had been collected within three multi-floored buildings. First two buildings were considered due to its typical features, rectangular footprint and square footprint, respectively. The third building was considered due to the existence of an indoor atrium within the building.

From the Distance-Dependant model parameter statistics, mean path loss exponents for rectangle footprint building are generally lower than square footprint building with the same number of floor obstruction

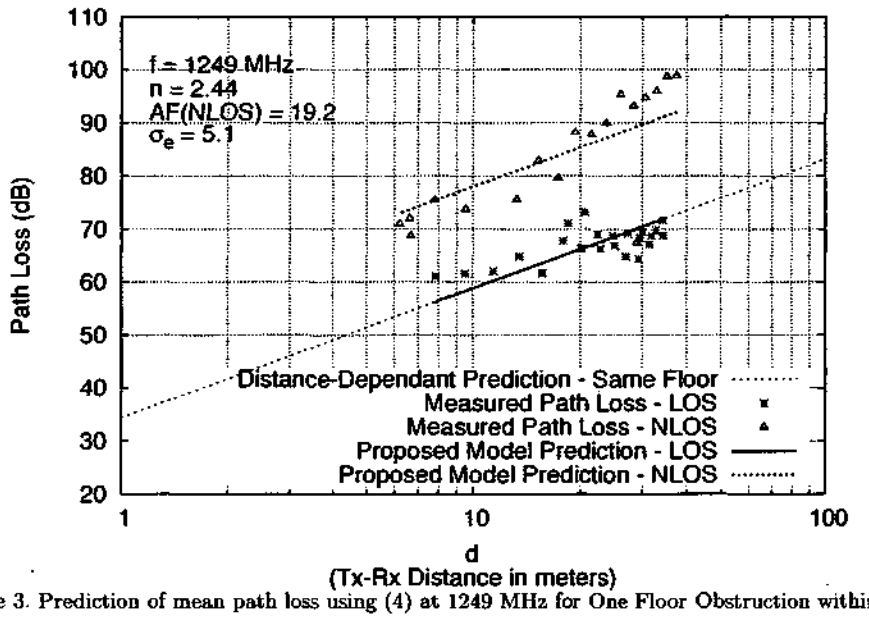


Figure 3. Prediction of mean path loss using (4) at 1249 MHz for One Floor Obstruction within B3.

between transmitter and receiver. This means square shaped footprint building attenuates wireless signal at higher rate than in a rectangular footprint, regardless of carrier frequency.

Comparison of mean path loss exponent among carrier frequencies has found that 869 MHz propagates with lowest path loss attenuation rate over a distance in most of considered environments. 433 MHz propagates with higher path loss attenuation rate since it has the highest mean path loss exponent in most environments. 1249 MHz is found being attenuated at slowest rate than other frequencies in an environment, where the transmitter (Tx) and the receiver (Rx) are within a straight waveguided environment with Line-of-Sight transmission between Tx and Rx, such as in a straight hallway or corridor.

Parameter tables of Floor Attenuation Factor model have shown that floor attenuation factor is a non-linear function of number of obstructed floor. Lower frequency signals are more robust to the floor obstruction than higher frequency signals. Floor Attenuation Factor statistics have shown that existence of atrium improves the average received signal power in other floors, as some signals are believed being guided through the atrium instead of penetrating the floors to reach the receiver.

A refinement of path loss prediction is proposed for multi-floor building with indoor atrium. Provided the location of Tx is located somewhere, where LOS and NLOS propagation path are possible between Tx and Rx during multi-floor transmission. Proposed model predicts indoor path loss by considering type of propagation path, either it is LOS or NLOS. Path loss of an area within other floors is predicted as Same Floor scenario if most of the measurement points within the area are LOS. Otherwise, an attenuation factor, which is denoted as AF(NLOS), is added to the predicted path loss. Proposed model has reduced standard deviation of error prediction, which indicates better prediction accuracy.

## ACKNOWLEDGMENTS

Authors would like to thank Alan Santillo and Ross Parlour from Faculty of Technology, the University of Plymouth, for their assistances in hardware preparation.

## REFERENCES


[1] Seidel, S. Y. and Rappaport, T. S., "914 MHz path loss prediction models for indoor wireless communications in multifloored buildings," *IEEE Transactions on Antennas and Propagation* **40**, 207–217 (February 1992).

[2] Andersen, J. B., Rappaport, T. S., and Yoshida, S., "Propagation measurements and models for wireless communications channels," *IEEE Communications Magazine* , 42–49 (January 1995).

[3] Valenzuela, R. A., Landron, O., and Jacobs, D. L., "Estimating local mean signal strength of indoor multipath propagation," *IEEE Transactions on Vehicular Technology* **46**, 203–212 (February 1997).

[4] Gibson, J. D., [*The Mobile Communications Handbook*], CRC Press Inc (1996). ISBN 0 849 38573 3.

[5] Affandi, A., Zein, G. E., and Citerne, J., "Investigation on frequency dependence of indoor radio propagation parameters," *Vehicular Technology Conference, 1999. VTC 1999 - Fall. IEEE VTS 50th* **4**, 1988–1992 vol.4 (1999).

[6] Turkmani, A. M. D. and de Toledo, A. F., "Radio transmission at 1800 MHz into, and within, multistory buildings," *IEE Proceedings I on Communications, Speech and Vision* **138**, 577–584 (December 1991).

[7] Molkdar, D., "Review on radio propagation into and within buildings," *IEE Proceedings H Microwaves Antennas and Propagation* **138**, 61–73 (Feb 1991).

[8] Rappaport, T. S. and Mcgillem, C. D., "UHF fading in factories," *IEEE Journal on Selected Areas in Communications* **7**, 40–48 (January 1989).

[9] Lafortune, J.-F. and Lecours, M., "Measurement and modelling of propagation losses in a building at 900 MHz," *IEEE Transactions on Vehicular Technology* **39**, 101–108 (May 1990).

[10] Phaiboon, S., "An empirically based path loss model for indoor wireless channel in laboratory building," *Proceedings of IEEE TENCON 2002* , 1020–1023 (2002).

[11] Huaiyi, J., Jian, G., and Hongqing, L., "The analysis and research of the radio propagation models in multifloored buildings," 331–334 (2002).

[12] Beauvarlet, D. and Virga, K. L., "Measured characteristics of 30-GHz indoor propagation channel with low-profile directional antennas," *IEEE antennas and wireless propagation letters* **1**, 87–90 (2002).

[13] Ju, K., Chiang, C., Liaw, H., and Her, S., "Radio propagation in office buildings at 1.8 GHz," *Personal, Indoor and Mobile Radio Communications, 1996. PIMRC'96., Seventh IEEE International Symposium on* **3**, 766–770 (1996).